

Dual-tracer Molecular Neuroimaging  
Methodological improvements and biomedical  
applications

Francisca Patuleia Figueiras

---

TESI DOCTORAL UPF / 2012

DIRECTOR DE LA TESI

Dr. Juan Domingo Gispert (Pasqual Maragall Foundation)

DEPARTAMENT OF EXPERIMENTAL AND HEALTH  
SCIENCES



*I would like to devote this thesis to my family, especially to...*

*My grandma Celinha and grandpa Patuleia...*

*My loving parents, Joana e Paulo...*

*My wonderful husband, Manel...*

*My sweet little boy, Benjamim...*



‘A scientist in his laboratory is not only a technician: he is also a child placed before natural phenomena, which impress him, like a fairy tale.’

*Marie Curie*



## Acknowledgements

The PhD has been a long and challenging journey, and I am extremely grateful to all who kept up with me this far.

I am very thankful to Dr. Juan D. Gispert for giving me the opportunity to work with PET imaging and develop my PhD thesis in his team. As PhD supervisor, I would like to thank him all the guidance, support and encouragement during these years.

I would like to thank to Dr. Santiago Rojas, Dr. Deborah Pareto, Dr. Santiago Bullich and to Dr. Alexandre Gironell for their scientific support and knowledge along the different projects.

During the PhD, I had the great opportunity to join Dr. Oliver Howes group at Medical Research Council (Hammersmith Hospital-Imperial College London), where I met exceptional people that I would like to mention here: Dr. Subrata Bose, Stacey Mccraw, Dr. Michael Bloomfield, Marleen le Cessie and Shazi Singh. Thank you all!

---

M'agradaria donar les gràcies a tots els membres passats i presents del Centre d'Imatge Molecular (CRC-CIM) per tota l'amistat, l'ajut i la bona companyia: Alba, Elia, Nuria, Cristina, Maria Luisa, Eva, Anna Doutres, Dolors, Aida, Natalia, Susi, Judith, Ignasi, Pili, Sergio, Raul H. y G., Jordi Ruiz, Francisco J. Fernández, Jesus, Rafa, Juanjo, Pilar, Carlos Trampal, Olga Millan, Laura Pla, Laura España, Ainhoa y Cecilia.

Gràcies en particular al Capi Xavi, per tota l'amistat i per ser el meu entrenador de Matlab i volei!

Mil gràcies a la Foti, la Beri i la Sandrix, les meves nenes preferides! Us trobo a faltar.

---

Obrigada Joana Margarida, Joana Cabral, Mónica e Inês Zimbarra, as minhas amigas doutorandas preferidas, por me ouvirem e compreenderem todos os meus dramas existenciais ao longo do PhD.

Obrigada família, por todo o Amor e ternura... papas, avos, mana Carlota e mano Baltazar, tios e primos... Adoro-vos a todos!

Obrigada Manel, por estares sempre comigo, por te rires das minhas palhaçadas, por aturares as minhas inseguranças... e ainda assim, gostares de mim!

Obrigada Benjamim, por existires na minha vida.



## Abstract

Positron emission tomography (PET) is a functional imaging method that allows studying physiological, biochemical or pharmacological processes *in vivo*. PET is being used in both research and clinical practice. In the brain, it has been used to investigate metabolism, receptor binding, and alterations in regional blood flow. This thesis involves both preclinical and clinical dual-tracer PET imaging studies of different neurological disorders. In this way, different radiotracers were used along the projects. The first project focused on the implementation and *in vivo* validation of the simultaneous dual-tracer PET imaging technique on the rat brain and its applications in the study of cerebral ischemia. In particular, in this project two biological processes were studied at the same time: cerebral blood flow and cerebral glucose metabolism. The second project consisted in a clinical correlation study of the GABAergic and serotonin systems in a population with Essential Tremor (ET), the most commonly movement disorders.

---

## Resum

La tomografia per emissió de positrons (PET) és un mètode d'imatge funcional que permet l'estudi *in vivo* de processos fisiològics, bioquímics i farmacològics. La PET s'utilitza tant en la pràctica clínica com en la recerca. Al cervell, s'ha utilitzat per investigar el metabolisme, la neurotransmissió, i les alteracions en el flux sanguini regional. Aquesta tesi implica estudis preclínic i clínic de la tècnica PET en diversos trastorns neurològics. D'aquesta manera, es van utilitzar diferents radiotracadors al llarg dels projectes. El primer projecte es va centrar en la implementació i validació *in vivo* de la tècnica PET del doble-marcador simultani en el cervell de rata i les seves aplicacions en l'estudi de la isquèmia cerebral. En particular, en aquest projecte es van estudiar en el mateix moment dos processos biològics: el flux sanguini cerebral i el metabolisme cerebral de la glucosa. El segon projecte va consistir en un estudi clínic de correlació dels sistemes GABAèrgic i serotoninèrgic en una població amb tremolor essencial (TE), el trastorn del moviment més comú.



## Preface

Positron emission tomography (PET) is a medical imaging modality, which expanded worldwide thanks to the availability of compact medical cyclotrons and automated chemistry synthesis modules for the production of PET radiopharmaceuticals. The first preparation of 2-deoxy-2-[<sup>18</sup>F]fluoro-D-glucose (<sup>18</sup>F-FDG) compound using <sup>18</sup>F-F<sub>2</sub> gas was achieved in 1978 (Ido et al., 1978). The real break-through was enabled in 1986 (Hamacher, Coenen et al. 1986), allowing for the production of high amounts of FDG on the basis of <sup>18</sup>F-fluoride. Since the 1970s several thousand PET radiotracers have been developed, almost 800 molecular imaging radiotracers have been listed with potential clinical applications. It is estimated that there are more than 650 biomedical cyclotrons in the world catering to about 2200 PET or PET/computed tomography (CT) systems. Recently, several reviews have been published that discuss the development of many new PET radiopharmaceuticals with potential clinical applications (Dunphy and Lewis 2009; Nagren, Halldin et al. 2010; Sioka, Fotopoulos et al. 2010; Vallabhajosula, Solnes et al. 2011). Despite the availability of many PET radiotracers, currently most clinical PET studies are performed with <sup>18</sup>F labelled radiotracers (IAEA 2006, IAEA, 2009), since it can be produced at high yields in biomedical cyclotrons, its decay mode is close to 100% positron emission, its positron energy is low when compared to other positron emitters and, most important, its relatively long half life permits the distribution from production centres to surrounding hospitals. The use of <sup>11</sup>C, and specially <sup>13</sup>N and <sup>15</sup>O, is restricted to those hospitals owning a cyclotron and a radiopharmaceutical laboratory, and consequently, this involves high costs of producing, specialized personnel and complex regulatory issues.

<sup>11</sup>C is a very interesting radionuclide because its stable isotope (<sup>12</sup>C) is present in all organic molecules and thus, the preparation of labelled analogs identical to any bioactive molecule is, *a priori*, achievable. Moreover, <sup>11</sup>C is an extremely useful tool in the process of drug development for the evaluation of new chemical entities, which do not contain a fluorine atom in their structure. <sup>11</sup>C became relevant in the 80's due to the widespread installation of biomedical cyclotrons, but its use is still strongly restricted due to the above-mentioned difficulties related to the distribution of <sup>11</sup>C-labelled tracers from centralized production

centres to surrounding hospitals. This limitation might be mitigated in the future thanks to the recent and currently on-going development of small low energy cyclotrons; the lower costs associated to the installation of such cyclotrons in terms of space and shielding could shift the PET scenario from its current situation to a new state in which each centre could produce their own short-lived positron emitter labelled radiotracers under the concept of ‘dose on demand’ (Nutt, Vento et al. 2007; Pascali, Nannavecchia et al. 2011). In this way, it is of great interest to explore potential applications of non-conventional radiotracers, which might be widely available in short-term.

The purpose of this thesis is to study different neuropathological processes of neurological disorders using the PET technique with different radiotracers. The thesis is divided in two parts.

The first part of this work focuses on the implementation and *in-vivo* validation of the simultaneous dual-tracer PET imaging technique on the rat brain and its applications in the study of cerebral ischemia. In particular, in this project two biological processes were studied at the same time: cerebral blood flow and cerebral glucose metabolism using the radiotracers  $^{13}\text{N}$ -Ammonium ( $^{13}\text{N}$ - $\text{NH}_4^+$ ) and  $^{18}\text{F}$ -FDG, respectively.

The second part of this thesis focuses in a clinical study in a population with essential tremor (ET), the most commonly movement disorder. Here, through PET imaging both serotonin transporters (SERT) and central benzodiazepine receptors were studied, separately, in ET patients, using the radiotracers  $^{11}\text{C}$ -DASB and  $^{11}\text{C}$ -flumazenil ( $^{11}\text{C}$ -FMZ), respectively. This work was carried out in collaboration with Dr. Alexandre Gironell and his team at the Hospital de la Santa Creu i Sant Pau (Autonomous University of Barcelona).

---

This thesis is submitted to obtain the degree of Doctor at the Pompeu Fabra University. The research described herein was conducted under supervision of Dr. Juan Domingo Gispert in the Centre d’Imatge Molecular (CRC-CIM), Barcelona, Spain. The PhD fellowship was sponsored by the Science and Technology Foundation (Portugal), from March 2008 until June 2012.

## **Additional Information**

\* PhD Trainee at the Psychiatric Imaging Group, Medical Research Council (Hammersmith Hospital-Imperial College London), from February 2010 until November 2010, under the supervision of Dr. Oliver Howes. The project consisted on the classification of schizophrenic patients, people at risk of psychotic disorders and healthy controls, using 18F-DOPA PET imaging and an artificial neural network.

### **\* Additional Publications**

Santiago Rojas, José Raul Herance, Sergio Abad, Xavier Jiménez, Deborah Pareto, Alba Ruiz, Èlia Torrent, Francisca P Figueiras, Foteini Popota, Francisco J Fernández-Soriano, Anna M Planas, Juan D Gispert (2011) *Evaluation of hypoxic tissue dynamics with 18F-FMISO PET in a rat model of permanent cerebral ischemia*. *Molecular imaging and biology* 13 (3) 558-564.

Elseline Hoekzema, Santiago Rojas, Raúl Herance, Deborah Pareto, Sergio Abad, Xavier Jiménez, Francisca P Figueiras, Foteini Popota, Alba Ruiz, Núria Flotats, Francisco J Fernández, Milagros Rocha, Mariana Rovira, Víctor M Víctor, Juan D Gispert (2011) *In vivo molecular imaging of the GABA/benzodiazepine receptor complex in the aged rat brain*. *Neurobiology of Aging*.

Elseline Hoekzema, Santiago Rojas, Raúl Herance, Deborah Pareto, Sergio Abad, Xavier Jiménez, Francisca P Figueiras, Foteini Popota, Alba Ruiz, Núria Flotats, Francisco J Fernández, Milagros Rocha, Mariana Rovira, Víctor M Víctor, Juan D Gispert (2011) *[11C]-DASB microPET imaging in the aged rat: Frontal and meso-thalamic increases in serotonin transporter binding*. *Experimental Gerontology* 46 (12) 1020–1025.

E Hoekzema, R Herance, S Rojas, D Pareto, S Abad, X Jiménez, FP Figueiras, F Popota, A Ruiz, È Torrent, FJ Fernández-Soriano, M Rocha, M Rovira, VM Víctor, JD Gispert (2010) *The effects of aging on dopaminergic neurotransmission: a microPET study of [11C]-raclopride binding in the aged rodent brain*. *Neuroscience* 171 (4) 1283–1286.

\* Conferences

Francisca P Figueiras, Xavier Jimenez, Deborah Pareto, Vanessa Gomez, Jordi Llop, Juan D Gispert (2009) *An evaluation of simultaneous dual-tracer technique for PET static studies*. Nuclear Science Symposium Conference Record (NSS/MIC), 2009 IEEE, 3225-3229.

Francisca P Figueiras, Xavier Jimenez, Deborah Pareto, Juan D Gispert (2009) *Partial volume correction using an energy multiresolution analysis*. Nuclear Science Symposium Conference Record (NSS/MIC), 2009 IEEE, 2724-2727.

# Index

	Page
Acknowledgements.....	vii
Abstract.....	ix
Preface.....	xi
List of abbreviations.....	xvii
1. INTRODUCTION.....	1
1.1. Positron Emission Tomography.....	1
1.1.1. PET Principles.....	1
a) Basic nuclear physics and positron emission.....	1
b) Data collection and PET system architecture.....	3
c) Image Reconstruction.....	7
d) PET data correction.....	11
e) Performance of PET systems.....	14
1.1.2. PET Image Acquisition .....	15
1.1.3. PET Image Analysis.....	17
1.1.4. Tracers Kinetic Modelling.....	18
1.1.5. PET Statistical Analysis.....	21
1.1.6. Regulatory aspects of PET radiopharmaceuticals.....	24
1.1.7. A prospect of PET technology.....	27
1.2. PET in Neurology.....	29
1.2.1. Dementias.....	29
1.2.2. Movement Disorders.....	36
a) Parkinson’s Disease.....	37
b) Essential Tremor.....	40
1.2.3. Cerebrovascular Disorders.....	43
1.3. Preclinical PET Studies.....	47
1.3.1. Animal models of neurological disorders.....	50
a) Stroke.....	50
b) ET.....	56
2. SUMMARY.....	59
3. OBJECTIVES.....	61

4. RESULTS.....	63
4.1. Publication 1.....	65
4.2. Publication 2.....	79
5. DISCUSSION.....	85
6. CONCLUSION.....	93
7. REFERENCES.....	95

## List of abbreviations

2D	Two-dimensional
3D	Three-dimensional
3DRP	Three-dimensional reprojection algorithm
4D	Four-dimensional
$^{13}\text{N-NH}_4^+$	$^{13}\text{N}$ -Ammonium
$^{11}\text{C-FMZ}$	$^{11}\text{C}$ -Flumazenil
$^{11}\text{C-PIB}$	$^{11}\text{C}$ -Pittsburgh compound
$^{18}\text{F-FDG}$	2-deoxy-2- $^{18}\text{F}$ fluoro-D-glucose
AADC	Aromatic amino acid decarboxylase
AC	Anterior commissure
AD	Alzheimer's Disease
AIPES	Association of Imaging Producers & Equipment Suppliers
BP	Binding potential
CBD	Aorticobasal degeneration
CBF	Cerebral Blood Flow
cBZR	Central benzodiazepine receptor
$\text{CMR}_{\text{glc}}$	Cerebral metabolic rate of glucose consumption
$\text{CMRO}_2$	Cerebral metabolic rate of oxygen
CT	Computed Tomography
CVD	Cerebrovascular disease
DA	Dopamine
DAT	Dopamine transporter
EMA	European Medicine Agency
ET	Essential Tremor
FBP	Filtered backprojection
FDA	Food and Drug Administration
FORE	Fourier rebinning
FOV	Field of view
FTLD	Frontotemporal lobar degeneration
FWHM	Full Width at Half Maximum
GABA	$\gamma$ -aminobutyric acid
GMP	Good Manufacturing Practice
HD	Huntington's disease
LOR	Line of response
MAO-B	Monoamine B oxidase
MA	Marketing Authority

MCAO	Middle cerebral artery occlusion
MCI	Mild cognitive impairment
MLEM	Maximum-likelihood expectation maximization
MRI	Magnetic resonance imaging
MSA	Multiple system atrophy
NAT	Noradrenaline transporter
OSEM	Ordered-subsets expectation maximization
PC	Posterior commissure
PD	Parkinson's disease
PET	Positron Emission Tomography
PSP	Progressive supranuclear palsy
PVE	Partial volume effect
PVC	Partial Volume Correction
RAMLA	Row-action maximum-likelihood algorithm
rCBF	Regional cerebral blood flow
rCMRO <sub>2</sub>	Regional cerebral metabolic rate for oxygen
RD	Ring difference
rOEF	Regional oxygen extraction fraction
ROI	Region-of-interest
SDTT	Simultaneous Dual-Tracer Technique
SERT	Serotonin transporter
SPECT	Single-photon Emission Computed Tomography
SNR	Signal-to-noise ratio
SPM	Statistical Parametric Mapping
SRTM	Simplified reference tissue model
SSDT	Simultaneous dual-tracer technique
SSRB	Single-slice rebinning
SUV	Standardized Uptake Value
TSPO	Translocator protein (18 kDa)
VaD	Vascular Dementia
VMAT2	Vesicular monoamine transporter

# 1. INTRODUCTION

## 1.1. Positron Emission Tomography

Positron emission tomography (PET) is a functional imaging method that allows studying physiological, biochemical or pharmacological processes *in vivo*. PET is a non-invasive nuclear medicine imaging technique and its outcome is the generation of three-dimensional (3D) images mapping the functional activity of a given tissue. PET is being used in both research and clinical practice. In research, it has supported investigations of underlying pathophysiology of different diseases and the evaluation of new drugs. In clinical practice, it has been used for the diagnosis, planning of treatment, and prediction outcome in several diseases. It is mainly used in oncology, neurology, and cardiology. In the brain, it has been used to investigate mostly glucose metabolism, receptor binding, alterations in regional blood flow and for the detection of pathological processes such as neuroinflammation or lesions like senile plaques. Subsequently, one of its major applications has been in favor of elucidating complex neurological and psychiatric disorders.

### 1.1.1. PET Principles

#### a) Basic nuclear physics and positron emission

PET relies on nuclear physics principles and involves the introduction, usually via an intravenous injection, of a short-lived radioactive tracer into a living body. A chemical structure designed to bind to the biological molecule of interest is labelled with a positron-emitting isotope, such as  $^{11}\text{C}$ ,  $^{13}\text{N}$ ,  $^{15}\text{O}$ ,  $^{18}\text{F}$ ,  $^{68}\text{Ga}$ , or  $^{82}\text{Rb}$ . As oxygen, carbon and nitrogen are included in most organic molecules, in principle it is possible to label the majority of natural substrates chemically indistinguishable from their unlabelled counterpart. As these isotopes generally present half-lives of

several minutes, it is mandatory to generate them *in situ*. The process takes place in a device called a cyclotron, which is an accelerator that forms a particle beam for bombarding a stable precursor (Birattari, Bonardi et al. 1987). Following emission from an ion source, a charged particle, generally containing a proton or deuteron is accelerated by the electric field along a path, which is made spiral by the combination of one static and one radiofrequency electromagnetic fields. The interaction of protons with the stable precursors of elements such as oxygen, nitrogen, and carbon will convert them to a radioactive condition. This radioactive condition is largely unstable because the created isotopes possess protons in excess and is called radioisotope.

Once the radioisotope has been generated, it is automatically transferred from the cyclotron to the radiochemistry laboratory. There, the isotope is incorporated into the molecular tracer of interest by using a synthesis module. These modules are devices that can be programmed to perform all the necessary chemistry steps to attach the radioactive label to the molecule to be administered. As the total amount of radioactivity arriving from the cyclotron could pose radiological hazards to exposed operators, all these operations take place in lead-shielded 'hot' cells.

The tracer of interest is labelled with a positron-emitting isotope such as carbon-11 ( $t_{1/2} \sim 20$  min), nitrogen-13 ( $t_{1/2} \sim 10$  min), oxygen-15 ( $t_{1/2} \sim 2$  min), and fluorine-18 ( $t_{1/2} \sim 110$  min) ( $t_{1/2}$  for radioisotopes is the amount of time it takes for half of the label to decay; faster the decay, less time between isotope production and scanning is available). Following intravenous administration, the tracer is distributed throughout the body according to its biochemical properties and when the radioisotope undergoes positron emission decay, it emits a positron, an antiparticle of the electron with opposite charge. The emitted positron travels in tissue for a short distance following a random path (typically less than 1 mm), during which it loses kinetic energy, until it decelerates to a point where it can interact with an electron. The encounter annihilates both electron and positron, such that their masses are converted to energy in the form of two photons being emitted back-to-back. If these two photons are simultaneously detected by two small detectors, we can infer that the annihilation must have occurred along the line connecting the two detectors, referred to as the line of response (LOR). This technique is known as 'coincidence detection' or 'electronic collimation' in opposition to absorptive collimation used in

SPECT to determine the location and direction of the emitted photons (Figure 1).

b) Data collection and PET system architecture.

To increase the sensitivity of the scanner, the object is surrounded by a 'ring' of small detectors rather than only two. Such a ring is shown in Figure 1. To image multiple planes simultaneously, several such rings are placed surrounding a cylindrical gantry to receive the subject. The electronics of the individual detectors are linked so that the detections of two photons occurring within a certain time window (10 ns) can be registered as a coincident event, most likely arising from the same annihilation.

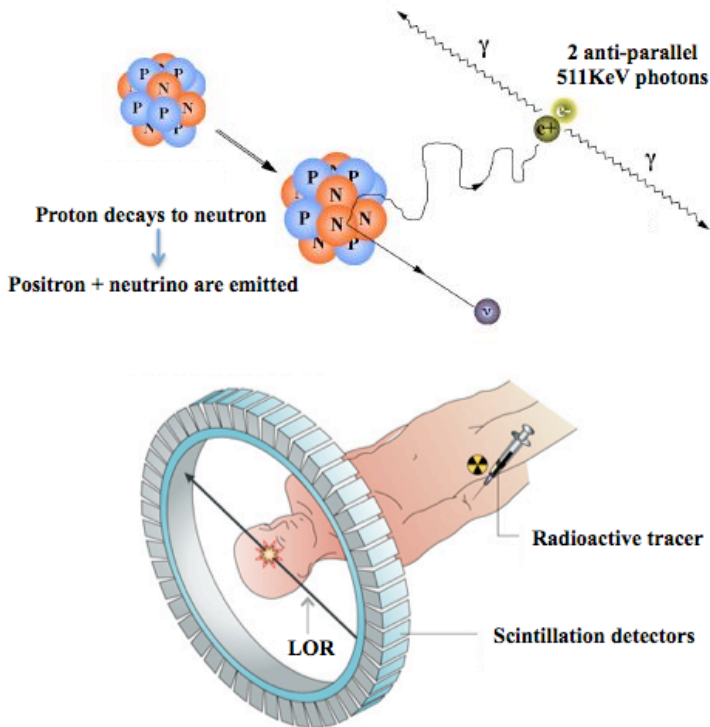


**Figure 1.** Positron emission and annihilation. LOR-Line of Response.

Each coincident event is assigned to a LOR joining the two relevant detectors (Figure 1) and it is usually histogrammed into a matrix, where each element in it corresponds to the number of events recorded by a particular pair of detectors (or along a specific LOR). The matrix is

arranged such that each row represents parallel line integrals or a projection of the activity at a particular angle, and each column represents the radial offset from the centre of the scanner gantry. This matrix is known as a sinogram because a point source at a location other than the centre of the scanner traces a sinusoidal path as given by the described geometry (Figure 2).

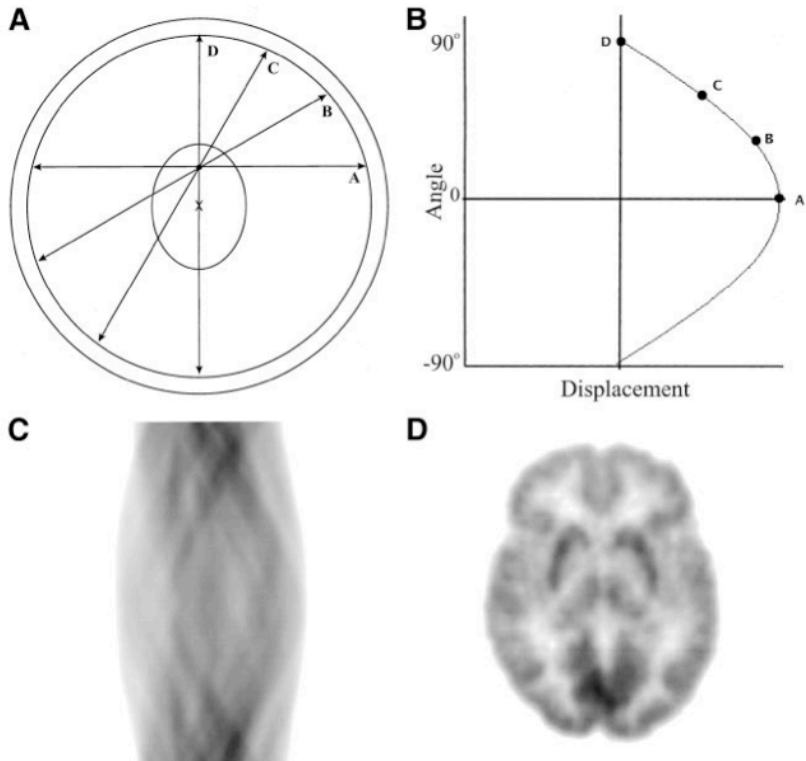


**Figure 2.** Sinogram formation. (A) Four LORs passing through locus of interest are labelled A, B, C, and D. (B) These 4 LORs are plotted on this sinogram where angular orientation is on  $y$ -axis and displacement from centre of gantry is on  $x$ -axis. If all possible LORs that pass through this point are plotted, it maps out half of sine wave turned on its side as shown here. (C) Sinograms of more complicated objects, such as sinogram of brain scan shown, are composed of many overlapping sine waves. (D) Reconstructed brain image corresponding to sinogram in (C) is shown (Fahey 2002).

In the first generation multi-ring PET scanners, coincidences were only recorded in direct and cross planes, where a direct plane is defined as coincidences between detector elements within the same detector ring and a cross plane are the coincidences recorded between detectors in two adjacent detector rings. Collecting coincidences in this way allows an improvement in axial sampling because the events collected by the cross

planes originate primarily from the volume between the planes. Thus, in a system built up of  $N$  detector rings,  $N$  direct planes and  $N-1$  cross planes can be defined, resulting in a total of  $2N-1$  coincidence planes. This mode of operation is known as two-dimensional (2D) data acquisition because the data collection is restricted to a set of almost parallel 2D planes. Note that if the scanner is exposed to a uniform source of activity, the cross planes will contain twice as many counts as a direct plane, since it combines the data from two sets of inter-plane LORs.

The sensitivity of the PET system can be further improved by defining additional coincidence plane combinations, where the ring difference extends well beyond that used in 2D data acquisition. These oblique coincidence planes are stored in separate sinograms, referred to as 'segments', with an associated azimuthal angle. This leads to  $N^2$  sinograms in a  $N$  ring PET scanner. Because the coincidence planes are no longer only limited to parallel planes, this acquisition mode is referred to as 3D data acquisition.

Even when acquiring in 3D mode, one may limit the range of allowable coincidences. The axial extent of the coincidences allowable in 3D PET is characterized by the 'maximum ring difference' (RD). Increasing the RD allowed in an acquisition results in an increase of sensitivity particularly at the centre of the gantry. Thus, this increase in absolute sensitivity comes at the expense of uniformity of axial sensitivity. The term 'span' is used to describe the extent of axial data combined. The span is the sum of the number of adjacent set of LORs combined into the same axial angle. Choosing a larger span will not result in a loss of data but a degradation of axial resolution. Once RD and span values have been chosen, the number of resulting segments (i.e. oblique sinograms) can be calculated as:  $(2RD + 1) / \text{span}$ .

In 3D mode operation, data is stored in sinograms each characterized by an average axial location and azimuthal angle or RD. Several approximate 'rebinning' methods seek to convert the collected 3D data into a set of parallel transverse sinograms so they can be reconstructed using conventional 2D methods. The simplest of these methods, often referred to as single-slice rebinning (SSRB), takes the average axial location of a detected event and places it in the sinogram that most closely corresponds to that axial average. Along the central axis of the scanner, this

approximation works fairly well. However, it steadily becomes worse with increasing radial distance. Therefore, this approach only yields reasonably acceptable images when the object being imaged takes up a small fraction of the field of view and when the axial acceptance angle (the maximum oblique angle accepted) is small. Otherwise, significant blurring of data occurs in the axial direction that becomes apparent when the data are resliced into sagittal or coronal views.

More recently, a technique known as Fourier rebinning (FORE) has been introduced (Defrise, Kinahan et al. 1997) and it is based on a principle that relates the 2D Fourier transform of the oblique sinograms to the 2D Fourier transform of the transverse sinograms. According to this method, each LOR can be characterized by four parameters: two in-plane parameters ( $s$ ,  $f$ ) and two longitudinal parameters ( $z$ ,  $d$ ) (Figure 3).  $s$  and  $f$  are the radial distance and angle, respectively, of the LOR projected onto a transverse plane.  $z$  is the midpoint of the LOR and  $d$  is the tangent of the angle the LOR makes with a transverse plane.

Any LOR can then be described as the projection  $p$ :

$$p(s, \phi, z, \delta) = \int_{-\infty}^{\infty} f(s \cos \phi - l \sin \phi, s \sin \phi + l \cos \phi, z + l\delta) dl.$$

For each  $z$  and  $d \neq 0$ , 2D data as a function of  $s$  and  $f$  is an oblique sinogram. The  $d = 0$  subset data are the in-plane sinograms. One can take a 2D Fourier transform of  $p$  with respect to  $s$  and  $f$  to get  $P(\omega, k, z, d)$ , where  $\omega$  and  $k$  are the frequency variables associated with  $s$  and  $f$ , respectively. One of the main results of (Defrise, Kinahan et al. 1997) is the approximation:

$$P(\omega, k, z, 0) \approx P[\omega, k, z + (k/\omega)\delta, \delta],$$

which suggests that one can rebin all of the oblique sinograms into in-plane sinograms. After the rebinning process, the data is in the form of a stack of in-plane 2D sinograms that can be reconstructed using any 2D algorithm. The data set is reduced in size, resulting in a very computationally efficient algorithm (Mazin and Pele 2008).

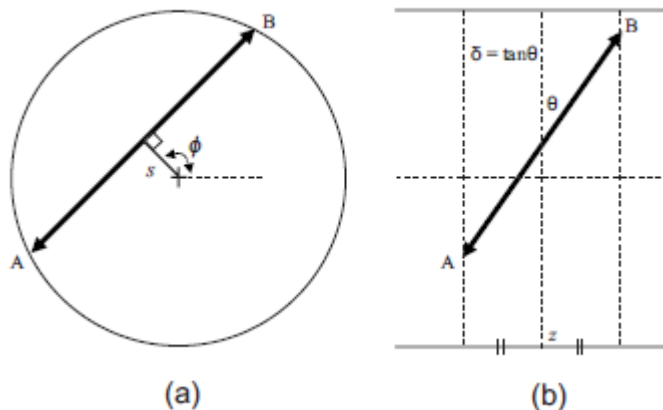


**Figure 3.** (a) Transverse view and (b) longitudinal view of a PET system. A LOR is characterized by four parameters,  $s$  and  $f$  are in-plane parameters,  $z$  and  $d$  are longitudinal parameters (Mazin and Pele 2008).

Although still an approximate method, it yields substantially better results than SSRB, even for larger objects and acceptance angles. Consequently, FORE has become the algorithm of choice for very large 3D datasets, for example from dynamic PET studies involving over 30 frames of 3D data.

### c) PET image reconstruction

The goal of image reconstruction is to provide quantitatively accurate cross-sectional images of the distribution of positron-emitting radiopharmaceuticals in the object that is being scanned, using the externally detected radiation along with the mathematical algorithms of computed tomography. There are two basic approaches to image reconstruction. One approach is analytic in nature and utilizes the mathematics of computed tomography that relates line integral measurements to the activity distribution in the object. These algorithms have a variety of names, including Fourier reconstruction and filtered backprojection (FBP). The second approach is to use iterative methods that model the data collection process in a PET scanner and attempt, in a series of successive iterations, to find the image that is most consistent with the measured data (Zeng 2001; Defrise and Gullberg 2006).

**Filtered Backprojection.** This method provides accurate estimation of 2D radiotracer distribution when projection data are noisy. The basic principles of FBP are to perform the Fourier transform of the angular projections, apply the ramp filter in the frequency domain, uniformly distribute the filtered data over the reconstructed matrix, and then antitransform (Cherry et al. 1996; Badawi et al. 1998; Bendriem et al. 1998; Townsend et al. 1993).

Conceptually, backprojection can be described as placing a value of  $p(s, \phi)$  back into an image array along the appropriate LOR, but, since the knowledge of where the values came from was lost in the projection step, a constant value is placed into all elements along the LOR. Figure 4 shows the backprojection along a fixed angle  $\phi$ .

After backprojection, the oversampling in the centre of Fourier space needs to be filtered in order to have equal sampling throughout the Fourier space. Basically, the Fourier transform of the backprojected image must be filtered with a 'cone' filter. This operation is summarized in:

$$F(u_x, u_y) = vB(u_x, u_y)$$

where  $B(u_x, u_y)$  is the 2-D Fourier transform of the backprojected image and  $F(u_x, u_y)$  is the 2-D Fourier transform of the backprojection-filtered image. The final step is the inverse Fourier transform of  $F(u_x, u_y)$  to obtain the image  $f(x, y)$ .

FBP consists on performing this filtering, before the backprojection step, in image space via the convolution of  $b(x, y)$  with  $F_2^{-1}\{v\}$ . FBP can be expressed by:

$$f(x, y) = \int_0^\pi p^F(s, \phi) d\phi$$

where the 'filtered' projection, given by

$$p^F(s, \phi) = \mathcal{F}_1^{-1} \{ |v_s| \mathcal{F}_1 \{ p(s, \phi) \} \}$$

can be regarded as pre-corrected for the oversampling of the Fourier transform of  $f(x, y)$ . The one-dimensional 'ramp' filter,  $|v_s|$ , is a section through the rotationally symmetric 2D cone filter.

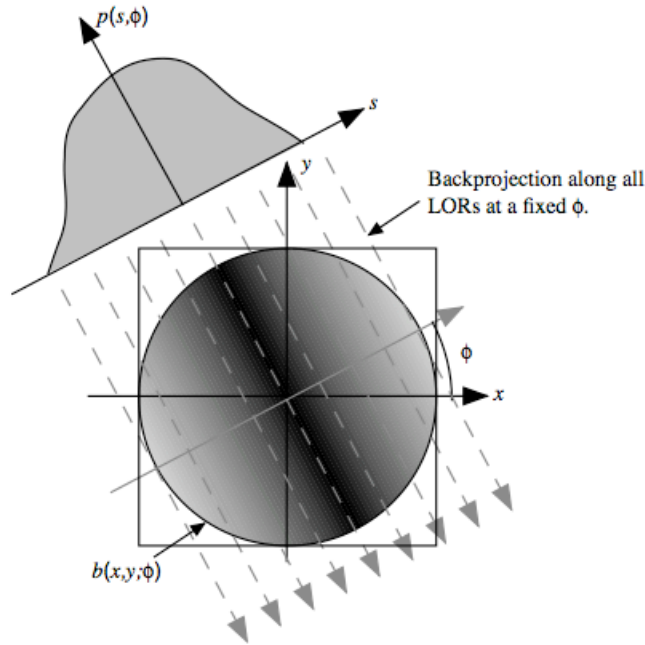


**Figure 4.** Backprojection,  $b(x, y; \phi)$ , into an image reconstruction array of all values of  $p(s, \phi)$  for a fixed angle value of  $\phi$ .

This method is simple to implement and fast in performing sections reconstruction. However, the ramp filter used to eliminate the star artefact and improve spatial resolution also amplifies the noise component, which is particularly important at low counting statistics. To compensate for these effects, low-pass smoothing filters are applied to cut-off frequencies higher than a certain limit, thereby producing more blurred images and worsening spatial resolution.

**Iterative algorithms.** Iterative algorithms are based on the attempt to maximize or minimize a target function determined by the particular algorithm used. The target is reached through repeating several analytic processes called iterations. A major advantage of this type of algorithm is the possibility of incorporating different a priori information, such as noise component, attenuation, or characteristics of detector non-uniformity, for more accurate image reconstruction; however, it must be pointed out that inclusion of additional parameters means increase in processing times.

Depending on the method, different numbers of iterations are required to reach the target function, keeping in mind that too many iterations can easily lead to noise amplification with image quality deterioration. For this reason, it is important to perform an accurate evaluation of the number of iterations needed to obtain the best image quality (Bendriem et al. 1998; Townsend et al. 1993). Different iterative algorithms are present in literature, some based on the methodologies of numeric linear algebra and others based on statistical approaches. To the latter class belongs the maximum-likelihood expectation maximization (MLEM), which is able to estimate more accurate radiotracer distribution.

The MLEM is based on the maximization of the logarithm of a Poisson-likelihood target function (Bendriem et al. 1998; Townsend et al. 1993; (Miller and Wallis 1992; Miller and Wallis 1992). The attempt is to obtain a reconstructed slice whose forward projection generates a projection dataset almost equal to the original one. The main feature of this reconstruction algorithm is to update the image during each iteration by using a multiplicative factor assessed as the ratio between the original acquired projections and the newly estimated ones. Advantages of this iterative method are very low noise amplification without loss of spatial resolution and the fact that all reconstructed values will be positive because a non-negativity condition is imposed on the original data (Bendriem et al. 1998; Townsend et al. 1993; (Miller and Wallis 1992; Miller and Wallis 1992). The main disadvantage is the large number of iterations required to converge to an optimal solution and then the long processing times, hampering its applicability in clinical routine.

To overcome the problem of slow convergence rate, the ordered-subsets expectation maximization (OSEM) algorithm was proposed in 1994, which is now the most widely used iterative reconstruction method in whole-body PET imaging (Hudson and Larkin 1994). The OSEM is a modified version of MLEM (the target is still the maximization of the log-likelihood function) with the main difference being that projections are grouped into subsets having projections uniformly distributed around the volume to be imaged. Within each iteration the target function is updated as many times as the number of subsets, proportionally accelerating convergence. An optimization of subsets and iterations number is required when the method is applied to real, noisy data, because the algorithm can

cycle without converging to the MLEM function (Hudson and Larkin 1994; Lonneux, Borbath et al. 1999; Boellaard, van Lingen et al. 2001; Riddell, Carson et al. 2001). More recently has been proposed the row-action maximum-likelihood algorithm (RAMLA), which in some extension can be considered a special case of OSEM requiring sequences of orthogonal projections and a relaxation parameter to control updating of the log-likelihood objective at each full iteration cycle (Browne and de Pierro 1996). Theoretically, these two conditions should guarantee a faster and better convergence to MLEM solution than OSEM.

**3D Image Reconstruction.** The gold standard for analytic 3D image reconstruction is the 3D reprojection algorithm (3DRP). It is based on the extension of the 2D FBP method to 3D. However, as the azimuthal projections are necessarily truncated given the geometry of the scanner, the 2D projections are used to reconstruct a first estimation of the object and, then, this estimation is used to estimate the oblique LORs that were not actually measured by the scanner. This process is known as reprojection or forward-projection and is the inverse process of back projection (Mazin and Pele 2008).

#### d) PET data corrections

A number of corrections are typically performed on PET data both before and/or during the reconstruction process. These include normalization, scatter correction, random correction, attenuation correction, dead time correction and partial volume correction (PVC).

**Attenuation Correction.** In human datasets, attenuation correction makes by far the biggest change among all corrections in the quantitative values as well as the visual appearance of the images. The sinograms used in image reconstruction in PET represent the distribution of activity in the scanned tissues, reduced by tissue attenuation. At 511KeV, a relatively high probability exists that one or both annihilation photons will be absorbed within the human body. It is therefore necessary to correct for this attenuation in order to allow true quantitative reconstruction (Phelps 1977; Phelps 2000). The tissue attenuation is measured by performing transmission and blank emission scans. A 5–10-min transmission scan is performed prior to injection of tracer to correct for tissue attenuation of gamma radiation. However, the use of PET scanners with combined CT

technology (PET/CT) significantly reduces the scanning time of attenuation. The magnitude of this correction for small animal subjects is much smaller than for humans (1.3 for a 3 cm diameter mouse versus 1.6 for a 5 cm diameter rat versus 45 for a 40 cm diameter human) (Chow, Rannou et al. 2005).

**Normalization.** Reconstruction algorithms usually rely on the assumption of an ideal scanner, that is, one for which all parts of the detector ring are uniformly sensitive to incoming photons. In real scanners, a number of factors deviate from this assumption. Normalization is a procedure that corrects the raw data to restore the conditions of an ideal scanner with uniform sensitivity prior to reconstruction. Normalization techniques can be based on the acquisition of data on the scanner, on mathematical models, or on a combination of these two methods (Defrise et al. 1991; Bailey et al. 1996; Badawi et al. 1998; Badawi et al. 1999; Badawi et al. 2000). Regardless of the technique used, normalization data do not need to be acquired for every study. However, because some factors, especially the calibration of the electronics, may drift over time, normalization should be part of quality control procedures and carried out periodically.

**Scatter Correction.** When a positron annihilates in the body, there is a reasonable chance that one or both of the annihilation photons will scatter in the body or in the detector itself. At 511 KeV, the most likely type of interaction is Compton scattering in which the photon transfers some of its energy to loosely bound electrons and deviates from its initial path (Figure 5). Since the coincidence LOR formed after one or both photons undergo Compton scattering is no longer colinear with the site of annihilation, such events degrade the PET measurement. In 3D mode the amount of scatter in the signal can become extremely large (Cherry, Dahlbom et al. 1991; Badawi, Marsden et al. 1996), and accurate scatter correction methods are required. Many schemes have been proposed for scatter correction in 3D mode. These include convolution-subtraction techniques (Bailey and Meikle 1994; Bentourkia, Msaki et al. 1995), Monte-Carlo modelling techniques (Levin et al. 1995), direct measurement techniques (Cherry, Meikle et al. 1993) and multiple energy window methods (Shao, Freifelder et al. 1994; Grootoenk, Spinks et al. 1996). The methods in widest use to date are the 'Gaussian fit' technique (Stearns 1995; Cherry and Huang 1995), and model-based scatter correction algorithms (Ollinger 1996).

**Dead time correction.** For detection systems that record discrete events, the dead time is the time after each event during which the system is not able to record another event. Since nuclear decay is a random process, there will always be a finite probability that some events will occur too close together to be distinguished even at very low average count-rates. At high count-rates such losses can become very significant. The fractional dead time of a system at a given count-rate is defined as the ratio of the measured count-rate and the count-rate that would have been obtained if the system behaved in a linear manner. This is usually one by modelling the dead-time losses as a combination of paralyzable and non-paralyzable components and obtaining parameters for the model by means of experiments involving repeated measurements of a decaying source (Casey et al 1995).

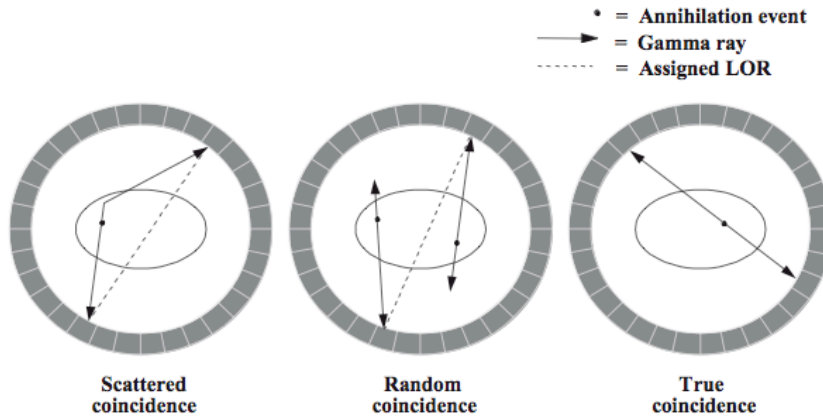


**Figure 5.** Different coincidence detections in PET imaging.

**Random Correction.** Random coincidences arise because of the finite width of the electronic time window used to detect true coincidences. This finite width allows the possibility that two uncorrelated single detection events occurring sufficiently close together in time can be mistakenly identified as a true coincidence event, arising from one annihilation. This is shown schematically in Figure 5. To obtain quantitative data in PET it is necessary to estimate and subtract the random coincidences from the measured data in each LOR to yield the sum of the true and scattered coincidences. The common implemented method for estimating the randoms rate in a particular LOR is the delayed coincidence channel method. Here timing signals from one detector are delayed by a time

significantly greater than the coincidence resolving time of the circuitry. There will therefore be no true coincidences in the delayed coincidence channel (although it is possible for an event from one true coincidence to be split from its partner and paired with an event from another), and the number of coincidences found is a good estimate of the number of random coincidences in the prompt signal. The estimate from the delayed channel may be subtracted from the prompt signal on-line, or stored as a separate sinogram for later processing (Casey and Hoffman 1986; Badawi, Miller et al. 1999).

**Partial Volume Correction.** The reconstructed image should map the radiotracer concentration with uniform accuracy and precision throughout the field of view. However, due to the partial volume effect (PVE), the bias in reconstructed pixel values may vary depending on the size of the structure being sampled and its radioactivity concentration relative to surrounding structures. The PVE may be described as follows. When the object or structure being imaged only partially occupies the sensitive volume of the PET scanner, its signal amplitude becomes diluted with signals from surrounding structures. The sensitive volume has dimensions approximately equal to twice the FWHM (Full Width at Half Maximum) resolution of the reconstructed image. For example, if a tomograph has isotropic reconstructed resolution of 6 mm FWHM, then a structure, which has any dimension less than 12 mm will have its signal diluted, and the degree of underestimation of radioactivity concentration will depend not only on its size but also on the relative concentration in surrounding structures. There are several possible approaches to correct or minimize the partial volume effect. These include methods that attempt to recover resolution losses before or during image reconstruction and methods that use side information from anatomical imaging modalities such as CT and MRI (Rousset, Ma et al. 1998; Harri, Mika et al. 2007).

#### e) Performance of PET systems

PET scanners typically present sensitivities in the pico to nanomolar range, spatial resolutions of about 4-8 mm FWHM for human devices and about 1-2 mm FWHM for small-animal systems and temporal resolution of up to several seconds. Scanners can be operated in a more sensitive 3D mode thus enabling scans of comparable quality to two-dimensional mode after administration of approximately four times less radiation. This

allows more scan repetitions to be performed. Use of 3D mode acquisition also enhances the ability to perform voxel rather than only region-based analyses. There are now several types of PET scanners operating in 3D mode that have enhanced sensitivity, improved signal-to-noise ratio and increased spatial resolution (Brix, Zaers et al. 1997; Spinks, Jones et al. 2000; Kemp, Kim et al. 2006). However, unlike other imaging techniques such as magnetic resonance imaging (MRI), a PET scan is not designed to show structural detail of organs. Instead, it yields images in reflecting radiation concentration, coded into gray or color scales for visualization purposes, to provide information about chemical activity within certain organs and tissues. This chemical activity may indicate areas of disease not detected by other scanning methods.

### 1.1.2. PET Image Acquisition

Normally, subjects in the scanner are positioned supine with their transaxial planes parallel to the line intersecting the anterior–posterior commissure line. They are made comfortable and their head position is maintained with the help of individualized foam holders. Head position, relative to the camera’s laser light, is monitored throughout the scans and is repositioned if movement is detected. PET scans can be carried out when subject is at rest, after administration of a medication challenge (Piccini, Pavese et al. 2003; de la Fuente-Fernandez, Sossi et al. 2004) or while performing certain tasks (Piccini, Lindvall et al. 2000; Goerendt, Messa et al. 2003; Sawamoto, Piccini et al. 2008). Some forms of PET studies require restrictions for the patients. For example, Parkinson’s disease (PD) patients undergoing PET scans with radioactive tracers relative to the dopamine (DA) system are commonly required to arrive for scanning in an OFF medication state after overnight withdrawal of their anti-PD medications. Also, smoking, consumption of alcohol, coffee, and other caffeinated beverages are not allowed for at least 12 h before scanning while eating and drinking are not allowed for at least 8 h before scan. Also some dietary products such as grapefruit can alter the rate of metabolization of the tracer molecules and, thus, have an impact on brain availability. PET scanning is a non-invasive procedure, but it does have safety issues involving exposure to ionizing radiation. The total dose of radiation is small, however, usually below 7 mSv for  $^{18}\text{F}$  tracer and below 3 mSv for  $^{11}\text{C}$  ones (Politis and Piccini 2012).

In animals, radionuclide tracers for Single-photon Emission Computed Tomography (SPECT) or PET imaging are typically injected via intraperitoneal or intravenous routes. Animals must be kept still during the imaging study and therefore almost all rodent PET studies involve anaesthesia. This can be a major confounding variable, particularly in brain studies (Gjedde and Rasmussen 1980). Characterization of the effects of different anaesthetics on biological systems and careful anaesthetic selection is key to minimize this difficulty (Matsumura, Mizokawa et al. 2003; Toyama, Ichise et al. 2004). In some cases, tracers that are irreversibly trapped, such as  $^{18}\text{F}$ -FDG, can be used, thus enabling distribution and uptake of the tracer to occur while the animal is conscious, followed by scanning of the anesthetized animal after uptake is complete. This approach also permits activation-stimulation type studies in awake animals. An alternative to anaesthesia is to completely restraint the animal but these methods cause enormous stress to the animal which leads to highly altered physiological conditions as stress, just as other factors in animal handling such as dietary conditions or ambient temperature, may impact cerebral PET measurements.

The PET investigation can be static or dynamic. In static recordings, the distribution of radiotracer is recorded in one time frame, and a single image for the whole investigation period is obtained. In dynamic recordings, the data is divided into a number of successive time frames, resulting in a series of images over time, resulting in a four-dimensional (4D) dataset. The 3D acquisition mode should be used to accommodate lower dosimetry and to improve the count statistics of the data. Measured attenuation correction is mandatory in human scanning but can be omitted in small-animal acquisitions, as this phenomenon is less acute in small bodies. The image should be reconstructed with the standard clinical reconstruction including all necessary corrections (such as for randoms, scatter, and attenuation). Quality control with calibration phantoms should be performed in order to assure qualitative accuracy (e.g., using the Hoffman brain phantom), and quantitative accuracy (e.g., using a uniform cylinder phantom) should be run periodically to assess scanner stability (Bartenstein, Asenbaum et al. 2002).

### 1.1.3. PET Image Analysis

PET image analysis also commonly involves the application of movement correction known as frame-by-frame realignment (Montgomery, Thielemans et al. 2006). PET data can be hard to assign to anatomical brain locations; the usual practice is to align the PET image to a MRI, in which anatomical regions are clearly defined, or available as templates. Co-registration of PET images to high resolution MRI enables the accurate anatomical localization of functional changes displayed on PET. The main techniques for co-registration of images are use of atlases (e.g. the Talairach atlas or the use of a computer based automated routine for aligning and reslicing tomographic image data using automated image registration algorithms (Woods, Cherry et al. 1992).

The Talairach atlas method relies on identification of the anterior (AC) and posterior (PC) commissures of the brain to define the AC-PC line. After the AC-PC line is identified, an origin is defined along this line. A perpendicular line is then drawn from the origin to the top of the brain. This gives longitudinal and vertical dimensions. The width of the brain is defined from the scan itself. Thus, in this coordinate system, three Cartesian axes are defined, with the edges of the brain identified to yield measurable dimensions. When comparing separate patients on PET scans, these dimensions are stretched proportionally such that the dimensions of the brain along this axis are the same lengths in all patients (Desco et al. 2001).

Automated image co-registration algorithms include computer routines for aligning and reslicing tomographic image data. A typical registration algorithm consists of four components: a correspondence basis, a transformation model, an optimization framework, and an interpolation method. Two images or two sets of images are involved in a registration algorithm; the source or moving image, and the target or reference image, are considered to be functions that assign scalar intensity values to the points in the 3D physical coordinates. The optimization framework is set up to find the appropriate parameters of the transformation model to maximize a measure of similarity based on correspondences between the source and target images. When the transformation is high-dimensional, a regularization term is also added to the optimization function to preserve the topology and smoothness of the source image. The target image is

fixed and the source image is transformed and resampled in each iteration of the registration algorithm by a fast and accurate interpolation method. The registration algorithm may be solved in a multiresolution or multiscale framework with a Gaussian filter, having a scale parameter. The termination condition is normally defined by a threshold on the variation of the optimization function (Gholipour, Kehtarnavaz et al. 2007).

The registration of the PET scans is followed by image quantification. Standardized Uptake Value (SUV) is often used in PET imaging for (semi-) quantitative analysis (Lucignani, Paganelli et al. 2004). It can be used when no arterial input function is available for kinetic modelling. The SUV is calculated either pixel-wise or over a region-of-interest (ROI) for each image of a dynamic series at time points  $t$  as the ratio of tissue radioactivity concentration (e.g. in MBq/kg=kBq/g) at time  $t$ ,  $c(t)$ , and injected dose (e.g. in MBq) at the time of injection ( $t=0$ ) divided by body weight (e.g. in kg):

$$SUV = \frac{c(t)}{\text{injected dose}(t_0) / \text{body weight}}$$

Some authors prefer to use the lean body weight (Zasadny and Wahl 1993) or the body surface area (Kim, Gupta et al. 1994) instead of the body weight. Also for  $c(t)$  either the maximum or mean value of a ROI is taken. SUVs can be affected by image noise, low image resolution and user biased ROI selection (Boellaard, Krak et al. 2004), thus it should be carefully interpreted and analysed.

#### 1.1.4. Tracers Kinetic Modelling

Obtaining precise quantitative measures of receptor concentrations in the brain *in vivo* is a challenging task. The measured binding of the ligand to the receptor will depend not only on the receptor concentration ( $B_{max}$ ), and also on the affinity of the ligand / the receptor complex, as measured by the dissociation coefficient ( $K_D$ ). The two parameters can be measured independently *in vivo* only through a complex experimental design with serial injection of tracer at two or more concentrations, including a non-tracer dose resulting in partial receptor occupancy. Generally, one carries out single PET examinations using a single tracer dose, and calculates the

so-called binding potential (BP), which is defined as the ratio of  $B_{max}$  to  $K_D$  (Innis, Cunningham et al. 2007). BP quantifies the equilibrium concentration of specific binding as a ratio to a reference concentration; the specific type of binding potential is designated according to the chosen reference tissue concentration (Innis, Cunningham et al. 2007):

- free plasma concentration (free, non-protein bound),
- concentration (not corrected for protein binding),
- non-displaceable uptake (concentration in reference region),

The general kinetic model contains one, two or more tissue compartments, as well as a plasma compartment. Compartments are mathematical abstractions that refer to the biochemical status of the tracers rather than anatomical locations. Typically, the first tissue compartment is the free ligand in blood plasma, and the second and third respectively refer to the specific and non-specific binding within the brain (i.e. after the tracer has crossed the blood-brain barrier). The unidirectional blood-brain clearance ( $K_1$ ) has units of cerebral blood flow ( $mLg^{-1}min^{-1}$ ), and the other defined processes ( $k_2, k_3, k_4, k_5, k_6$ ) are fractional rate constants ( $min^{-1}$ ) (Figure 6).

In most cases it is not possible, given the noise properties of PET recordings, to separately determine the masses occupying the three tissue compartments. Therefore, the free and non-specific compartments are often regarded as a single compartment, and only four rate constants are used to describe the biological system. Thus, the number of compartments should not be viewed strictly in biological terms, since the number of rate constants to be measured depends on what can in actual practice be separated kinetically. Thus, for example, the reference tissue may have two compartments (free and non-specific compartments), while the tracer kinetics in the high binding tissue maybe best described with only one. Here, it is important to notice that the kinetic model only represents a workable simplification of a much more complex behaviour of the tracer for quantification purposes.

Measuring the plasma input curve to the brain requires invasive arterial cannulation and labour-intensive measuring of tracer free fraction in plasma and radiolabeled metabolites along image acquisition, which often introduces noise into the measurements. In the case of humans, blood samples may be an inconvenience, but are relatively easy to obtain. On the

other hand, rats have a blood volume of just ~30 ml, of which roughly 3 ml can be safely withdrawn over a period of an hour. In mice, direct sampling becomes extremely difficult as their blood volume is of just ~1.3 ml of which 0.13 can be withdrawn. Even though several microsampling or external detection systems have been developed for rodents (Yamamoto, Imaizumi et al. 2010), they are not available widespread and investigators often rely on other solutions such as obtaining the input function from imaging the left ventricle blood pool (Fang and Muzic 2008). Still, studies that require metabolite analysis are still problematic and may require additional modelling or assumptions such that only a small number of arterial or, preferably, venous blood samples will suffice.

However, if brain region exists, demonstrably devoid of specific binding, and with similar non-specific binding as the rest of the brain, it can be used as a reference and enable non-invasive quantification using appropriate reference tissue models (Hume, Lammertsma et al. 1992). Fitting the region of interest with the reference region serving as an indirect input function, provides robust estimates for  $BP_{ND}$ ,  $k_2$  and  $R1 = K1/K1'$  (relative delivery,  $K1'$  is the rate constant of the reference tissue).

The widely used simplified reference tissue model (SRTM) (Lammertsma and Hume 1996) (Lammertsma and Hume 1996) assumes:

- that the non-displaceable distribution volume ( $V_{ND}$ ) is the same in region of interest and reference tissue is the same, i.e.  $K1'/k2' = K1/k2$
- that tracer kinetics in the target region (as well as the reference tissue) are such that it is difficult to distinguish between free and specific compartments, i.e. can be fitted satisfactorily with a one-tissue compartment model, without distinct  $k_3$  and  $k_4$  terms. The SRTM is expressed as:

$$C_T(t) = R_1 C_{ND}(t) + \left( k_2 - R_1 \frac{k_2}{1 + BP_{ND}} \right) C_{ND}(t) \otimes e^{\frac{-k_2 t}{1 + BP_{ND}}}$$

where  $t$  is time, and  $\otimes$  denotes convolution,  $C_T$  is the concentration in the target region, and  $C_{ND}$  the concentration in the reference region.

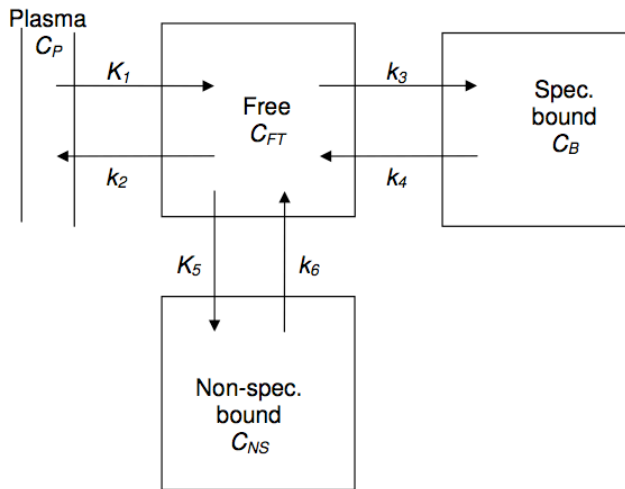


**Figure 6.** The possible compartments in a kinetic model. The rate constants  $K_1$ ,  $k_2$ ,  $k_3$ ,  $k_4$ ,  $k_5$  and  $k_6$  describe the transport of tracer between plasma and the three tissue compartments (free, specifically bound and non-specifically bound). In most applications, a maximum of only two tissue compartments can be distinguished kinetically.

The SRTM or other reference methods (Ichise, Liow et al. 2003) are very useful, as they obviate the need for labour-intensive blood sampling, and have lower levels of noise in the estimated parameters make, such that pharmacologically-evoked changes in binding potential can be more readily detected. However, the end point, i.e. binding potential relative to non-displaceable binding ( $BP_{ND}$ ) is vulnerable to changes in non-displaceable binding, the outcome parameter can change, even with the specific binding is actually unchanged (Slifstein, Parsey et al. 2000). Thus, the risk of biased estimates is higher with SRTM than with arterial input models. Figure 7 provides a schematic overview as an example of PET procedures and analysis.

### 1.1.5. PET Statistical Analysis

There are two main methods of quantitative analysis in PET studies: ROI and voxel based.

The ROI analysis method involves defining an area of interest in the brain within which to make measurements. ROIs can be drawn manually by

using appropriate software, or (semi-)automatically by ad hoc computer algorithms and brain atlases. However, either method has own drawbacks. There can be user bias in manually defining the regions of interest. Given the low resolution of PET images, the orientation plane and positions of the slices could cause significant variability in the diffusion measurements, particularly for small structures. The placement of the ROI can also have a marked effect on the results of the analysis. Outlining the ROIs according to the shape of the structure can help minimize the inclusion of other structures (Schneider, Il'yasov et al. 2004; Snook, Paulson et al. 2005) in comparison to the faster but more simplistic method of placing circles, squares, or ovals over a certain area (Shimony, McKinstry et al. 1999; Abe, Aoki et al. 2002; Suzuki, Matsuzawa et al. 2003; Yoshiura, Mihara et al. 2005). Finally, ROI analysis has the simple limitation in that it is not feasible to measure every region of the brain given time constraints, particularly for large sample sizes.

This limitation is evident in that several studies acquire whole brain data and then measure just a handful of brain regions. To overcome these limitations, there are automated morphometric approaches for the study of large datasets. Some of the challenges to developing automated methods to measure brain ROI volumes relate to anatomical variability across subjects, since it involves image co-registration, already discussed above, and the use of brain atlas or templates. The major limitation of ROI based analysis is the fact that researchers should to know a priori which specific brain regions they want to study.

The voxel-based analysis method, essentially voxel-by-voxel statistical comparisons throughout the brain, may resolve some of these issues. Typically, this method consists of the spatial normalization of each set of brain images to a template, and thus in the assignment of an 'address' to each voxel. For instance, the method of spatial normalization using the program statistical parametric mapping (SPM) (Ashburner and Friston 2000) warps the brain to account for global brain shape differences using a 12-parameter affine transformation, and then applies a non-linear step which estimates the deformations, i.e., attempts to match the internal structures of the brain to the template. Regardless of the technical particularities of the different algorithms, this approach assumes the fact that the functional analogies are established based on anatomical locations. Despite this important limitation, voxel-based analysis methods

have been widely accepted in the imaging community due to the simplicity of their use, although not without criticism (Ashburner and Friston 2000; Bookstein 2001; Davatzikos 2004)

Then, a voxel-by-voxel statistical comparison of the subject brains can be performed, with the assumption that each individual voxel represents the same anatomic location between subjects. While this method does resolve the ROI method issues of user bias as well as a priori knowledge by essentially checking every possible location of the brain, it does have some drawbacks that are not present with an ROI-based method of analysis. For example, since this method performs so many statistical comparisons, the chance of an error due to multiple comparisons is very high (Loring, Meador et al. 2002).

SPM refers to the construction and assessment of spatially extended statistical processes used to test hypotheses about functional imaging data. When two image data sets are evaluated by SPM, all voxels contained within the scans are compared in the same space on a voxel-by-voxel basis using linear constraints to test hypotheses for specific focal effects using a univariate parametric statistical test. The resulting statistics are then assembled onto an image (i.e. the statistical parametric map). Statistical differences are interpreted as regionally specific effects, attributable to some effect in brain function associated to the independent factors in the study. The statistical significance of these differences is assessed using statistical tests (usually the t or F statistic). Criteria for accepting voxels (those intended to represent true changes in regional cerebral perfusion can be set for voxel height ( $p$ ) and extent of contiguous cluster of supra-thresholded voxels ( $k$ ). For visualization of the results, a pseudo-color scale can be applied to accepted significant voxels, which are then overlaid in a semi-transparent fashion onto the MRI of either the normative atlas or the patient's own MRI anatomy. The most recent versions of SPM combines the general linear model to create the statistical map and the random field theory to make statistical inference about regional effects. Software for SPM analysis is available as Freeware from several sources, including the Wellcome Department of Imaging Neuroscience (<http://www.fil.ion.ucl.ac.uk/>). There are numerous software packages for medical image processing available such as FSL, Freesurfer, AFNI and others.

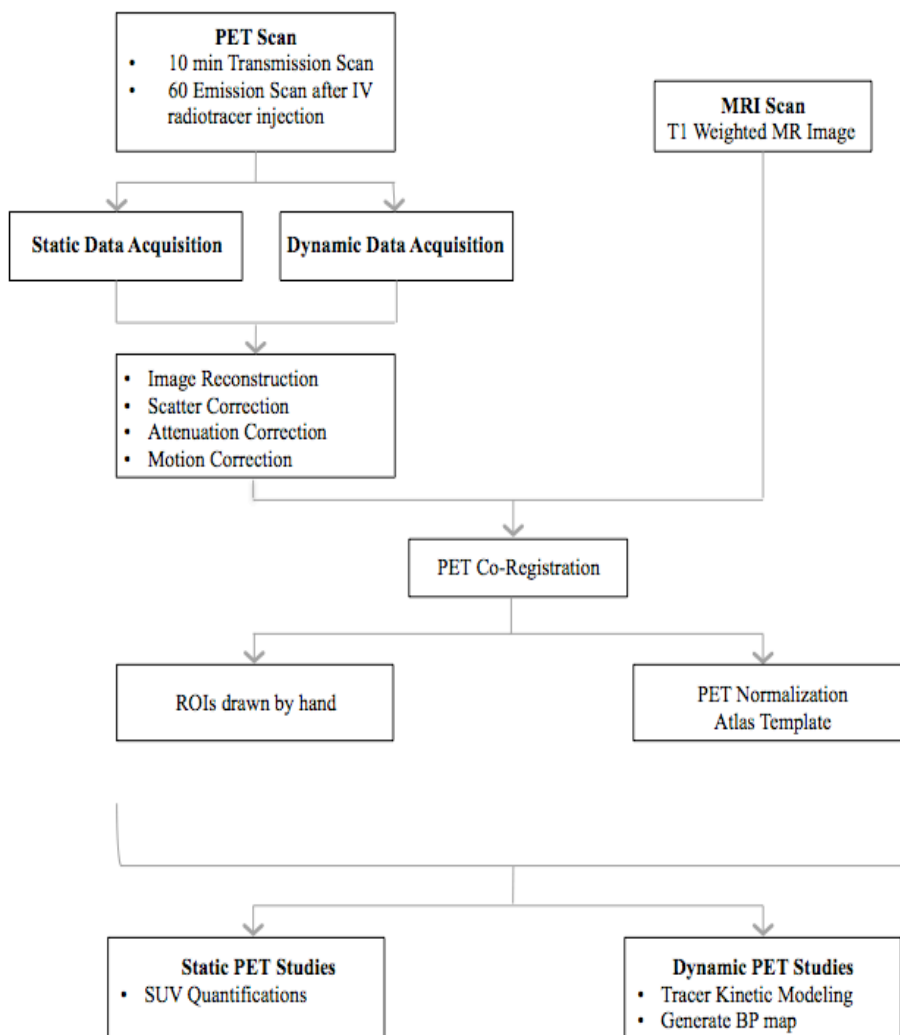


**Figure 7.** Schematic overview of PET scanning procedures and analysis. (ROI- Region of interest; SUV- Standard Uptake Value; BP- Binding Potential)

### 1.1.6. Regulatory aspects of PET radiopharmaceuticals

Radiolabeling techniques depend on the selected radionuclide, the structure of the drug to be radiolabeled, and vary accordingly in complexity; therefore the manufacturing and compounding processes are usually unique for a given radioactive drug. Successful outcomes in the use of radioactive drugs depend on their proven quality. Almost all

radioligand applications can be performed in conditions of very high specific activity so that no macroscopic effect linked to product chemical toxicity or pharmacological effect is detected in the subject. As a matter of fact they are considered medicinal products and their production and use comply with specific laws.

As a consequence, there are some regulatory limitations since PET radiotracers are considered as pharmaceuticals and consequently, they have to meet certain standards such as the strict manufacturing quality standards of conventional pharmaceuticals, i.e. the current Good Manufacturing Practices (cGMP). Radiopharmaceuticals production, unlike conventional pharmaceuticals production, is still on a relatively small scale and implementing the cGMP guidelines which are applicable for the drugs industry is both difficult and expensive. Ensuring cGMP compliance is a demanding task for a small scale manufacturer, as it involves taking care of several aspects prior to, during and after production. These include the development of well qualified personnel, use of controlled materials and procedures, availability of qualified equipment, production of the products in designated clean areas, applying validated processes and analytical methods, full documentation of the process and release of the final product by a qualified person. Application of clean room requirements in radioisotope laboratories in general and hot cells in particular, is technically demanding to be compatible with the requirements for both radiological and pharmaceutical safety.

Unlike non-radioactive medications, radioactive drugs are by their very nature unstable, i.e., contain a decaying radioactive nucleus, and their clinical use, either in diagnosis or therapy, is wholly dependent on the presence of this radioactive entity. The intrinsic instability of radioactive drugs creates a need for special quality assurance requirements. Manufacturing and all quality controls are often performed on location, immediately prior to the administration into the patient. Nonetheless radioactive drugs must be manufactured and dispensed in accordance with the basic principles of cGMP.

The dimension of nuclear medicine as compared to other diagnostics market, and the unpredictable direction of industrial strategies have led to the reduction of the number of radiopharmaceuticals and the clustering of manufacturers. PET has appeared as a lighthouse in this landscape,

bringing new impulse to research first, and gaining clinical value later on; most of the work has been done with one radiopharmaceutical, i.e. 18F-FDG, mentoring the clinicians' community and the pharmaceutical researchers around the secrets of molecular medicine. Since the Directive 89/343/EC, nothing has been really done to clarify the situation of radiopharmaceuticals. From certain point of view, things have worsened because pharmaceutical regulations have been always kept as unique code, mostly focused on conventional medicinal products, and regulators have been reluctant to adopt separate regulations for special situations such as that of radiopharmaceuticals.

To make the issue even more complicated, the role of European Medicine Agency (EMA) cannot be compared to that, for instance, of the equivalent Authority in US: FDA (Food and Drug Administration). European directives need to be adopted (implemented) by single Member States and this usually happens with the possibility of introducing changes and with different timeframes (Hartmann and Hartmann-Vareilles 2006). Although this fragmentation can be avoided for Marketing Authorisation (MA) applications, the situation is quite complex for clinical trials where researchers have to refer and apply to their national Competent Authority. The evolution of the regulations has introduced tighter rules; latest Directives have extended GMP to R&D medicinal products and non-profit and academic research. Recently, Association of Imaging Producers & Equipment Suppliers (AIPES) has made a lobbying effort to draw attention of regulators on a simplification of registration procedures for radiopharmaceuticals or, even better, on adopting a separate regulation (AIPES conference 2007).

This situation is going beyond radiopharmaceuticals and in general affects small-scale preparations used for research such as spontaneous, academic, no-profit programs that, at least in principle, should be run under full Good Clinical Practice. As a consequence of actual legislation, the investigational product(s) should be prepared under official European GMP standards and this would have an extreme impact on premises and organisation.

Serious concern on the future of this kind of research was expressed by many interested parties, mostly from Academia and Scientific Associations (Hartmann and Hartmann-Vareilles 2006). Applicable rules

to radiopharmaceuticals are still quite vague and the response to the problem remains variable from Country to Country in Europe. Some Countries (e.g. Italy) have recently issued GMP guides for hospital pharmacies and, as a separate issue, on Good Practice for radiopharmaceutical preparation in Nuclear Medicine. Some others (e.g. UK) have adopted detailed guidance on radiopharmaceuticals and radiopharmacies since a long time; some other Countries have fair or unexisting specific regulation. In this situation, the possibility to conduct multicentric clinical trials with radiopharmaceuticals is of major concern.

### 1.1.7. A prospect of PET technology

One relevant challenge in PET technology is attaching the radioactive isotope to the biological agent. Conventional chemical processes require almost 1 hour to perform this task, and with limited effective yield. There is newer technology, however, referred to as microfluidic chemistry (Lee, Sui et al. 2005), that markedly shortens the time for labelling the compounds and increases the chemical yields. Another major improvement resulting from the use of microchemistry is that it requires as much as 1,000 times less precursor. Using much smaller quantities of initial reagent potentially simplifies the quality-control process primarily to passing the final product through a separation column to meet the standard purification requirements.

With the labelling process considerably improved, the issue turns to cost effectiveness of the production of the isotope. Currently, the design of new 'microcyclotrons' is dramatically simplified as compared with the typical cyclotrons. The new self-shielded microcyclotron normally operates at 1  $\mu$ A of positive ion beam current, as compared with the 100  $\mu$ A of the PET cyclotrons. Additionally, these microcyclotrons, which are physically about one-fifth the size are designed to be integrated with the microchemistry process described above to produce a single human dose of a desired biomarker in approximately 15–20 minutes. The new microcyclotron could be designed so as to be installed with-out building modification in a 3.66 by 3.66 m room, be operated without additional personnel, and cost four to five times less than conventional accelerators. Coupled with the microchemistry labelling, the new biomarker generator could have 'kits' supplied by a manufacturer containing all required

precursors and the purification columns necessary to produce approved imaging biomarkers under the clinical Good Medical Practices guidelines enforced by the FDA. Any such 'biomarker generator' will, of course, need to undergo the FDA approval process for medical devices.

Ultimately, given the need for smaller amounts of starting reagent, a smaller and less costly cyclotron, on-site cyclotron installation requiring less radiolabeled product due to decreased transport time, and faster labelling of isotope to a biological agent could lead to a marked reduction in cost and bring this capability to the community medical setting where it can have the greatest impact.

The last remaining challenge is regulatory hurdles. Important biomarkers cannot be used to measure critical human cellular functions except under research protocol, and in many cases this can be very difficult and time-consuming in itself. Therefore, these important in vivo biomarkers are limited in use to a very small number of research programs instead of being potentially available for clinical practice. The reasonably low radiation dose to the patient and the extremely small amounts of the biomarker injected into humans are two fundamental reasons that the FDA process for approval of imaging biomarkers should differ from that for therapeutic drugs. When the FDA's regulatory processes are simplified and shortened to a point more in keeping with investigational new drug applications and the medical device approval guidelines that are in place when similar devices have been approved a very significant hurdle will be eliminated (Nutt, Vento et al. 2007).

## 1.2. PET imaging in neurological disorders

PET plays a critical role in both clinical and research applications with regard to neurological disorders (Politis and Piccini 2012). PET is useful in the initial diagnosis of patients presenting several neurological diseases and can help clinicians determine the best course of each therapy. PET studies can also be useful for studying the response to therapy. Table 1 lists some of the commonly used tracers and their specific applications.

### 1.2.1. Dementias

Dementias are a group of disorders that are expected to affect more than 100 million people by 2050 raising remarkable financial costs for healthcare (Wimo, Winblad et al. 2003). Alzheimer's Disease (AD) is the most common cause of dementia and the most common neurological disorder of the elderly. AD is characterized by the presence of amyloid plaques, neurofibrillary tangles and activated microglia and PET enables a broad range of assessments of the in vivo AD brain.

Studies using 18F-FDG PET have shown that there is a progressive reduction in glucose metabolism years in advance of clinical symptoms in patients with pathologically verified AD (Mosconi, Mistur et al. 2009) and that the decreases in cortical glucose metabolism in AD correlate with the severity of dementia (Mosconi 2005). 18F-FDG PET can be also used as a diagnostic tool in the early stages of the AD. Moreover, longitudinal 18F-FDG PET studies have been able to predict the development of mild cognitive impairment (MCI) in healthy elderly people and the development of AD in patients with MCI (Drzezga, Lautenschlager et al. 2003; Drzezga, Grimmer et al. 2005; Mosconi, Brys et al. 2007; Tartaglia, Rosen et al. 2011).

Other studies have also shown the relevance of 18F-FDG PET imaging on the differential diagnosis of dementias. Specific patterns of 18F-FDG hypometabolism are now identified in association with the most common neurodegenerative dementia (Bohnen, Djang et al. 2012) (Figure 8). Dementia with Lewy bodies (DLB) is the second most frequent type of dementia, Minoshima et al. found that the sensitivity in discriminating DLB and AD using 18F-FDG PET was greater than that with clinical

diagnostic criteria applied retrospectively to the data from medical charts (Luis, Barker et al. 1999; Minoshima, Foster et al. 2001). Frontotemporal dementia (FTD) is characterized clinically by prominent initial changes in personality and behaviour, such as apathy or disinhibition, whereas memory impairment may be less conspicuous (Neary, Snowden et al. 1998). FTD is readily identified on 18F-FDG PET scans by distinct frontal or frontotemporal metabolic impairments that typically are quite asymmetrically centred in the frontolateral cortex and the anterior pole of the temporal lobe, from where they may extend to other association areas (Friedland, Koss et al. 1993; Diehl-Schmid, Grimmer et al. 2007). Panegyres et al. reported a specificity of greater than 95% for 18F-FDG PET in the differential diagnosis of different dementias, including FTD, DLB, and primary progressive aphasia, in a prospective cohort study of 102 individuals presenting consecutively to a primary care centre for examination of suspected early-onset dementing diseases (Panegyres, Rogers et al. 2009).

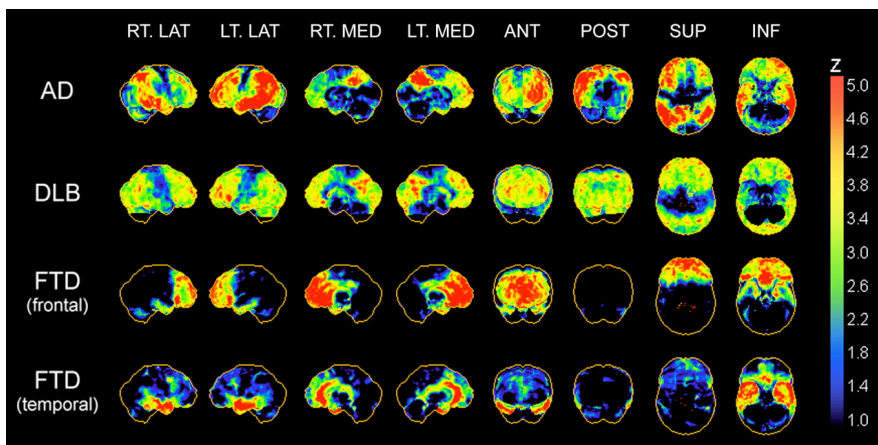


**Figure 8.** Typical regional cerebral 18F-FDG hypometabolism patterns in AD, DLB, and frontal and temporal FTD. Patterns are presented as z score maps based on significantly hypometabolic voxels relative to non-demented comparison population. AD pattern of glucose hypometabolism involves predominantly temporoparietal association cortices and posterior cingulate and precuneus cortices. In advanced disease, prefrontal association cortices show additional hypometabolism. Primary sensorimotor and visual neocortices are relatively spared. DLB has cortical hypometabolism similar to that of AD but with additional involvement of occipital cortex. FTD demonstrates frontal lobar or frontal and temporal polar cortical hypometabolism with relative sparing of parietal association cortex and preservation of primary somatomotor and visual cortices. ANT = anterior; INF = inferior; LAT = lateral; MED = medial; POST = posterior; SUP = superior (Bohnen, Djang et al. 2012).

**Table 1.** Commonly used PET radiotracers.

<b>PET tracer</b>	<b>Target</b>	<b>Assessment</b>
18F-DOPA	AADC	Monoaminergic systems (e.g., Presynaptic dopaminergic system)
11C-CFT (WIN35, 428) 18F-CFT 11C-nomifensine	DAT	Presynaptic dopaminergic system
11C-RTI32	DAT	Presynaptic dopaminergic system
	NAT	Presynaptic noradrenergic system
11C-SCH23390	VMAT2	Presynaptic dopaminergic system
11C- DTBZ	D1 receptors	Postsynaptic dopaminergic system
11C-raclopride	D2/D3 receptors	Postsynaptic dopaminergic system Dopamine release (medication challenge)
11C-DASB	SERT	Presynaptic serotonergic system
13-NH4+	rCBF	Brain metabolism
15-O2	rCMRO <sub>2</sub>	Brain metabolism
15-H2O	rCBF	Brain metabolism
18F-FDG	Relative regional CMRglc	Brain metabolism
11C-flumazenil	cBZR	GABAA/cBZR complex
11C-PK11195	TSPO	Microglial activation
11C-PIB	Fibrillar $\beta$ -amyloid	$\beta$ -amyloid plaque load
18F-Flutemetamol (GE-067) 18F-Florbetapir (AV-45) 18F-Florbetaben	Fibrillar $\beta$ -amyloid	$\beta$ -amyloid plaque load

AADC aromatic amino acid decarboxylase, cBZR central benzodiazepine receptor, CMRglc cerebral metabolic rate of glucose consumption, DAT dopamine transporter, NAT noradrenaline transporter, rCBF regional cerebral blood flow, rCMRO<sub>2</sub> regional cerebral metabolic rate for oxygen, SERT serotonin transporter, TSPO translocator protein, VMAT2 vesicular monoamine transporter 2.

Amyloid- $\beta$  plaques and hyperphosphorylated tau neurofibrillary tangles, together with associated reactive gliosis, are the neuropathological hallmarks of AD. Prior to the development of radiotracers specific for such pathological lesions, AD diagnosis could only be confirmed post-mortem or after an unacceptably hazardous and extremely invasive brain biopsy. Probably, the most representative of these pathology-specific tracers is 11C-Pittsburgh compound (11C-PIB), a sensitive and specific marker of amyloid- $\beta$  deposition. Increases in 11C-PIB cortical binding have been reported in more than 90% of patients with AD (Rabinovici and Jagust 2009) and studies have demonstrated that 11C-PIB PET uptake can be used to differentiate between AD and age-matched healthy people (Price, Klunk et al. 2005; Archer, Edison et al. 2006; Kempainen, Aalto et al. 2006; Mintun, Larossa et al. 2006).

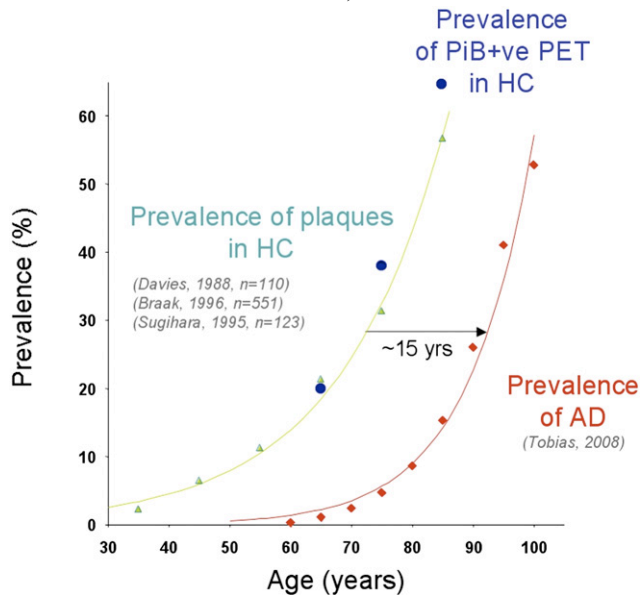


**Figure 9.** Comparison of the age prevalence of beta amyloid ( $A\beta$ ) deposition as detected at post-mortem in cognitively unimpaired subjects (green triangles), the age prevalence of AD in the general population (red diamonds), and the prevalence of high PIB binding in healthy controls (HC) from the Australian Imaging, Biomarkers and Lifestyle (AIBL) cohort (blue dots). The post-mortem and epidemiological data behave in a similar exponential fashion. PIB PET results are closely related to the post-mortem data, both suggesting that  $A\beta$  deposition precedes the diagnosis of AD by  $\approx 15$  years (Rowe, Ellis et al. 2010).

However, the frequency of increased 11C-PIB cortical binding in healthy people increases rapidly above the age of 70 (Rowe, Ellis et al. 2010) (Figure 9). 11C-PIB could be a valuable tool for the prognosis of

developing dementia (Devanand, Mikhno et al. 2010) (Figure 10). MCI patients with increased 11C-PIB uptake (PIB-positive) have a high risk of progressing to AD, whereas for MCI patients with low 11C-PIB uptake (PIB-negative) the risk is very low (Forsberg, Engler et al. 2008; Okello, Koivunen et al. 2009; Jack, Wiste et al. 2010). The degree of 11C-PIB uptake has been found to correlate with the degree of cognitive decline in non-demented elderly individuals (Villemagne, Pike et al. 2008).

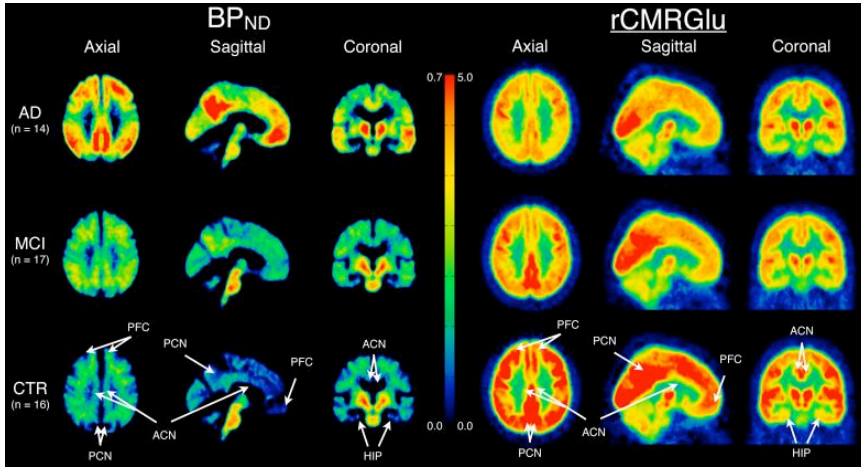


**Figure 10.** Comparison of Controls (CTR) (n=14; age  $68.5 \pm 9.4$ ), MCI (n=17; age  $69.5 \pm 9.2$ ), and AD (n=16; age  $67.9 \pm 8.1$ ), subjects' BP<sub>ND</sub> (left) and rCMRglu (right) data derived from PET 11C-PIB and 18F-FDG scans respectively. All PET data was non-linearly registered, using each individual's MRI, to the SPM5 MNI single subject MRI template using the Automated Registration Toolbox (ART). MNI space BP<sub>ND</sub> and rCMRglu maps were averaged voxel-by-voxel in the AD (first row), MCI (second row), and CTR (third row) groups. The middle color bar represents the BP<sub>ND</sub> (left side) and rCMRglu (right side) value in the images. Arrows point to regions of interest for the prefrontal cortex (PFC), precuneus (PCN), anterior cingulate (ACN), and hippocampus (HIP) (Devanand, Mikhno et al. 2010).

Recently new amyloid tracers labelled with 18F are being investigated in clinical trials. Due to the long half-life of 18F, these ligands could be widely used as a diagnostic tool. These include tracers with high-affinity binding for amyloid, similar to 11C-PIB, such as 18F-Flutemetamol (GE-067) (Koole, Lewis et al. 2009), 18F-Florbetaben (AV-1) (Rowe, Ackerman et al. 2008) and 18F-Florbetapir (AV-45) (Choi, Golding et al. 2009). This last one has received marketing authorization by the FDA on April 2012.

<sup>11</sup>C-PK11195 PET is a marker of microglial activation by specifically binding to the translocator protein 18KDa (TSPO) that is upregulated when microglia become activated. <sup>11</sup>C-PK11195 has been used to demonstrate the presence of activated microglia in vivo in AD and compared with healthy individuals. AD patients exhibit increased binding in hippocampus and temporal and parietal cortices (Cagnin, Brooks et al. 2001). In contrast, patients with MCI or mild AD demonstrate only low levels of microglial activation (Okello, Edison et al. 2009; Wiley, Lopresti et al. 2009; Carter, Scholl et al. 2012) (Figure 11). On the other hand, more conclusive results have been found using <sup>11</sup>C-DED, an irreversible inhibitor of the monoamine B oxidase (MAO-B) which can be used as an indirect marker of astrocytosis. In a study with this tracer and PIB, (Carter, Scholl et al. 2012) showed increased astrocytosis in MCI patients, particularly in PIB positive ones, as compared to healthy controls and AD patients (Figure 12).

Differential diagnosis of dementias based on multitracer studies has also been reported. <sup>11</sup>C-PIB has shown to allow differentiation between AD and other forms of dementia such as PD dementia, DLB and FTD (Drzezga, Grimmer et al. 2008; Edison, Rowe et al. 2008; Engler, Santillo et al. 2008; Maetzler, Reimold et al. 2008). <sup>18</sup>F-florbetaben PET images have shown clear differences when comparing cortical binding in controls, PD, Vascular dementia (VaD), and Frontotemporal lobar degeneration (FTLD) with MCI, DLB, or AD patients (Villemagne, Ong et al. 2011) (Figure 13). <sup>11</sup>C-DTBZ PET in conjunction with <sup>18</sup>F-FDG PET have shown some improvements on the discrimination between AD, FTD and DLB patients (Koepp, Gilman et al. 2005) (Figure 14).

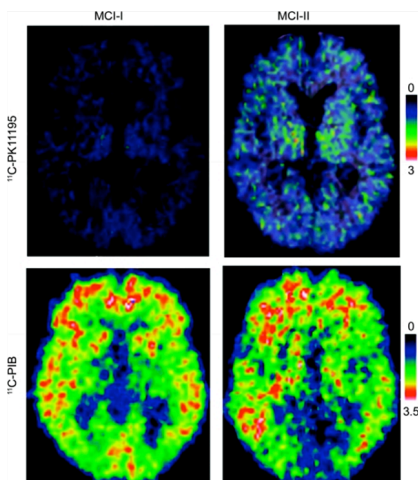


**Figure 11.** While amyloid deposition and microglial activation can be detected in vivo in around 50% of patients with MCI, these pathologies can occur independently (Okello, Edison et al. 2009)

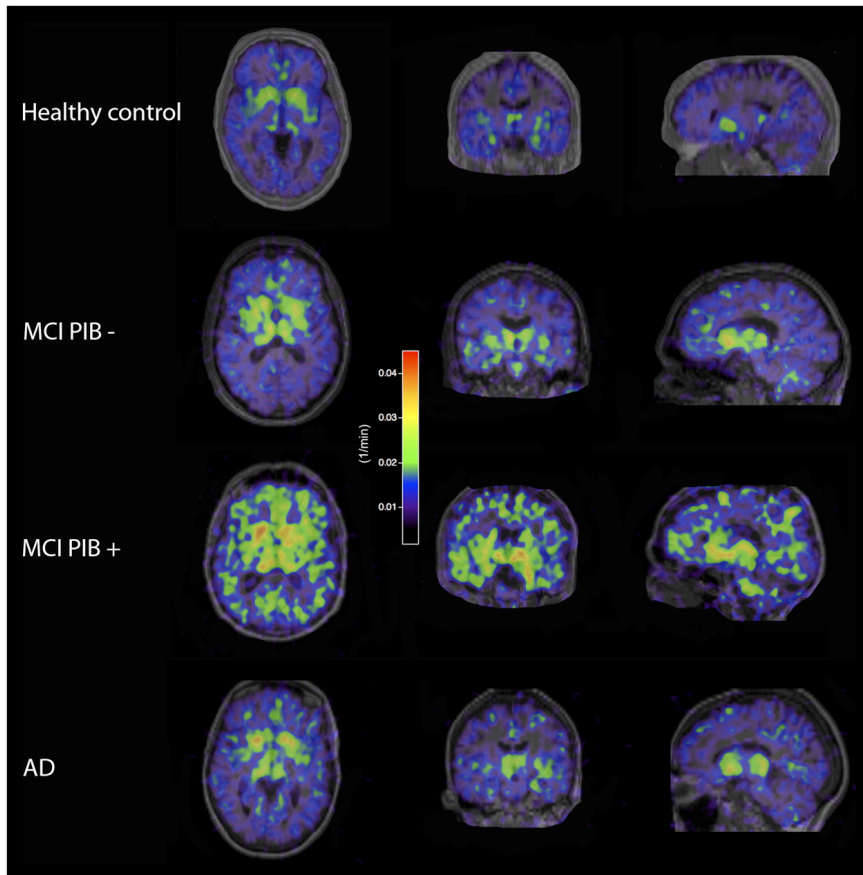


**Figure 12.** 11C-PIB images of AD and MCI patients and healthy controls (Carter, Scholl et al. 2012).

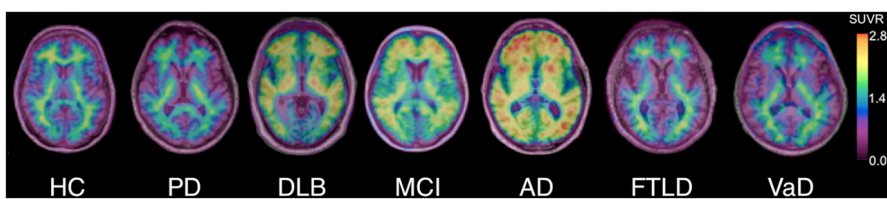


**Figure 13.** 18F-florbetaben imaging with PET. Representative 18F-florbetaben PET transaxial images overlaid on individual co-registered MR images of 68-y-old healthy control (HC), 73-y-old patient with PD, 73-y-old patient with DLB, 70-y-old subject with MCI, 80-y-old AD patient, 62-y-old patient with FTL D, and 79-y-old patient with VaD. All images are scaled to same SUVR maximum (Villemagne, Ong et al. 2011).

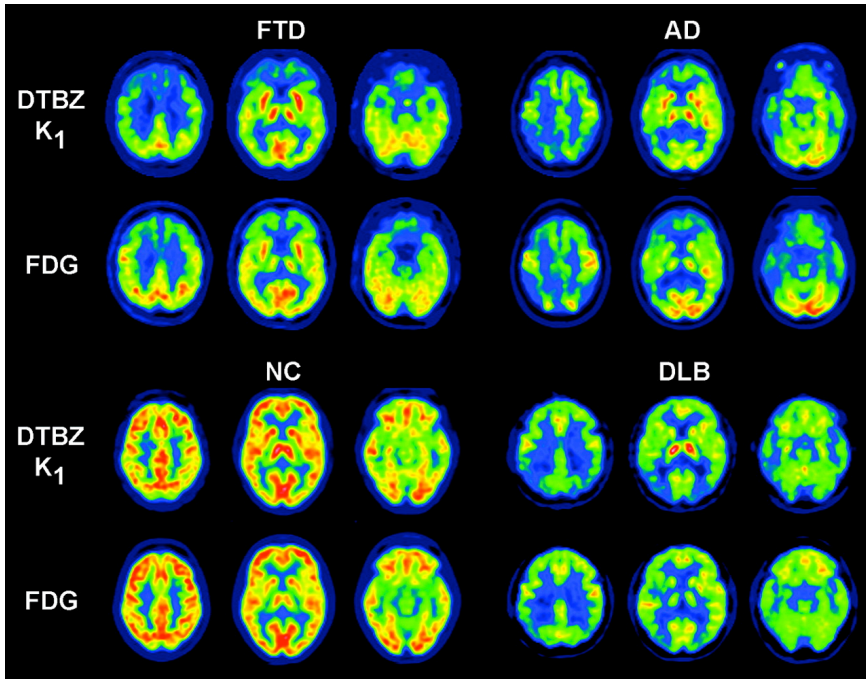


**Figure 14.**  $^{11}\text{C}$ -DTBZ  $K_1$  and  $^{18}\text{F}$ -FDG images at 3 brain levels for one representative subject from FTD, AD, DLB patients and normal controls (NC). All images are normalized to cerebellar vermis (Koeppel, Gilman et al. 2005).

### 1.2.2. Movement disorders

Imaging with PET represents a valuable clinical and research tool to visualize pathological changes in movement disorders. During the past decade, PET imaging has provided diagnostic agents as well as tools for the evaluation of novel therapeutics, and has served as a powerful means for revealing *in vivo* changes at different stages of movement disorders.

The discovery of several radiopharmaceuticals useful for assessment of movement disorders has enormously simplified the clinical management of patients. Emphasis has been placed on imaging of the dopaminergic system, as well as other neurotransmission systems, which are affected in several movement disorders. Additionally, PET imaging with  $^{18}\text{F}$ -FDG has been extensively used to assess local synaptic activity at rest and to highlight local changes in brain metabolism accompanying movement disorders (Berti, Pupi et al. 2011). Neurological movement disorders include Parkinson's disease (PD), essential tremor (ET), atypical

parkinsonism [multiple system atrophy (MSA), progressive supranuclear palsy (PSP), corticobasal degeneration (CBD)], Huntington's disease (HD), ataxia and dystonia.

#### a) Parkinson's disease

PD is the second most common neurodegenerative disorder of the elderly. The DA-ergic nigrostriatal pathway is most seriously affected in PD, while other systems such as the serotonergic are affected as well. 18F-DOPA PET has been used to assess the storage of AADC in DA terminals and therefore allow to be used as a measure of DA terminal functionality (Garnett, Firnau et al. 1983). Studies have shown that loss of striatal 18F-DOPA uptake correlates with an increase in motor disability (Vingerhoets, Schulzer et al. 1997; Broussolle, Dentresangle et al. 1999). It has been demonstrated that the decline of DA function starts in the dorsal-caudal putamen contralateral to the clinically affected side (Fearnley and Lees 1991) and that the rate of degeneration in the caudate nucleus is slower than that of the putamen in early PD (Bruck, Aalto et al. 2009). 18F-DOPA PET has also been used longitudinally and showed degeneration of the DA-ergic nigrostriatal pathway over time correlating with the progression of the disease (Hilker, Schweitzer et al. 2005; Nandhagopal, Kuramoto et al. 2009). Other markers of presynaptic DA-ergic terminal function include 11C-DTBZ labelling VMAT2 (Lee, Samii et al. 2000; de la Fuente-Fernandez, Sossi et al. 2009), also labelled with 18F (Lin, Weng et al. 2010), and 11C-nomifensine, 11C-RT132, 11C-CFT, 18F-CFT labelling DAT (Leenders, Salmon et al. 1990; Salmon, Brooks et al. 1990; Tedroff, Aquilonius et al. 1990; Frost, Rosier et al. 1993; Marie, Barre et al. 1995; Guttman, Burkholder et al. 1997).

The postsynaptic striatal DA-ergic system has been assessed with PET using 11C-SCH23390 or 11C-NNC112 for D1 receptors or 11C-raclopride, among several others, for D2/D3 receptors and it has been shown that in early PD, there is an abnormal binding of D2 but not of D1 receptors (Rinne, Laihininen et al. 1995). 11C-raclopride PET has also demonstrated evidence of D2 receptor dysfunction in the hypothalamus of PD patients, which may have relevance to the occurrence of non-motor symptoms (Politis, Piccini et al. 2008).

Differential diagnosis across the different types of parkinsonism can be

difficult by using conventional imaging such as MRI, which often do not reveal abnormalities. PET imaging in early PD cases could aid the clinical diagnosis. In PD, the most significant 18F-DOPA uptake decreases are seen in the putamen contralateral to the most affected side, while the caudate nucleus is affected later in the disease (Brooks 1993). In MSA and progressive PSP there is a symmetrical loss of 18F-DOPA uptake in the entire putamen from the beginning of the disease. In CBD, there is an asymmetric and equivalent reduction in 18F-DOPA uptake of both putamen and caudate. 18F-DOPA PET can discriminate PD from MSA in 70% of cases and from PSP in 90% of the cases (Burn, Sawle et al. 1994), however it is less effective in discriminating between the atypical parkinsonian syndromes. Moreover, Ghaemi et al. has reported in a multitracer PET imaging study, a marked decrease of putaminal volume (MRI), glucose consumption (18F-FDG), and dopamine D2 receptor binding (11C-raclopride) in patients with striatonigral variant of MSA (MSA-P). These decreases were not found in PD patients neither healthy controls (Ghaemi, Hilker et al. 2002) (Figure 15).

In addition to loss of dopaminergic neurons, damage to subcortical structures alters the functional connectivity across brain regions in a disease-specific manner. A recent meta-analysis of quantitative 18F-FDG PET studies revealed widespread cortical hypometabolism in PD (Borghammer, Chakravarty et al. 2010). Non quantitative 18F-FDG PET studies using normalization to the global gray matter activity consistently showed a pattern of relative cortical hypometabolism, particularly involving temporoparietal regions and increased metabolism in the putamen, globus pallidus, thalamus, brainstem, central cerebellum, white matter, and primary sensory-motor areas of PD patients (Eidelberg, Moeller et al. 1994; Eckert, Barnes et al. 2005). Conversely, hypermetabolism is seen in subcortical structures and is evidenced by increased neuronal firing rates in animal models of PD (Bezard, Crossman et al. 2001). However, caution is necessary because relative metabolic increases may be artifactual due to normalization of the global gray matter mean, which is reduced in PD patients, as demonstrated in several quantitative 18F-FDG PET studies (Borghammer, Cumming et al. 2009). Figure 16 shows the 18F-FDG images of four patients, each with a different movement disorder: PD, MSA, PSP, and CBD (Berti, Pupi et al. 2011).

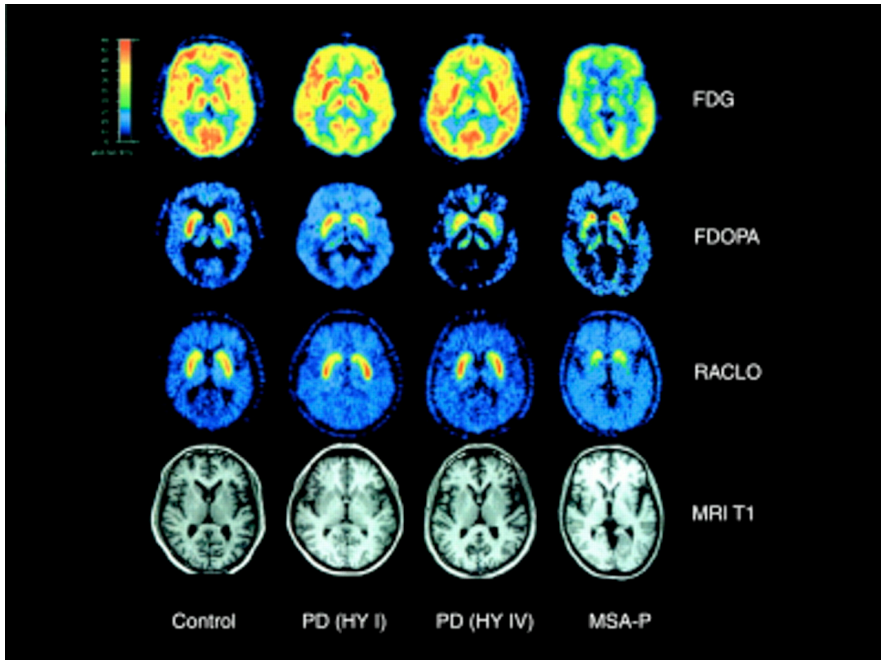


**Figure 15.** Transaxial slices of FDG-PET, FDOPA-PET, and RACLO-PET as well as T1 weighted MRI (from top to bottom) of a healthy control subject (control), two patients with idiopathic Parkinson’s disease (early stage PD HY I and advanced stage PD HY IV), and a patient with striatonigral variant of multiple system atrophy (MSA-P) (from left to right). (Ghaemi, Hilker et al. 2002).

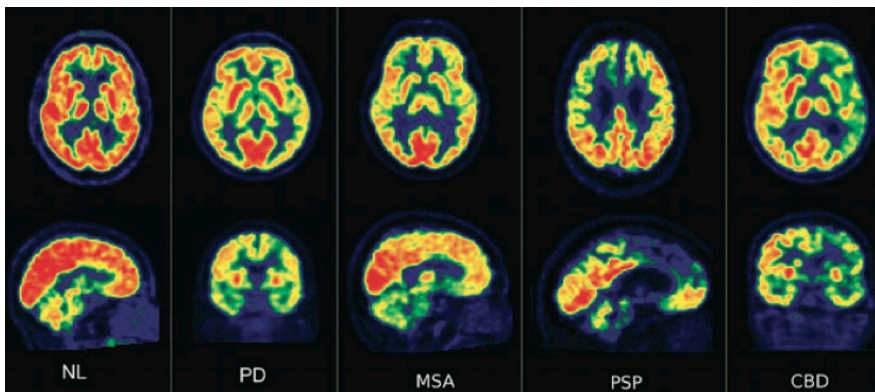


**Figure 16.** 18F-FDG PET scans of a representative cognitive normal individual (NL, left) and of four patients, each with a different movement disorder (from left to right): PD, MSA, PSP, and CBD (Berti, Pupi et al. 2011).

Non-motor symptoms represent significant PD patient complaints in both early and advanced disease (Politis, Wu et al. 2010) and the serotonergic

system is thought to modulate mood, emotion, sleep, and appetite, so changes in its function may contribute to the non-motor features commonly associated with PD (Fox, Chuang et al. 2009). 11C-DASB PET, a marker of serotonin transporter availability has been used in PD to provide a staging of presynaptic serotonergic terminal dysfunction (Politis, Wu et al. 2010). The results of this study indicated a widespread decrease of presynaptic serotonergic terminal function in striatal, brainstem, and cortical regions in PD patients with early, established, and advanced disease that does not correlate with the duration of the disease, the locomotor disability or medication intake (Politis, Wu et al. 2010). Further studies using 11C-DASB PET have shown correlations between SERT dysfunctions and depressive symptomatology (Politis, Wu et al. 2010) and abnormal changes in body mass index (Politis, Loane et al. 2011). Moreover, 11C-raclopride PET studies in PD patients with impulsive–compulsive behaviours has shown increased DA release in ventral striatum following reward-related cue exposure compared to neutral cue exposure following a challenge with l-DOPA, suggesting a sensitization to appetitive behaviours with DA-ergic therapy in vulnerable individuals (O'Sullivan, Wu et al. 2011).

#### b) Essential tremor

ET is the most common movement disorder, characterized by postural and kinetic tremors that most frequently occur in hands, arms, head, and neck. Tremor may occur at the beginning of, or during, voluntary movements (initial or kinetic tremor) or at the end of the movement (intentional tremor) (Jankovic 2002). Recent data have challenged the traditional view of essential tremor's being a monosymptomatic disorder: although postural and kinetic tremors are still considered as the core symptomatology of essential tremor, other symptoms (e.g., cognitive deficits, psychiatric abnormalities, and ataxia) are increasingly recognized, and they increase the clinical diversity of essential tremor (Louis 2009). Although the clinical course of essential tremor is usually slowly progressive over decades, advanced disease stages can be physically and socially highly disabling and warrant effective treatment.

Imaging studies show that the nigrostriatal dopaminergic system is relatively preserved in ET (Berti, Pupi et al. 2011). Two multicenter studies using SPECT with DAT tracers demonstrated DAT reductions in

parkinsonism but not in ET, reflecting a preserved dopaminergic system integrity in the latter condition (Benamer, Patterson et al. 2000). However, several ET patients with initial postural tremor develop resting tremor and accompanying dysfunction of the dopaminergic system. An 18F-DOPA PET study reported a 50% reduction of tracer uptake in the striatum of nine out of 11 patients with resting tremor, compared to only two out of 12 patients with postural tremor in parkinsonism (Brooks, Playford et al. 1992).

Activation studies with PET indicate abnormally increased regional cerebral blood flow in the cerebellum both at rest and when tremor is provoked by unilateral arm extension (Colebatch, Findley et al. 1990; Wills, Jenkins et al. 1994; Boecker, Wills et al. 1996; Boecker and Brooks 1998). This bilateral cerebellar overactivity distinguishes essential-tremor patients from healthy volunteers, in whom mimicking of unilateral tremor or passive unilateral wrist oscillation by an experimenter causes predominantly ipsilateral cerebellar activation (Boecker, Wills et al. 1996; Boecker and Brooks 1998) (Figure 17). Cerebellar involvement in essential tremor is also supported by work with MRI, including spectroscopy (Louis, Shungu et al. 2004), voxel-based morphometry (Daniels, Peller et al. 2006), and functional MRI (Bucher, Seelos et al. 1997).

ET is also associated with reduced GABAergic function and increased availability of benzodiazepine receptor sites in brain regions implicated specifically in tremor genesis. This finding is thought to reflect overactivity of cerebellothalamic circuits and, hence, lends support to the ‘GABA hypothesis’ of ET (Boecker, Weindl et al. 2010) (Figure 18).

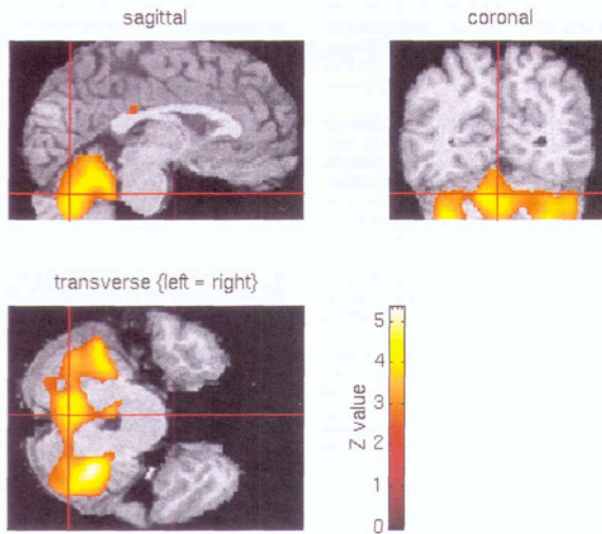


**Figure 17.** Characteristic pattern of bilateral cerebellar activation induced by postural tremor of the extended right arm compared with rest. Group (n=6 patients with classic ET) SPM of H<sub>2</sub><sup>15</sup>O PET data superimposed on standard MRI;  $p < 0.001$  (Boecker and Brooks 1998).

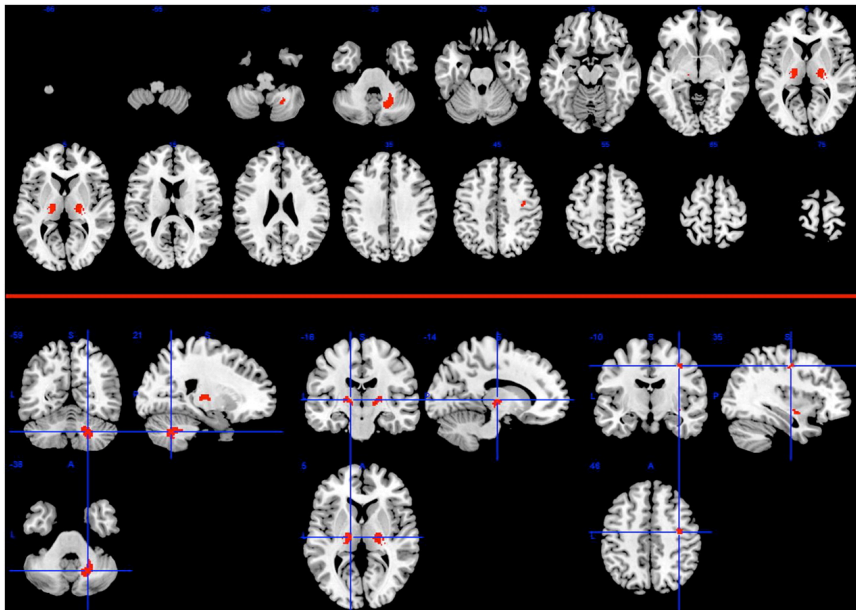


**Figure 18.** SPM analysis of changes in 11C-FMZ binding in essential-tremor group. Regions of abnormally increased 11C-FMZ binding in patients, compared with healthy controls, are seen in ventrolateral thalamus, dentate nucleus, and premotor cortex ( $P < 0.05$ : extended region-of-interest analysis; family wise error-corrected; extent threshold,  $k > 10$ ). Changes in 11C-FMZ binding are most prominent in subcortical regions (Boecker, Weindl et al. 2010).

### 1.2.3. Cerebrovascular Diseases

Cerebrovascular disease (CVD) includes all disorders in which an area of the brain is transiently or permanently affected by ischemia or bleeding and where one or more of the cerebral blood vessels are involved in the pathological process. Stroke is often associated with a poor outcome, however, in part because of the lack of understanding of the mechanisms that underlie stroke and the process by which recovery may take place. PET imaging has been of great benefit in advancing the understanding of the pathophysiology of cerebrovascular disorders (Newberg and Alavi 2005). Further, PET imaging has been useful in evaluating the extent of the functional damage, because areas not immediately affected by the infarct may show hypometabolism or decreased blood flow. Initial stroke severity has been shown to correlate with the initially affected volume as determined by PET, whereas neurologic deterioration during the first week after stroke correlates with the proportion of the initially affected volume that infarcted, and functional outcome correlates with the final infarct volume (Read, Hirano et al. 2000).

In patients who have suffered a stroke, there is a characteristic uncoupling between cerebral blood flow (CBF) and metabolism in the infarcted area (Kuhl, Phelps et al. 1980; Lenzi, Frackowiak et al. 1982). Several studies using  $^{15}\text{O}$ -H $_2\text{O}$  have described “misery perfusion” in and near areas of infarct within the first hours to days after a stroke. This misery perfusion is described as a relative decrease in regional CBF compared with the regional glucose or oxygen metabolism. Further studies have shown that there is a marked increase in the regional oxygen extraction fraction (rOEF) in response to the diminished blood flow (Wise, Bernardi et al. 1983; Baron, Rougemont et al. 1984).

Approximately 1 week after infarct ‘luxury perfusion’ occurs, which is a relative increase of rCBF compared with cerebral metabolism (Lassen 1966). Wise et al (Wise, Bernardi et al. 1983) found that rCBF increased compared with rCMRO $_2$  over several days post-infarct. Further, there was a subsequent decrease in the rOEF in the infarcted area 18 hours to 7 days after the infarct. This is believed to reflect mitochondrial dysfunction and energy failure of the damaged tissue. In addition to the infarcted area, there exists a penumbral zone, a hypometabolic and presumably ischemic area that surrounds the infarct core. This area also has increased rOEF suggesting that this area has decreased perfusion relative to the necessary

oxygen requirements. If blood flow to this ischemic area is restored before irreversible damage occurs, then the tissue will likely recover and resume normal function (Baron, Bousser et al. 1981; Heiss 2000) (Figure 19).

There have been several studies correlating the functional recovery in patients with stroke to functional changes on PET scans (Heiss, Kessler et al. 1993). Cerebral metabolic rates of glucose measured early after stroke have shown that receptive language disorders best correlate with metabolism in the left superior temporal cortex, and word fluency best correlates with metabolism in the left prefrontal cortex (Karbe, Kessler et al. 1995). A PET study of patients with left inferior frontal gyrus strokes and resulting aphasia demonstrated a stronger-than-normal response in the homologous right inferior frontal gyrus (Rosen, Petersen et al. 2000). Although the level of activation in the right inferior frontal gyrus did not correlate with verbal performance, increased activity in the perilesional area occurred in the two patients who gave the best performance in certain verbal tasks and who also showed the most complete recovery from aphasia. Similar results were described in several other studies of patients with aphasia secondary to stroke that demonstrated increased right temporal lobe activity as a mechanism to compensate for the impaired left hemispheric function (Ohyama, Senda et al. 1996; Karbe, Thiel et al. 1998). The best degree of speech restoration, however, has been found in those patients with at least some preservation of activity in the left temporal lobe that can ultimately be incorporated into the functional language network (Heiss, Kessler et al. 1999; Warburton, Price et al. 1999). Another study measuring CBF associated with passive elbow movement showed that hemiplegic stroke initially activated the bilateral inferior parietal cortex, contralateral sensori-motor cortex, and ipsilateral dorsolateral prefrontal cortex, supplementary motor area, and cingulate cortex, but later included activation of the ipsilateral premotor area (Nelles, Spiekramann et al. 1999). These results suggested that recovery from hemiplegia is accompanied by changes of brain activation in sensory and motor systems.

PET studies have also been used to monitor the success of various treatment regimens. PET has been used to evaluate the effects of thrombolytic therapy in acute stroke and has found that critically hypoperfused tissue can be preserved by early reperfusion and that large infarcts can be prevented by early reperfusion to misperfused but

viable tissue (Heiss, Grond et al. 1998). Imaging of benzodiazepine receptors by FMZ PET has been found to distinguish between irreversibly damaged and viable penumbra tissue early after acute stroke (Heiss, Grond et al. 1998) (Figure 20). Hakim et al (Hakim, Evans et al. 1989) found that stroke patients treated with nimodipine had a greater increase in the rCBF in the ischemia core (7 days after the infarct) than did patients receiving placebo. There was also an increase in rCBF in the penumbral zone in the nimodipine group compared with the placebo group (but these results were not statistically significant). Another study using  $^{18}\text{F}$ -FDG PET found that patients on nimodipine had greater increases in glucose metabolism in the affected areas compared with controls (Heiss, Holthoff et al. 1990).

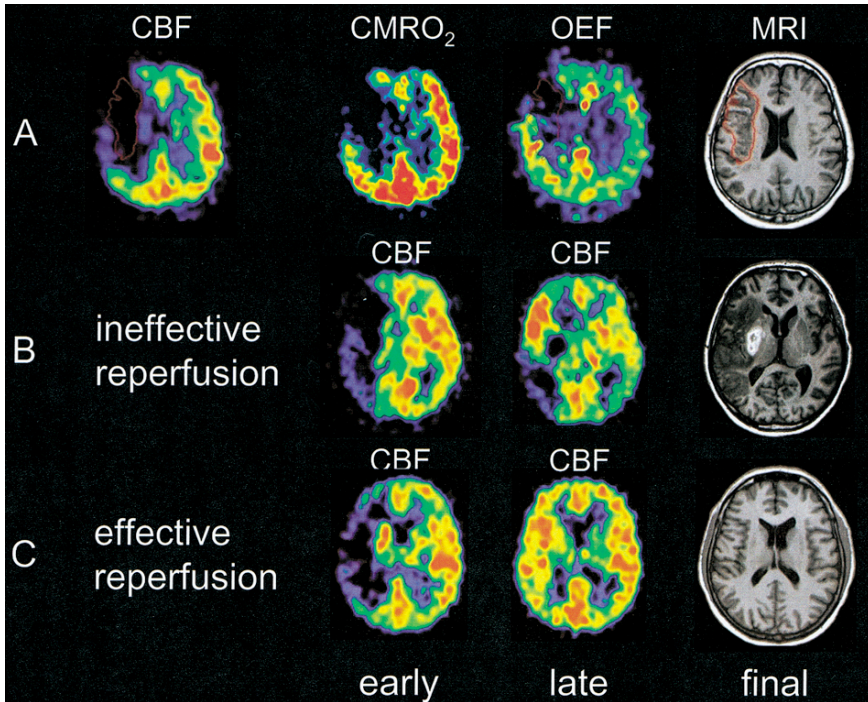


**Figure 19.** Ischemic stroke in MCA territory. **(A)** Low flow area with irreversible damage on final MRI predicted by low oxygen consumption and decreased OEF. Penumbra tissue outside the final infarct is characterized by preserved oxygen consumption and increased OEF. **(B)** Reperfusion is not effective if tissue is already damaged. **(C)** Effective reperfusion to viable (penumbra) tissue (Heiss 2000).

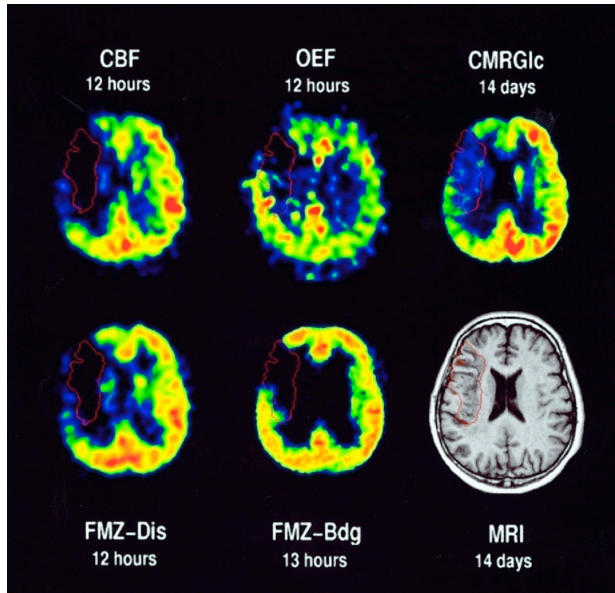


**Figure 20.** Co-registered transaxial PET images at the caudate/ventricular level of CBF, early FMZ distribution (Dis) and steady state FMZ binding (Bdg), and OEF at 12 hours and  $CMR_{glc}$  and MRI at 2 weeks after moderate left hemiparesis and hemihypesthesia of acute onset in a 52-year-old male patient. The large territorial defect is visible in all PET modalities with different extensions. The contour delineates the cortical infarct as determined on late MRI. FMZ binding precisely predicts the extension of the final infarct, whereas CBF and FMZ distribution (as a marker of perfusion) delineate a considerably larger volume of disturbed perfusion. In the cortical region outside the infarct with initially disturbed perfusion, OEF is increased, indicating preserved  $CMRO_2$  at 12 hours after ictus. The permanently decreased  $CMR_{glc}$  in this region could be caused by neuronal loss and/or diaschisis (Heiss, Grond et al. 1998).

### 1.3. Preclinical PET Studies

The exponential advances in the biological inquiry in the recent years, focused in the molecular bases of the functions of the systems of the body (e.g. cells, agencies and entire organism) along with the successful use of PET imaging in humans, has increased the demand for the instrumentation for molecular imaging of small laboratory animals.

Small animal experiments (generally rodents) constitute an integral part of biomedical and pharmacological research. Because of their genetic and resemblance with humans and the feasibility of gene transfer or modification, many different genetically modified small animal models have been developed to study the mechanism of human diseases.

During the past few years, dedicated small animal PET scanners with enhanced spatial resolution were developed to overcome the limitation of using human PET scanners with small species. The first dedicated small animal scanner RATPET was introduced in 1995. Since then, the development of small animal PET has become a promising area for technological innovation. To date, the spatial resolution has exceeded the 1 mm value.

Small animal PET imaging, namely in mice, rats, or small nonhuman primates, offers the added benefit that the animals can be their own control, reducing the inter-animal variability, and enabling repeated studies on the same animal. It is particularly useful for testing hypotheses during the study of diseases and the development of new imaging and therapeutic drugs. It is thus not surprising that small animal PET now provides the best tool for the accurate measurement of the pharmacokinetics of imaging agents *in vivo*.

A mouse is more than three orders of magnitude smaller than a human based on body weight (70 Kg for a human and 20 to 30 g for a mouse). Because of this, an animal PET system must have very high spatial resolution and sensitivity to achieve the same level of details and accuracy currently achievable in human PET studies (Jagoda, Vaquero et al. 2004). Current human clinical PET scanners have a typical image resolution

ranging from 4 to 10 mm FWHM and an absolute sensitivity of 0.5% to 5%, depending on the mode of operation (2D versus 3D). To improve the volumetric resolution of human PET systems by three orders of magnitude, the image resolution of animal PET systems needs to be reduced to 1 mm FWHM or less in each of the three dimensions.

Imaging techniques based on radionuclide decay rely on photon counting for signal detection. Photon counting is a stochastic process that follows Poisson statistics. With Poisson statistics, the variance equals the mean, thus the signal-to-noise ratio (SNR) of photon counting measurement is proportional to the square root of the number of counts detected. When the image resolution of a PET system is improved, the volume of each image voxel is reduced accordingly. If the radiotracer concentration remains the same, the number of coincidence events originating from each image voxel is reduced proportionally. So, to improve the counting statistics of an animal study, one may increase the radio-tracer concentration, extend the scan duration, or improve the sensitivity of the PET scanner itself. Extending the acquisition time is feasible only for a static imaging protocol where the process under observation is assumed to have reached a steady state prior to the scan. However, in many animal experiments, the objective is to measure the dynamics of a specific biological process. To provide adequate temporal resolution of the measurements, the number of counts collected per unit time is more critical than the total number of counts collected. Ideally, to accomplish this, one would like to improve the sensitivity of an animal PET scanner to a value much higher than that of a human PET system.

Whole-body human PET scanners detect on the order of 0.3 to 0.6% of the coincident annihilation photons in 2D mode and 2 to 5% in 3D acquisition mode (Cherry 2003; Bailey 2003; Bailey 2005). Based on the same argument of scale presented for spatial resolution and to preserve the number of counts per resolution element, the sensitivity for mouse imaging would need to improve by a factor of 1000 relative to human imaging, which is clearly not possible. Even with perfectly efficient detectors and complete solid angle coverage around the animal, the best that can be achieved is about a 200-fold increase in 2D mode and a 30-fold increase in 3D mode. Although this relative reduction in sensitivity from mouse to human can partly be solved by injecting larger amounts of radioactivity. Another approach to compensate for the sensitivity problem

is to use more sophisticated reconstruction algorithms that make better use of the available counts. Iterative statistical algorithms that accurately model the physics of the scanner and the statistics of the raw data will probably play an important role in very high resolution PET studies because they can produce improvements in either resolution or SNR relative to analytic reconstruction algorithms.

The amount of activity that can be administered during a small animal imaging study is limited by the mass effect coupled to the specific activity of the radiochemical (the ratio of labelled to unlabelled chemical in the injection), by the total volume that can be injected into a mouse, by the radiotoxicity effects of the radiotracer, and by the maximum counting rate capability of a PET system. A fundamental requirement of imaging is to not disturb the biological systems under observation either through pharmacological effects or radiation dose to tissues. In receptor studies in small animals the mass effect is quite often the limiting factor for radioactivity dose administration. When too much radioligand is administered, in such a situation that the compound affects the system, it can no longer be considered a tracer (Hume et al., 1998). Thus, higher tracer specific activity corresponds higher allowable radioactivity dose, since less 'cold' compound is co-administered, and consequently the statistically better the images. A typical animal PET imaging protocol administers 7.4 MBq (200  $\mu$ Ci) radiotracer into a 20 g mouse, and a typical clinical PET study administers 370 to 555 MBq (10 to 15 mCi) into a 70 Kg patient. What appears to be a small amount of radiotracer in an animal experiment can result in a radiotracer concentration 40 to 70 times higher than that of a typical human study.

As discussed before in section 1.1.2, the animal must be kept still during the imaging study and therefore almost all animal PET studies involve anaesthesia. Schulz et al. (Schulz and Vaska 2011) developed a method for imaging awake, behaving rats with PET that allows the simultaneous study of behavior. Key components include the 'rat conscious animal PET' or RatCAP, a miniature portable PET scanner that is mounted on the rat's head, a mobility system that allows considerable freedom of movement, radiotracer administration techniques and methods for quantifying behavior and correlating the two data sets. The simultaneity of the PET and behavioral data provides a multidimensional tool for studying the functions of different brain regions and their molecular constituents.

### 1.3.1. Animal models of neurological disorders

PET studies in animal models of neurological conditions have focused primarily on diseases for which PET has proved useful within the clinic. Progressive neurodegenerative diseases such as AD, PD and HD, as well as other neurological conditions encompassing neurodegenerative mechanisms including stroke, epilepsy and traumatic brain injury have used PET to study aspects of disease pathogenesis, progression and prognosis and treatment (Virdee, Cumming et al. 2012). In this chapter, only stroke and ET animal models will be described in detail.

#### a) Stroke

Ischemic stroke is one of the leading causes of death and disability in developed countries. As such, considerable efforts have been made to develop animal models of stroke. There are, however, considerable inter-species and inter-model differences in vulnerability for infarct (Howells, Porritt et al. 2010). While reversible global ischemia is a useful model for resuscitation after cardiac arrest, focal ischemia has more general clinical relevance. Focal ischemia can be obtained with embolization or by targeted infusion of the vasoconstrictive peptide endothelin-1. Middle cerebral artery occlusion (MCAO) can be obtained without craniotomy through intravascular insertion of a filament, or by ligation after exposure of the cortical surface. MCAO models emulate the most common site of clinically relevant strokes and can furthermore be reversible so that the effects of reperfusion injury can be followed. Cortical infarcts arising in spontaneously hypertensive rats, while of variable location, are considerably more invariant in volume than are infarcts in the MCAO model (Howells, Porritt et al. 2010). PET studies in animal models of stroke have investigated metabolic and cellular responses to ischemia and their relationship to histological and functional outcomes.

Energy metabolism in post-ischemic rat brain has been monitored in a number of studies with <sup>18</sup>F-FDG and other predictors of tissue viability. In a semi-quantitative study, cerebral <sup>18</sup>F-FDG uptake correlated with neurological impairment scores during recovery from MCAO (Fu, Chang et al. 2009). However, reduced <sup>18</sup>F-FDG uptake at 2 h after reperfusion in the reversible rat MCAO model preceded any measurable change in mitochondrial activity measured *ex vivo* and did not entirely predict the

ultimate extent of the infarct (Figure 21) (Martin, Rojas et al. 2009).  $^{18}\text{F}$ -FDG uptake was also enhanced in the peri-infarct area 7 days after MCAO, presumably indicating microglial activation. In contrast,  $^{11}\text{C}$ -FMZ PET indicated only neuronal damage, thus suggesting that  $^{18}\text{F}$ -FDG might not be an appropriate ligand for detecting ischemic neuronal damage in the acute to subacute phase (Fukumoto, Hosoya et al. 2011).

$^{18}\text{F}$ -FMZ PET has been used to monitor the viability of cerebral cortex following MCAO with and without reperfusion in rats (Fukumoto, Hosoya et al. 2011; Rojas, Martin et al. 2011) (Figure 22). Rojas et al. demonstrated that *in vivo*  $^{11}\text{C}$ -FMZ binding is preserved up to 24 h following ischemia/reperfusion in spite of extensive neuronal death, suggesting that GABA-A receptor binding is maintained under certain conditions in the rat brain.  $^{11}\text{C}$ -FMZ binding was significantly depressed in the ipsilateral cortex at 24 h following permanent ischemia (Rojas, Martin et al. 2011) (Figure 23).

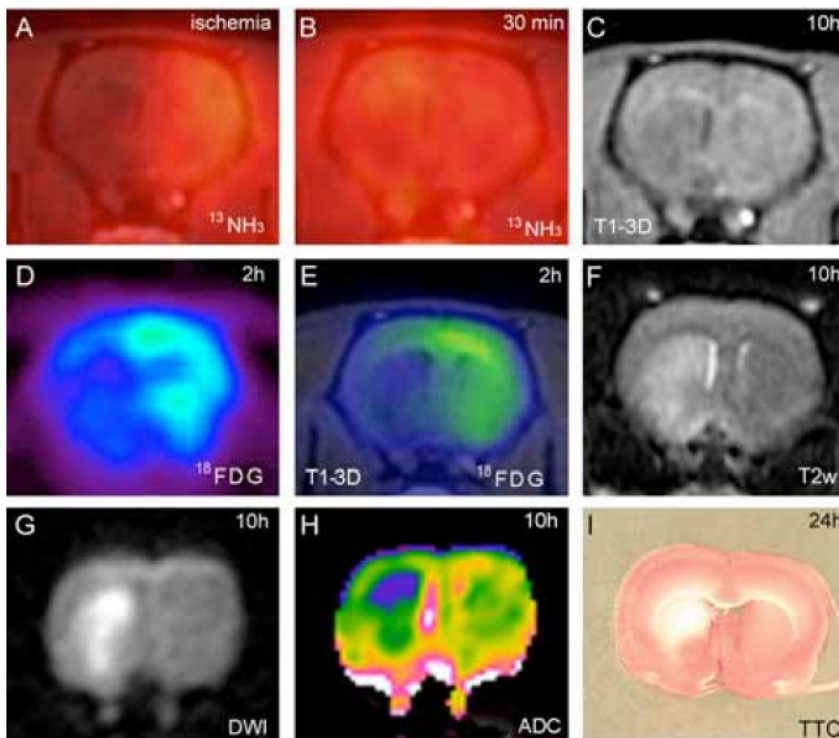


**Figure 21.** Illustration of the different imaging studies obtained in the same rat. A, B) Perfusion PET images obtained *in vivo* with  $^{13}\text{NH}_3$  during ischemia (A) and 30 min after reperfusion (B). Reduced signal intensity is observed in the

ipsilateral hemisphere (left side of the image) during ischemia (A), whereas the signal recovers at reperfusion (B). The PET images shown in A, B, and E are co-registered with an MRI T1-3D image obtained from the same rat (C). D) 18F-FDG PET image obtained between 2-3h of reperfusion showing reduced uptake in the ipsilateral hemisphere (left side of the image). E) The same 18F-FDG PET image is co-registered with the MRI data to obtain anatomical information. (F-H) MRI images showing T2w (F), DWI (G), and the ADC map (in false color) (H) of the same rat, illustrating damage in the striatum but not in the cortex. (I) The rat shown here did not develop cortical infarction at 24h in spite of reduced 18F-FDG uptake in the cortex after reperfusion, as illustrated in the postmortem tissue section stained with TTC and obtained at 24h (Martin, Rojas et al. 2009).

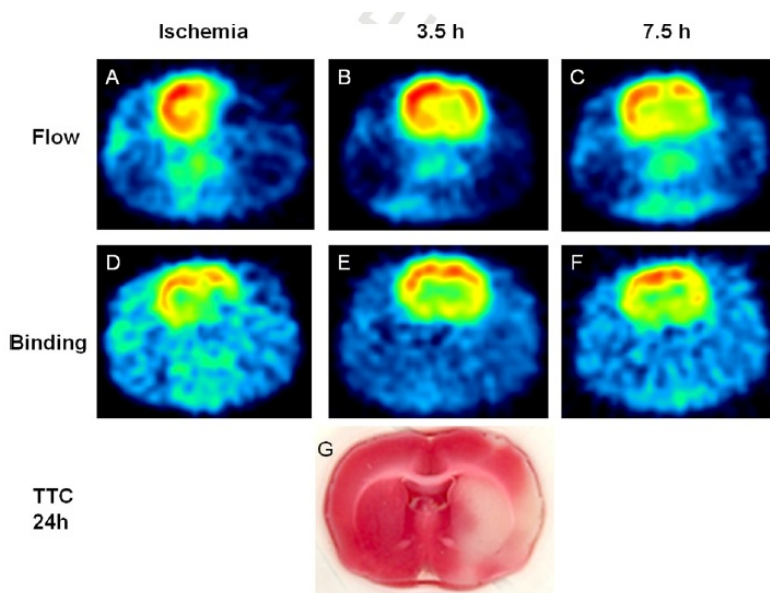


**Figure 22.** PET images of 11C-FMZ binding in the transient ischemia model. Images show one representative animal of the transient ischemia study. (A–C) show the flow image obtained from the reconstruction of the first 10 min after 11C-FMZ injection. (D–F) show the binding image obtained from the reconstruction of later time frames (10–30 min after injection). Asymmetry in the brain is only apparent during the occlusion in the flow image (A). (G) Post-mortem tissue TTC staining of the same animal clearly demonstrates the presence of corticostriatal infarction at 24 h, despite the lack of alteration in 11C-FMZ binding within the first 8 h following brain ischemia (Rojas, Martin et al. 2011).

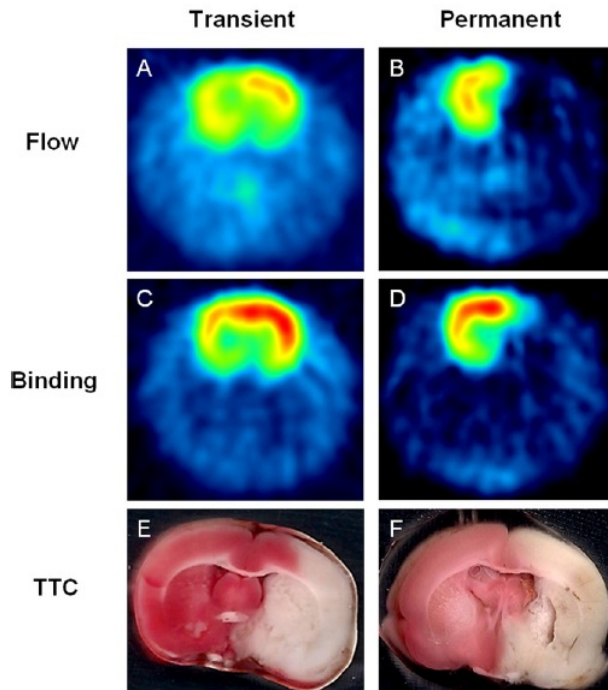


**Figure 23.**  $^{11}\text{C}$ -FMZ binding after transient vs. permanent ischemia at 24 h. Animals were imaged at 24 h after transient (A, C, E) or permanent (B, D, F) ischemia. Both animals developed cortical and striatal infarct at 24 h that appears in the TTC staining as a pale area (E, F). However, the PET image at this time point is very different depending on whether ischemia was followed by reperfusion or was permanent. (A) The flow images (A, B) show lack of asymmetry between both hemispheres after transient ischemia, indicating successful reperfusion (A), whereas after permanent ischemia (B) a strong interhemispheric asymmetry and lack of reperfusion is observed in the ipsilateral hemisphere. (C, D)  $^{11}\text{C}$ -FMZ binding in the same animals as in (A, B) shows no reduction in the ischemic area after transient ischemia, despite the presence of infarction (E). (D) In contrast,  $^{11}\text{C}$ -FMZ binding is strongly reduced in the ipsilateral hemisphere after permanent ischemia (Rojas, Martin et al. 2011).

More specific indication of tissue viability may be provided by  $^{18}\text{F}$ -FMISO, which is preferentially retained within hypoxic brain tissue amenable to rescue (Takasawa, Beech et al. 2011). Serial  $^{18}\text{F}$ -FMISO studies in rats with permanent distal MCAO suggested that the ischemic penumbra remains viable for approximately 8h (Saita, Chen et al. 2004; Rojas, Herance et al. 2011) (Figure 24).

Microglial activation, a hallmark of the inflammatory response, is thought

to contribute to both degeneration and neuroplasticity following ischemia. A number of TSPO ligands have been used to visualize microglial activation in models of ischemia; 11C-PK11195 (Rojas, Martin et al. 2007; Fukumoto, Hosoya et al. 2011; Hughes, Jones et al. 2012) (Figure 25), 18F-DPA-714 (Martin, Rojas et al. 2009), 18F-FEAC and 18F-FEDAC (Yui, Maeda et al. 2010) and 11C-DAC (Yui, Hatori et al. 2011). PET studies in the rat MCAO model showed the development of considerable uptake of the TSPO tracer 11C-PBR28 adjacent to the cerebral infarction (Imaizumi, Kim et al. 2007).

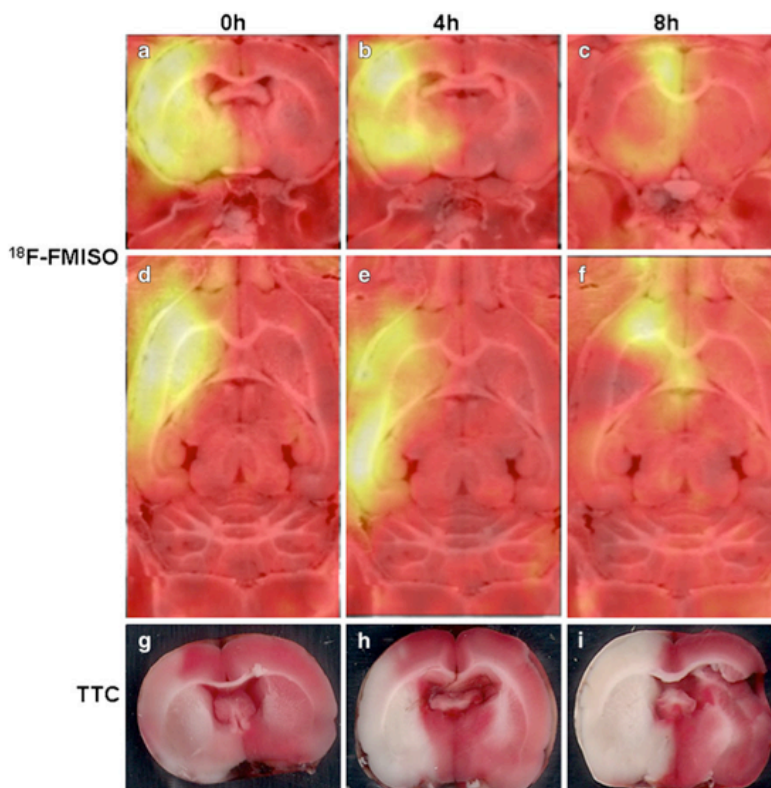


**Figure 24.** Uptake of 18F-FMISO persists up to 8 h after ischemia. Co-registered images from three different animals with permanent ischemia studied at different time points. a, d Immediately after the occlusion; b, e after 4 h and c, f after 8 h of occlusion. After 8 h of ischemia some hypoxic but viable areas remain in the periphery of lesion. g, h, i TTC staining obtained immediately after the PET study. The infarcted area is clearly seen in the three cases (Rojas, Herance et al. 2011).

Most rodent studies of  $^{18}\text{F}$ -FDG uptake in stroke have been qualitative, avoiding the requirement for arterial blood sampling. However, the region of somatosensory cortex sensitive to whisker stimulation (the barrel field) has served as a reference tissue for back-calculation of the arterial input function, allowing non-invasive quantification of  $^{18}\text{F}$ -FDG uptake in the rat MCAO model (Backes, Walberer et al. 2011). More conventionally, an image-derived  $^{18}\text{F}$ -FDG arterial input function has been obtained by placing a VOI in the murine heart ventricle (Tantawy and Peterson 2010), but this quantitative approach has not been tested in an ischemia model.

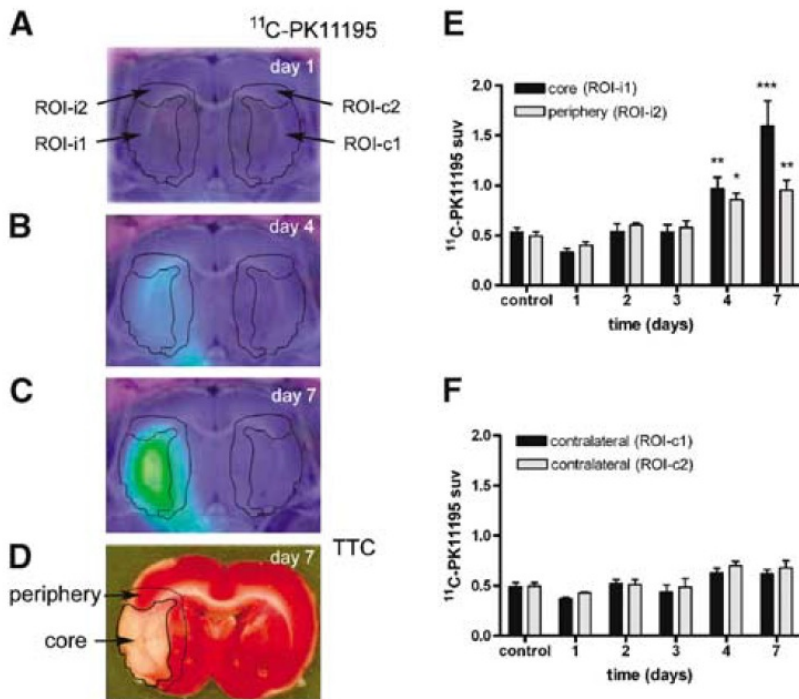


**Figure 25.** Progression of the  $^{11}\text{C}$ -PK11195 PET signal after ischemia. Images are from one representative rat showing  $^{11}\text{C}$ -PK11195 signal at various time points after ischemia (A to C). PET images were co-registered with a rat brain atlas for illustration of anatomical regions. Two ROIs were defined in the core of infarction (ROI-i1) and at the periphery (ROI-i2) (A to C) on the basis of the information obtained from the tissue (D). Also the corresponding homologous contralateral regions (ROI-c1 and ROI-c2) were examined. (D) TTC image of the post-mortem brain tissue at day 7 showing the core (pale area) and the surrounding peripheral region. Images correspond to coronal rat brain sections approximately at the level of Bregma. (E and F) SUVs in the ipsilateral (E) and contralateral (F) hemispheres. (E) The ROIs in the core and periphery in the ipsilateral hemisphere were defined for each animal on the basis of the

corresponding region of infarction and periphery, evaluated post mortem in the TTC-stained sections. (F) ROI-c1 and ROI-c2 correspond to the homologous contralateral region of infarction and periphery, respectively. Significant increases versus control became apparent at 4 and 7 days in the core (ROI-i1), and, to a lesser extent, in the periphery (ROI-i2) (Rojas, Martin et al. 2007).

## b) ET

Animal models cannot entirely mimic the kinematics of ET or any other human tremor. Furthermore, even skilled clinicians occasionally have difficulty distinguishing classic ‘tremor’ disorders such as ET and Parkinson disease from one another. For instance, diagnostic confusion can arise because some patients with severe ET may exhibit a rest tremor and most patients with Parkinson disease have an action tremor. Thus, finding consensus on the face validity of animal models of human tremor disorders is often problematic. Many animal models of action tremor are currently available to the research community. Action tremors are a prominent phenotypic feature of many rodents with spontaneous mutations; examples include trembler, vibrator, shiverer, and jumpy mice and zitter rats. Unlike humans with ET, however, these mutant rodents show severe pathological changes such as demyelination or spongiform degeneration of the peripheral and/or central nervous systems. In contrast, GABA<sub>A</sub> receptor  $\alpha$ -1 subunit knock-out mice are pathologically normal and show an action tremor with both postural and kinetic components (Kralic, Korpi et al. 2002).

Numerous pharmacological agents can induce action tremors. Unfortunately, only the tremors induced by harmaline and closely related compounds may have both face and predictive validity as models of ET. The drug harmaline has been shown to produce a generalized tremor at frequencies of 5–14Hz in rodents, rabbits, cats, and primates by producing oscillatory firing of neurons within the inferior olive. Harmaline-induced tremor has been proposed as a model for ET by different groups (Poirier, Sourkes et al. 1966; Llinas and Volkind 1973; Batini, Buisseret-Delmas et al. 1981; Bernard, Buisseret-Delmas et al. 1984). ET and harmaline tremor share numerous similarities and, as such, the latter may be a useful tool for understanding and treating the former.

In the other hand, for example the muscarinic-agonist tremorogenic agent, oxotremorine, produces a generalized tremor in a variety of mammalian species that does not require an intact olivocerebellar system. The oxotremorine tremor frequency (>12 Hz) is outside the range of human ET. Moreover, unlike ET, the tremor induced by oxotremorine does not improve significantly with moderate doses of ethanol (Rappaport, Gentry et al. 1984).

Reproducing psychiatric and neurological disorders in a meaningful mechanistic way remains a challenging task. The ET animal models developed up to date, poorly represent the ET in humans. Unfortunately, there are other limited animal models, such as AD (Spires and Hyman 2005) and PD (Fleming, Fernagut et al. 2005), which do not reproduce the full pathology and progression of the disease seen in patients. New opportunities emerge for mammalian genetic models with the development of transgenic rats, and even primates, and a wider range of non-mammalian models (Chesselet 2005). The development of animal models of neurological disorders is a work in progress and will continue to fuel new discoveries for neurotherapeutics.



## 2. SUMMARY

PET imaging allows studying physiological, biochemical or pharmacological processes *in vivo*, and it is being used in both research and clinical practice. In research, it has aided investigations of underlying pathophysiology of different diseases and the development of new drugs. In clinical practice, it has been used for the diagnosis, planning of treatment, and prediction outcome in several diseases. In the future, with the continuous development of new radiotracers and improvements in PET technology, the relevance of multitracer PET studies in both research and clinical practice will be even more marked.

Animal models of stroke are, up to date, among the best models in neurology, since their physiopathological mechanisms are translationable to humans and its invasive intervention treatments are also possible to be applied in rodents. Individual rodent stroke models capture each elements of the human disease. With careful attention to size, mechanism, and purpose, selected rodent models can be used to study the major targets of human neuroprotective therapies - reperfusion injury, delayed apoptotic cell death, and inflammatory cascades; or the cellular elements of neural repair. Rodent models can be easily shifted to study cell death and repair in aged animals, the actual population target for stroke therapies, without prohibitive cost and time constraints (Carmichael 2005).

Multitracer studies are of clinical interest since they do provide information of different pathophysiologic mechanisms, however they do require separate scans. Besides, the high costs and time consuming of separate scans, there are problems relating to image alignment and physiological changes inherent in successive imaging. Therefore, conditions in which physiological process evolve rapidly would especially benefit from the simultaneous assessment of different biological functions. Simultaneous dual-tracer PET imaging was originally proposed by Huang et al., however, it is not routinely applied since it increases image noise (Huang, Carson et al. 1982). Since the current generation of PET scanners is more sensitive and provides better image resolution, this technique could be feasible and should be evaluated in

detail. Accurate simultaneous dual-tracer imaging techniques are a promising and challenging issue and can provide large improvements in PET research.

ET is one good example of the added value of PET imaging in research: PET has recently pinpointed the physiopathological causative effect of ET. Previously, ET was thought to be associated with a dysfunction of the dopaminergic system. A recent study have demonstrated that ET is associated with reduced GABAergic function and increased availability of benzodiazepine receptor sites in brain regions implicated specifically in tremor genesis. This finding is thought to reflect overactivity of cerebellothalamic circuits and, hence, lends support to the “GABA hypothesis” of ET (Boecker, Weindl et al. 2010). Nevertheless, further studies are needed to better understand the involvement of the GABAergic system in ET and investigate the correlation between symptoms and the level of GABAergic dysfunction.

Another relevant neurotransmitter system in tremor disorders is the serotonergic system. Studies have been done in rats and in humans with selective serotonin reuptake inhibitors in ET (Koller 1989; Arshaduddin, Al Kadasah et al. 2004). The radiotracer 11C-DASB is a compound that binds to the serotonin transporter and it is a perfect tool to investigate the possible involvement of the serotonergic system in ET. Interestingly, abnormalities in the serotonergic system have been found in patients with tremor caused by PD (Doder, Rabiner et al. 2003).

## **3. OBJECTIVES**

### **3.1. Preclinical PET Studies**

- \* Evaluate the performance of simultaneous dual-tracer technique (SDTT) in static PET studies using  $^{18}\text{F}$ -FDG and  $^{13}\text{N}$ - $\text{NH}_4^+$  as radiotracers.
  
  - \* Measure cerebral glucose metabolism and cerebral blood flow, simultaneously, in the study of cerebral ischemia.
- 

### **3.2. Clinical PET Studies**

- \* Measure the serotonin transporters (SERT) and central benzodiazepine receptors, in a dynamic PET study of patients with Essential Tremor (ET), using the radiotracers  $^{11}\text{C}$ -DASB and  $^{11}\text{C}$ -flumazenil ( $^{11}\text{C}$ -FMZ), respectively.
  
- \* Test the hypothesis that the serotonin neurotransmission system may play a role in ET as it does in tremor in Parkinson's disease (PD).
  
- \* Investigate the possible association between the severity of tremor symptoms and the GABAergic and serotonergic neurotransmission systems in ET.



## 4. RESULTS

In this section, the scientific results are presented in the form of research papers.

### 4.1. Publication 1

Francisca P. Figueiras, Xavier Jiménez, Deborah Pareto, Vanessa Gómez, Jordi Llop, Raul Herance, Santiago Rojas and Juan D. Gispert. **Simultaneous Dual-tracer PET Imaging of the Rat Brain and its Application in the Study of Cerebral Ischemia.** *Mol Imaging Biology*, 2011 Jun;13(3):500-10.

---

### 4.2. Publication 2

A.Gironell, F.P. Figueiras, J.Pagonabarraga, J.R.Herance, B.Pascual, C.Trampal, and J.D. Gispert. **Molecular Neuroimaging of Gabaergic and Serotonergic systems in Essential Tremor: A clinical correlation Study.** *Parkinsonism and Related Disorders* (2012), doi:10.1016/j.parkreldis.2012.04.024 (*in press*)



Contents lists available at [SciVerse ScienceDirect](http://www.elsevier.com/locate/locate/parkreldis)

## Parkinsonism and Related Disorders

journal homepage: [www.elsevier.com/locate/parkreldis](http://www.elsevier.com/locate/parkreldis)

# Gaba and serotonin molecular neuroimaging in essential tremor: A clinical correlation study

Q1 A. Gironell<sup>a,\*</sup>, F.P. Figueiras<sup>b</sup>, J. Pagonabarraga<sup>a</sup>, J.R. Herance<sup>b</sup>, B. Pascual-Sedano<sup>a</sup>, C. Trampal<sup>c</sup>, J.D. Gispert<sup>b</sup>

<sup>a</sup> Movement Disorders Unit, Department of Neurology, Sant Pau Hospital, Autonomous University of Barcelona, Catalonia, Spain

<sup>b</sup> Institut d'Alta Tecnologia, Parc de Recerca Biomèdica, CRC Corporació Sanitària, Barcelona, Catalonia, Spain

<sup>c</sup> Centre de Imatge Molecular, Parc de Recerca Biomèdica, CRC Corporació Sanitària, Barcelona, Catalonia, Spain

## ARTICLE INFO

## Article history:

Received 11 January 2012

Received in revised form

13 April 2012

Accepted 20 April 2012

## Keywords:

Essential tremor

PET

GABA

Serotonin

## ABSTRACT

**Background:** Essential tremor is the most common movement disorder in adults, but its exact etiology and pathophysiology are still not fully understood. There is some consensus, however, about the involvement of the cerebellum and accumulating evidence points towards a dysfunction of the gabaergic system. We hypothesize that the serotonin neurotransmission system may also play a role as it does in tremor in Parkinson disease. This study aimed to investigate the association between the severity of tremor symptoms and the gabaergic and serotonergic neurotransmission systems in essential tremor. **Material and methods:** We measured the tremor clinical rating scale score and acquired DASB and Flumazenil PET scans in 10 patients who presented with essential tremor at different stages of clinical severity. Statistically significant correlations were sought between the scale scores and parametric binding potential images.

**Results:** The correlation analysis of cerebellar Flumazenil uptake and tremor clinical rating scale scores reached statistical significance ( $R^2 = 0.423$ ,  $p = 0.041$ ), whereas no association was detected in the DASB scans.

**Conclusions:** The severity of tremor correlated with the abnormalities found in GABA receptor binding, suggesting a primary gabaergic deficiency or a functional abnormality at the level of GABA<sub>A</sub> receptor subtypes. These results may assist in the rational development of new pharmacological treatments for essential tremor.

© 2012 Published by Elsevier Ltd.

## 1. Introduction

Essential tremor (ET) is a common movement disorder in adults, characterized by rhythmic action tremor of the arms and other parts of the body [1]. It is often referred to as a benign disorder but moderate and advanced stages of ET can be physically and socially disabling. The few medications that have been used to treat ET have demonstrated only modest efficacy [2].

The etiology and pathophysiology of ET are not yet well understood, and this limits the rational development of new pharmacological therapies for ET. Although there is some consensus about the involvement of the cerebellum in ET, the exact neurochemical abnormalities underlying ET remain to be

identified. Increasing evidence points to a dysfunction of the gamma-aminobutyric acid (GABA)ergic system [3]. To our knowledge, only one PET study using [<sup>11</sup>C]Flumazenil exploring *in vivo* the GABAergic system in ET patients has been undertaken [4].

Another relevant neurotransmitter system in tremor disorders is the serotonergic system. Studies have been done in rats and in humans with selective serotonin reuptake inhibitors in ET [5,6]. Moreover, abnormalities in the serotonergic system have been found in patients with tremor caused by Parkinson's disease (PD) [7].

The aim of the present study was to investigate the association between the severity of tremorsymptoms and the GABAergic and serotonergic neurotransmission systems in ET. To this end we acquired PET images in a group of ET patients at different stages of clinical severity. To obtain the images we used [<sup>11</sup>C]Flumazenil which specifically bind to the central benzodiazepine receptor sites of the GABA<sub>A</sub> receptor complex, and [<sup>11</sup>C]DASB that bind to the central serotonin transporters (SERT).

\* Corresponding author. Department of Neurology, Hospital de Sant Pau, Av.Sant Antoni Maria Claret, 167, 08025 Barcelona, Catalonia, Spain. Tel.: +34 935565986; fax: +34 935565902.

E-mail address: [agironell@santpau.cat](mailto:agironell@santpau.cat) (A. Gironell).

## 2. Materials and methods

### 2.1. Subjects

Ten patients with mild to severe ET (6 males, 4 females; mean age  $66 \pm 7$  y; age range 49–73 y) were included in the study. The study protocol was approved by the institutional ethics committee and by the Spanish Agency of Drugs and Health Products, and performed in accordance with international regulations. All subjects provided written informed consent.

Diagnosis was established on the basis of chronic (i.e., longer than 5 years), persistent (although the amplitude may fluctuate), bilateral (though it may be asymmetrical) postural tremor, with or without kinetic tremor, involving hands or forearms (although tremor of other body parts may be present in addition to upper limb tremor). All the patients fulfilled neurophysiological criteria for ET [8].

Exclusion criteria were other neurological abnormalities related to systemic or other neurological disease (with the exception of tremor, cogwheeling and Froment's sign) and alternative explanations for tremor (e.g. presence of known causes of enhanced physiological tremor, concurrent or recent exposure to drugs known to cause tremor, or the presence of a drug withdrawal state) [9]. Patients were also excluded from the trial based on the presence of psychiatric or mental illness, substance abuse, or tremor active drugs. Tremor active drugs included central cholinergic drugs (acetylcholine, muscarine and nicotinic agonists, anticholinergases, aminopropranolols), central monoaminergic drugs (neuroleptics, phenylethylamines, indoles), peripheral adrenergic drugs (lithium, amphetamine, adrenocorticosteroids, thyroid hormone supplements), and drugs such as anticonvulsants (valproic acid), bronchodilators (theophylline, terbutaline) or antidepressants (amitriptyline). Patients with pacemakers and contraindications for MRI, including claustrophobia, were also excluded. Patients were asked to avoid alcohol, caffeine and smoking during the 24 h before PET scanning.

Patients were recruited from the pool of our Movement Disorders Unit according to the level of tremor severity indicated by the Glass Scale [10]. The Glass Scale measures disease severity in ET with upper limb involvement. The scale is administered by asking the patient the question: "Over the last week, when you were sitting down at the table, how did you drink water from a glass?" Scores: I – I have no difficulties. II – I can drink with one hand, but I have to fill the glass with less liquid to avoid spills. III – I cannot drink with one hand, I need both hands. IV – I cannot drink with my hands, I need a straw. We recruited two patients who had mild symptoms (Glass Scale I), three with moderate symptoms (Glass Scale II), three with moderate-severe symptoms (Glass Scale III) and two with severe symptoms (Glass Scale IV). The study was offered to 13 patients, and three refused to participate.

The main clinical measurement consisted of parts 1 and 2 of the tremor clinical rating scale (TCRS), proposed by Fahn et al. [11], with minimal modifications. Specifically, postural and kinetic tremor of the hands, legs, head and trunk (Part 1) was classified according to the following scale: 0 = none; 1 = mild (amplitude < 0.5 cm); 2 = moderate (amplitude 0.5–1 cm); 3 = marked (amplitude 1–2 cm); and 4 = severe (amplitude > 2 cm) (maximum score = 40). We did not include scores for face, tongue and voice. Measures of motor task performance (Part 2) (handwriting, drawing spirals and lines, and pouring liquids from one cup to another) were scored as follows: 0 = normal, 1 = mildly abnormal, tremulous; 2 = moderately abnormal, considerable tremor; 3 = markedly abnormal; and 4 = severely abnormal and unable to do the task (maximum score = 36). The same clinician (A.G.) conducted all the clinical assessments in all the patients.

Eight patients had a positive family history for ET. Two patients had head tremor as well as hand tremor. None of the study patients were alcohol sensitive. Three patients received no antitremor medication and the rest were taking treatment. None of the patients were taking either benzodiazepines or selective serotonin reuptake inhibitors (SSRIs). To exclude pharmacologic interference with the GABA or SERT receptors at the time of PET, any medication that might interact with these was withdrawn before PET for a period based in at least two times the respective half-lives of the compounds (Table 1). The PET scans were acquired with the patients at rest and without tremor.

**Table 1**  
Patients' demographic data.

Patient	Age	Gender	Family	Disease duration <sup>a</sup>	Glass scale	TCRS	Drugs
1	69	M	+	5	I	4	–
2	70	F	–	9	I	4	–
3	49	M	+	15	II	15	–
4	73	M	–	20	II	29	b-blockers
5	62	F	+	16	II	13	b-blockers
6	70	F	+	11	III	30	Gabapentin
7	68	M	+	5	III	30	b-blockers
8	68	M	+	10	III	28	Gabapentin
9	71	F	+	15	IV	34	Primidone + gabapentin
10	64	M	+	19	IV	36	Primidone + b-blockers

TCRS: tremor clinical rating scale.

<sup>a</sup> Years.

### 2.2. Radiopharmaceutical preparation

Precursors and reference standards for [<sup>11</sup>C]Flumazenil (ethyl 8-fluoro-5,6-dihydro-5-[<sup>11</sup>C]methyl-6-oxo-4H-imidazo [1,5-a] [1,4]benzodiazepine-3-carboxylate; [<sup>11</sup>C]RO 151788) and [<sup>11</sup>C]DASB (N,N-Dimethyl-2-(2-amino-4-cyanophenylthio)-benzylamine) were obtained from Advanced Biochemical Compounds (ABX, Radeberg, Germany). Ligands were synthesized by a methylation reaction using [<sup>11</sup>C]CH<sub>3</sub>I as radioactive precursor according to procedures described in the literature with minor changes [12,13]. Subsequently, the tracers underwent a quality control procedure consisting of chemical purity by UV-HPLC, radiochemical purity by radio-HPLC, residual solvents by GC, radionuclidic purity by multichannel gamma-spectrometry, pH, sterility, and endotoxin testing. The radiochemical and chemical purity was over 95% for both tracers and the mean specific activities were 119.45 GBq/μmol for [<sup>11</sup>C]DASB and 48.76 GBq/μmol for [<sup>11</sup>C]Flumazenil.

### 2.3. Image acquisition

Each patient underwent two 90 min high-resolution [<sup>11</sup>C]Flumazenil and [<sup>11</sup>C]DASB PET scans, approximately one week apart. Patients were placed on the scanner bed with their head held firmly in place by means of a thermoplastic mask fixed to the bed to minimize head movements during each scan.

PET acquisitions were performed using a Siemens ECAT EXACT HR + camera. To correct for attenuation, a 10-min transmission scan was carried out before emission scanning with the <sup>68</sup>Ge/<sup>68</sup>Ga rods in the scanner. The [<sup>11</sup>C]DASB/[<sup>11</sup>C]Flumazenil radiotracers (range 8.63–13.36 mCi [319.31–494.32 MBq]) were administered intravenously with a scan protocol of 26 time frames, starting after the injection of the radiotracer (8 × 15 s, 3 × 60 s, 5 × 120 s, 5 × 300 s, 5 × 600 s). PET data were reconstructed using the filtered back projection algorithm with a Hann filter (4.9 mm FWHM). Corrections were applied for attenuation (through transmission data), scatter, randoms and dead time. The reconstructed volumes had a matrix size of 128 × 128 × 63 voxels; with a voxel size of 2.57 × 2.57 × 2.43 mm.

In addition to the PET scans, each subject underwent a magnetic resonance imaging (MRI) scan [GE Signa 1.5 T scanner, spin-echo sequence, proton density weighted image (voxel dimensions): x (1 mm), y (1 mm), and z (1.5 mm)] within one month of the PET scans.

### 2.4. Image quantification and analysis

The spatial pre-processing of the images was performed using SPM5 (Wellcome Department of Cognitive Neurology, London, U.K.). A post frame-by-frame realignment procedure was applied to compensate for head movement in the scanner. Frames were realigned to a single, 'reference' frame acquired 25 min post injection. This frame had a high signal to noise ratio, and the transformation parameters were then applied to the corresponding attenuation corrected dynamic images. MRI images were superimposed on the PET images. To enable between-subject voxel-by-voxel comparisons all the images were spatially normalized to a standard. Normalizing scans of elderly patients to the standard SPM5 templates might present some difficulties as brain structures change over time. We based normalization on the patients' MRI. MRIs were segmented into gray matter (GM), white matter (WM), and cerebrospinal fluid (CSF). The GM image was then normalized to the GM *a priori* template which already fits the Montreal Neurological Institute (MNI) standard space. The individual normalization parameters obtained using the previous method were applied to both the MRI and PET dynamic images. Normalization of PET images using individual MRI scans has previously been described to yield more sensitive SPM maps [14].

Images were voxel-wise modeled to yield parametric images of the non-displaceable binding potential (BP<sub>ND</sub>) with PMOD 2.7 (PMOD Technologies, Zurich, Switzerland) and using the simplified tissue reference model (SRTM-2) [15,16]. For [<sup>11</sup>C]DASB, the cerebellum is a suitable reference region because studies report either undetectable or extremely low 5-HTT density [17]. On the other hand, the bilateral hypothalamus was selected as a region with high specific binding since

uptake is high and homogeneous in this region [18]. Regarding [<sup>11</sup>C]Flumazenil, the pons was used as the reference region to estimate non-displaceable uptake (free plus nonspecifically bound), whereas the occipital cortex was used as the receptor-rich region [19]. Since all the images were in the MNI standard space, the WFU Pickatlas template was used to define ROI.

The correlation between clinical parameters and BP<sub>ND</sub> parametric images was tested prospectively in the whole brain using SPM8. Additionally, driven by previous reports of cerebellar GABAergic dysfunctions in ET and SERT alterations in the raphe in PD [7]. ROIs were drawn in the cerebellum for the [<sup>11</sup>C]Flumazenil scans and in the raphe nucleus for the [<sup>11</sup>C]DASB scans. TCRS scores were used as covariate to find regions showing statistically significant correlations (two-tailed; uncorrected  $p$ -value of  $p < 0.001$  and  $k > 300$  for the whole brain voxel-wise analysis and  $p < 0.05$  for the ROI analysis) across all BP<sub>ND</sub> parametric images. No intensity scaling or global calculation was needed. To improve localization of the voxel-wise results, SPM maps were overlaid onto the single-subject-T1 anatomical brain template.

### 3. Results

All the patients' demographic and clinical details are summarized in Table 1. Fig. 1 shows a cluster of statistically significant positive correlation between [<sup>11</sup>C]Flumazenil BP<sub>ND</sub> and TCRS scores in the cerebellum. Specifically, this cluster includes the cerebellar vermis, bilateral posterior lobes and right anterior lobe. Partially, it also extends to the bilateral lingual, fusiform and inferior occipital gyri, probably arising from a spill-over effect given the limited resolution of PET imaging. SPM results are shown in Table 2 showing the statistical maximum and the corresponding coordinates in the standardized space of the Montreal Neurological Institute. As usual when using the SPM software, the statistical maximum is expressed as uncorrected  $p$ -value ( $p_{\text{uncorr}}$ ), equivalent T and Z scores, and  $p$ -values corrected for multiple comparisons

using two methods: the Family Wise-Error ( $p_{\text{FWE-corr}}$ ) and the False Discovery Ratio ( $p_{\text{FDR-corr}}$ ). The table also shows the results at the cluster level (i.e. the probabilities that a particular number of contiguous voxels survive the threshold for statistical significance). At this level, reported extent of the cluster ( $k_E$ ), the uncorrected  $p$ -value and the  $p$ -values corrected for multiple comparisons with the two aforementioned methods. In this analysis, it is worth noting that the extent of the cluster survives the level of  $p < 0.05$  corrected for multiple comparisons. Accordingly, the ROI correlation analysis of cerebellar [<sup>11</sup>C]Flumazenil uptake (Fig. 2) also reached statistical significance ( $p = 0.0419$ ). The negative correlation between [<sup>11</sup>C]Flumazenil BP<sub>ND</sub> and TCRS scores rendered no statistically significant results in the SPM analysis. Similarly, no statistically significant correlations were found between [<sup>11</sup>C]DASB uptake and TCRS scores neither in the ROI ( $p = 0.9059$ ) nor in the SPM analysis.

### 4. Discussion

Our exploratory study suggests that ET is associated with a GABAergic neurotransmission dysfunction in the cerebellum. Tremor severity correlated with the abnormalities found in GABA receptor binding, suggesting a functional abnormality at the level of GABA<sub>A</sub> receptor subtypes. On the other hand, no serotonergic transporter dysfunction was found to be associated with the symptom scales.

The results of our study agree with the "GABA hypothesis" in ET [3]. This is supported by the tremorl responses to ethanol and gabapentin (an anticonvulsant drug that is structurally similar to

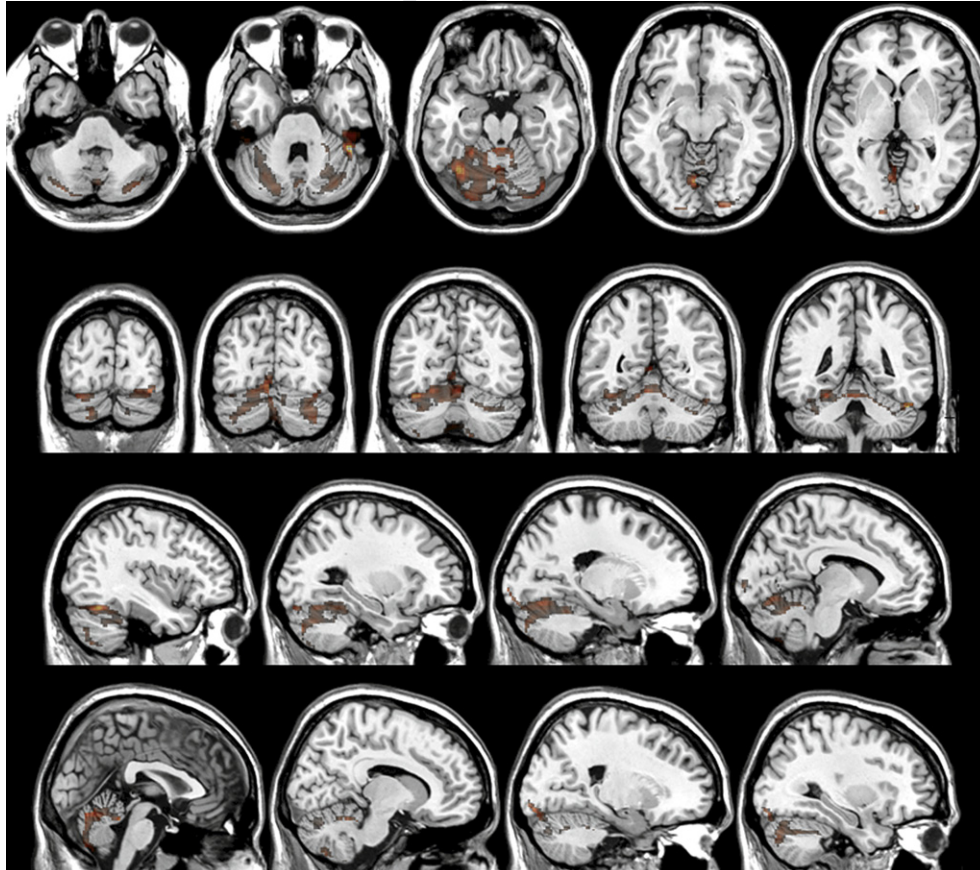


Fig. 1. Brain regions with statistically significant correlations between [<sup>11</sup>C]Flumazenil binding and TCRS, which mainly include the cerebellar vermis, bilateral posterior lobes and right anterior lobe.

**Table 2**  
SPM results. See the 'results' section for details.

SPM results: positive correlation [ <sup>11</sup> C]-Flumazenil binding vs. TCRS										
Cluster-level					Peak level					x, y, z (mm)
P <sub>FWE-corr</sub>	P <sub>FDR-corr</sub>	k <sub>E</sub>	P <sub>uncorr</sub>	P <sub>FWE-corr</sub>	P <sub>FDR-corr</sub>	T	Z <sub>E</sub>	P <sub>uncorr</sub>		
0.016	0.023	5088	<0.001	0.993	0.999	4.99	3.37	<0.001	46, -42, -30	

the inhibitory neurotransmitter GABA) in ET [20], and by GABA findings in human cerebrospinal fluid [21]. Post-mortem studies have also revealed structural abnormalities in the cerebellum, particularly at the level of the GABA-containing Purkinje cells. A recent study has found a decrease in GABA<sub>A</sub> and GABA<sub>B</sub> receptors in the dentate nucleus [22,23]. It may be hypothesized that a decrease in receptor number probably results in an increase in function with a GABA receptor up-regulation at the level of the deep cerebellar nuclei, explaining the increase of binding of [<sup>11</sup>C]Flumazenil. Furthermore, our results are in agreement with the previous [<sup>11</sup>C]Flumazenil PET study which studied eight ET patients and found significant binding increases in the cerebellum (dentate nucleus), the ventrolateral thalamus, and the lateral premotor cortex [4].

The cerebellum and thalamus are the main regions involved in the pathophysiology of tremor in humans. Clinical case studies have shown that lesions of these structures can alleviate tremor [24]. The ventral intermediate nucleus is the most effective target for stereotactic interventions to treat tremor. A study using repetitive transcranial magnetic stimulation applied over the cerebellum found a tremorolytic action in ET patients [25]. Furthermore, activation studies with PET indicate an abnormally increased regional cerebral blood flow in the cerebellum [26,27]. Microscopic cerebellar pathology has also been identified in these patients [22]. MRI studies are also in agreement with cerebellar involvement in ET, including spectroscopy, voxel-based morphometry and functional MRI [28].

According to this mounting evidence, the cerebellum and GABAergic system appear to play a central role in ET pathophysiology. There are several examples of tremorolytic effects induced by increasing GABAergic transmission in the thalamus and the cerebellum. Microinjections of the GABA<sub>A</sub> agonist muscimol into the ventral intermediate thalamus of ET patients undergoing stereotaxy are effective in reducing tremor [24]. However, increasing GABAergic stimulation alone does not improve tremor in ET. One study using gabapentin [29], two trials using the GABA-agonist

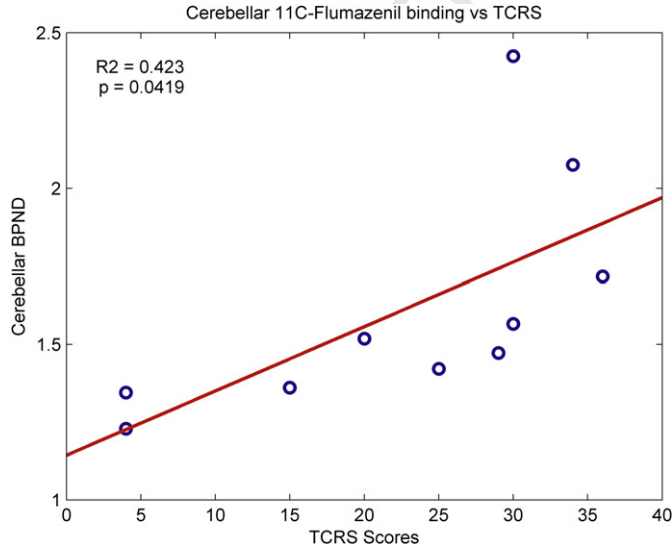


**Fig. 2.** Scatterplot of TCRS scores vs cerebellar [<sup>11</sup>C]Flumazenil binding.

progabide [30,31], and one study using tiagabine in patients with ET failed to elicit therapeutic benefit [32].

There is some evidence of involvement of the serotonergic system in ET pathophysiology: one study in rats with citalopram, an SSRI, augments harmaline-induced tremor in rats; tremor is one of the signs of serotonin syndrome, and trazodone, an SSRI, has been proved in ET in humans with inconclusive results [5,6]. Moreover, in a PET study using [<sup>11</sup>C]WAY-100635, a specific tracer for 5-HT<sub>1A</sub> receptors, Doder et al. revealed that serotonergic neurotransmission is decreased in PD [7]. Interestingly, they found an association between 5-HT<sub>1A</sub> receptor availability in the raphe and the severity of parkinsonian tremor, and concluded that serotonergic agents are worth studying for the relief of this kind of tremor. In our study with ET patients, however, we found no abnormality in serotonergic system transport. However, both studies represent an indirect measure of 5HT neuronal counts in the rafe. We can not fully exclude a role for 5HT in ET.

This preliminary study has several limitations. First, the relatively small number of patients included in this study might have prevented us from detecting subtler effects in either the GABAergic or serotonergic systems. Nevertheless, our sample size is similar to those of previous PET studies. Second, while the benzodiazepine receptor is part of the GABA<sub>A</sub> complex it may not be directly influenced by synaptic GABA levels or reflect GABA transmission. Thus we cannot absolutely conclude that GABA deficiency underlies ET. Third, PET does not allow us to discern whether increased ligand binding results from decreased competition with endogenous GABA<sub>A</sub>, increased concentration of the receptors, or increased receptor-ligand affinity. Another limitation is that GABAergic effects may remain after the withdrawal of antitremor drugs. However, in our study patients treated with gabapentin (BP<sub>ND</sub> = 1.569) showed cerebellar binding levels very similar to those not taking this drug (BP<sub>ND</sub> = 1.633), thus reflecting a correct wash-out of the medication prior to the PET scan. Finally, the lack of control data in the present study may indicate that the observed positive correlation represent a secondary phenomena rather than being causative. However, previous controlled PET study using the same methods and radiotracer, showed compatible results with our study [4].

In conclusion, our results provide further *in vivo* neuroimaging evidence of abnormally increased cerebellar GABA<sub>A</sub> receptors in ET, and support the role of cerebellar GABAergic dysfunction as the main physiopathological hypothesis of the disease. We did not detect any abnormalities in the serotonergic transporting system in our subjects with ET. These results may facilitate the rational development of new pharmacotherapies for ET.

#### Acknowledgements

Study supported by a grant from "Fondo de Investigaciones Sanitarias" (PI 052309), Government of Spain.

#### References

- [1] Louis ED. Essential tremor. *Lancet Neurol* 2005;4:100–10.
- [2] Deuschl G, Raethjen J, Hellriegel H, Elble R. Treatment of patients with essential tremor. *Lancet Neurol* 2011;10:148–61.

- [3] Louis ED. A new twist for stopping the shakes? Revisiting GABAergic therapy for essential tremor. *Arch Neurol* 1999;56:807–8.
- [4] Boecker H, Weindl A, Brooks DJ, Ceballos-Baumann AO, Liedtke C, Miederer M, et al. GABAergic dysfunction in essential tremor: an 11C-Flumazenil PET study. *J Nucl Med* 2010;51:1030–5.
- [5] Koller WC. Trazadone in essential tremor. Probe of serotonergic mechanisms. *Clin Neuropharmacol* 1989;12:134–7.
- [6] Arshaduddin M, Al Kadasah S, Biary N, Al Deeb S, Al Moutaery K, Tariq M. Citalopram, a selective serotonin reuptake inhibitor augments harmaline-induced tremor in rats. *Behav Brain Res* 2004;153:15–20.
- [7] Doder M, Rabiner EA, Turjanski N, Lees AJ, Brooks DJ. Tremor in Parkinson's disease and serotonergic dysfunction. An 11C-WAY 100635 PET study. *Neurology* 2003;60:601–5.
- [8] Gironell A, Kulisevsky J, Pascual-Sedano B, Barbanoj M. Routine neurophysiological tremor analysis as a diagnostic tool for essential tremor: a prospective study. *J Clin Neurophysiol* 2004;21:446–50.
- [9] Deuschl G, Bain P, Brin M, Ad Hoc Scientific committee. Consensus statement of the movement disorder Society on tremor. *Mov Disord* 1998;13(Suppl. 3): 2–23.
- [10] Gironell A, Martínez-Corral M, Pagonabarraga J, Kulisevsky J. The glass scale: a simple tool to determine severity in essential tremor. *Parkinsonism Rel Disord* 2010;16:412–4.
- [11] Fahn S, Tolosa E, Marín C. Clinical rating scale for tremor. In: Jankovic J, Tolosa E, editors. *Parkinson's disease and movement disorders*. Baltimore-Munich: Urban & Schwarzenberg; 1988. p. 225–34.
- [12] Maziere M, Hantraye P, Prenant C, Sastre J, Comar D. Synthesis of ethyl 8-fluoro-5,6-dihydro-5-[11C]methyl-6-oxo-4H-imidazo [1,5-a] [1,4]benzodiazepine-3-carboxylate (RO 15.1788-11C): a specific radioligand for the in vivo study of central benzodiazepine receptors by positron emission tomography. *Int J Appl Radiat Isot* 1984;35:973–6.
- [13] Wilson AA, Ginovart N, Hussey D, Meyer J, Houle S. In vitro and in vivo characterisation of [11C]-DASB: a probe for in vivo measurements of the serotonin transporter by positron emission tomography. *Nucl Med Biol* 2002; 29:509–15.
- [14] Gispert JD, Pascau J, Reig S, Martínez-Lázaro R, Molina V, García-Barreno P, et al. Influence of the normalization template on the outcome of statistical parametric mapping of PET scans. *Neuroimage* 2003;19:601–12.
- [15] Ichise M, Liow JS, Lu JQ, Takano A, Model K, Toyama H, et al. Linearized reference tissue parametric imaging methods: application to [11C]DASB positron emission tomography studies of the serotonin transporter in human brain. *J Cereb Blood Flow Metab* 2003;23:1096–112.
- [16] Wu Y, Carson RE. Noise reduction in the simplified reference tissue model for neuroreceptor functional imaging. *J Cereb Blood Flow Metab* 2002;22: 1440–52.
- [17] Meyer JH, Wilson AA, Guinovart N, Goulding V, Hussey D, Hood K, et al. Occupancy of serotonin transporters by paroxetine and citalopram during treatment of depression: a [(11C)DASB PET imaging study. *Am J Psychiatry* 2001;158:1843–9.
- [18] Voineskos AN, Wilson AA, Boovariwula A, Sagrati S, Houle S, Rusjan P, et al. Serotonin transporter occupancy of high-dose selective serotonin reuptake inhibitors during major depressive disorder measured with [11C]DASB positron emission tomography. *Psychopharmacology (Berl)* 2007;193:539–45.
- [19] Odano I, Halldin C, Karlsson P, Varrone A, Airaksinen AJ, Krasikova RN, et al. [18F]flumazenil binding to central benzodiazepine receptor studies by PET—quantitative analysis and comparisons with [11C]flumazenil. *Neuroimage* 2009;45:891–902.
- [20] Gironell A, Kulisevsky J, Barbanoj M, López-Villegas D, Hernández G, Pascual B. A double-blind placebo-controlled trial of gabapentin and propranolol in patients with essential tremor. *Arch Neurol* 1999;56:475–80.
- [21] Mally J, Baranyi M, Vizi ES. Change in the concentrations of amino acids in CSF and serum of patients with essential tremor. *J Neural Transm* 1996;103: 555–60.
- [22] Louis ED, Faust PL, Vonsattel JP, Varrone A, Airaksinen AJ, Krasikova RN, et al. Neuropathological changes in essential tremor: 33 cases compared with 21 controls. *Brain* 2007;130:3297–307.
- [23] Paris-Robidas A, Brochu E, Sintès M, Emond V, Bousquet M, Vandal M, et al. Defective dentate nucleus GABA receptors in essential tremor. *Brain* 2012; 135:105–16.
- [24] Pahapill PA, Levy R, Dostrovsky JO, Davis KD, Rezaei AR, Tasker RR, et al. Tremor arrest with thalamic microinjections of muscimol in patients with essential tremor. *Ann Neurol* 1999;46:249–52.
- [25] Gironell A, Kulisevsky J, Lorenzo J, Barbanoj M, Pascual-Sedano B, Otermin P. Transcranial magnetic stimulation of the cerebellum in essential tremor: a controlled study. *Arch Neurol* 2002;59:413–7.
- [26] Colebatch JG, Findley LJ, Frackowiak RS, Marsden CD, Brooks DJ. Preliminary report: activation of the cerebellum in essential tremor. *Lancet* 1990;336: 1028–30.
- [27] Louis ED, Shungu DC, Chan S, Mao X, Jurewicz EC, Watner D. Metabolic abnormality in the cerebellum in patients with essential tremor: a proton magnetic resonance spectroscopic imaging study. *Neurosci Lett* 2002;333: 17–20.
- [28] Bucher SF, Seelos KC, Dodel RC, Reiser M, Oertel WH. Activation mapping in essential tremor with functional magnetic resonance imaging. *Ann Neurol* 1997;41:32–40.
- [29] Pahwa R, Lyons K, Hubble JP, Busenbark K, Rienerth JD. Double-blind controlled trial of gabapentin in essential tremor. *Mov Disord* 1998;13:465–7.
- [30] Koller WC, Rubino F, Gupta S. Pharmacologic probe with progabide of GABA mechanisms in essential tremor. *Arch Neurol* 1987;44:905–6.
- [31] Mondrup K, Dupont E, Pederson E. The effect of the GABA-agonist, progabide on benign essential tremor. *Acta Neurol Scand* 1983;768:248–52.
- [32] Gironell A, Martínez-Corral M, Pagonabarraga X, Kulisevsky J. Tiagabine for essential tremor: an open-label trial. *Mov Disord* 2008;23:1955–6.

## Errata

Line 102: ‘tremorsymptoms’ → ‘tremor symptoms’

Line 106: ‘which specifically bind to the’ → ‘which specifically binds to the’

Line 107: ‘that bind to’ → ‘that binds to’

Line 207: ‘SPM5’ → ‘SPM8’

Line 246: ‘Additionally, driven by’ → ‘Additionally, we conducted an ROI-based analysis driven by’

Line 333: ‘tremorl’ → ‘tremorlytic’

Line 459: ‘rafe’ → ‘raphe’

Line 471: ‘GABA-A’ → ‘neurotransmitter’

And paragraph starting in line 385, which states:

‘It may be hypothesized that a decrease in receptor number probably results in an increase function with a GABA receptor up-regulation at the level of deep cerebellar nuclei, explaining the increase of binding of [11C]-FMZ’.

Should be substituted by:

‘It might be hypothesized that a decrease in receptor number probably results from a decrease in function and after a GABA receptor up-regulation at the level of deep cerebellar nuclei, explaining the increase of [11C]FMZ binding which could also arise from molecular alterations at the at the level of GABA-A receptor subunits’.

## 5. DISCUSSION

In the first study, ‘Simultaneous dual-tracer PET imaging of the rat brain and its application in the study of cerebral ischemia’, an evaluation of the performance of SDTT in static microPET studies using  $^{18}\text{F}$ -FDG and  $^{13}\text{N}$ - $\text{NH}_4^+$  was presented.

The dual-tracer approach is useful for understanding the relationship between simultaneous pathophysiologic processes in the brain. Imaging cerebral blood flow and cerebral glucose metabolism provide complementary physiological information, and the dual-tracer approach may potentially provide perfectly co-registered images, faster throughput and less time consuming. However, its main benefit comes from the confirmation of successful reperfusion after MCA occlusion. In addition, the injury mechanisms that occur in ischemic damage change rapidly over time and, therefore, it may not be possible to study two different processes in the same animal using two separate single-tracer acquisitions.

The methodological details limitations of SDTT have already been discussed in depth in the section 4.1. However, it is worth noting the superior performance of SSRB over FORE found in our comparison of rebinning methods for SDTT. This behaviour can be attributed from the fact that the used phantom was relatively small and centred in the field-of-view (FOV), thus meeting the assumptions of the approximations in SSRB. Nevertheless, Figueiras et al showed for the first time that the SDTT, as here described, is feasible to be applied *in vivo*.

Small animal PET imaging is an evolving technology that makes possible to probe biological processes *in vivo* using minimally invasive procedures. Small animal PET, coupled with human PET imaging capabilities, provides an outstanding platform for translational science. Because the small animal and human PET technologies and methodologies provide essentially the same information, and because PET imaging studies of both humans and small animals are based on the same molecular imaging agents, knowledge gained in one area can rapidly be

employed in the other. The strong translational science potential of small animal and human PET holds a great promise to dramatically advance our understanding of human disease.

The size differences between humans and small animals present a considerable challenge in efforts to translate this technology from the human to preclinical imaging applications. The first PET images of rat brain were obtained using a clinical PET scanner (Ingvar, Eriksson et al. 1991). Because of resolution issues, rodent scanning only became practical with the advent of RATPET, the first dedicated small-animal scanner (Bloomfield, Rajeswaran et al. 1995). Improvements in instrumentation continue apace, such that current detectors approach the theoretical limit of spatial resolution.

In parallel, the palette of available radiopharmaceuticals continues to increase. Most molecular brain imaging has so far focused on brain energy metabolism and neurotransmitter receptors and transporters, labelled with small molecules. *In vivo* imaging of gene expression promises to emerge as an important method for detecting endogenous genes or genes that have been transfected (transgenes) into cells or organ systems, for example in studies of disease progression or therapeutic interventions. *In vivo* imaging of gene expression is one potential major new area of PET research.

Application of post-processing techniques routinely used in human brain imaging to the rodent brain such as SPM, partial volume effect correction, automated segmentation and co-registration also represent an important area for continued development within the field. A number of studies have already demonstrated the use of SPM techniques in rodent models (Casteels, Vermaelen et al. 2006; Mirrione, Schiffer et al. 2007; Soto-Montenegro, Vaquero et al. 2009; Hoekzema, Rojas et al. 2011). However, with the exception of Atlas3D (Hjornevik, Leergaard et al. 2007), no standard rat or mouse brain imaging atlas space has been developed. There are significant inter-strain differences in brain shape and size (Airey, Wu et al. 2006), which complicates development. Partial volume correction has been attempted for cardiac blood input function in rats (Su, Lee et al. 2009), however the applicability of these algorithms to the brain have not been tested. The advent of combined-modality systems

such as PET/MRI and PET/CT should assist in the continued optimization of these techniques.

While no systematic preclinical PET studies have been carried out on the effects of sex differences on brain activity and function, it is evident from emerging human imaging studies that the uptake of some tracers is strongly influenced by gender differences. For example, it has been reported that males with AD have significantly higher PIB binding than females, suggesting that a greater amyloid burden is necessary before males manifest the disease (Rowe, Ellis et al. 2010). Thus, the development and evaluation of tracers for specific neurological or neuropsychiatric disorders should consider putative sexually dimorphic effects on PET-derived measures.

While PET offers the ability to non-invasively assess alterations in receptor function, it does routinely require restraint of the animal in order to keep it stationary during the period of data acquisition; this is achieved by general anaesthesia and other supplementary devices to fix, for example, the head in one position. The recent development the RatCAP has provided the technical possibility to acquire PET recordings in awake, behaving animals (Schulz and Vaska 2011). The tomograph has a resolution of <2 mm FWHM, and in proof-of-concept experiments, was sufficiently sensitive to demonstrate reductions in striatal 11C-raclopride binding related to anaesthesia. Whether the temporal resolution of RatCAP system will prove sufficiently sensitive to detect ‘real time’ changes in receptor occupancy related to behaviour has yet to be demonstrated. Nevertheless, the ratCAP system does represent a significant stride forward in allowing simultaneous functional whole-brain imaging of awake and freely mobile rats.

With the development of novel radiopharmaceuticals with specificity for non-dopaminergic targets in the brain and the increasing sophistication of animal models and continued optimization of image processing techniques, PET has emerged as a powerful tool to investigate the brain mechanisms of neuropsychiatric and neurological disorders in humans.

In the second study, ‘Molecular Neuroimaging of Gabaergic and Serotonergic systems in Essential Tremor: A clinical correlation Study’, it has been investigated the association between the severity of tremoric

symptoms and the GABAergic and serotonergic neurotransmission systems in ET.

As with any PET ligand, it cannot be answered with surety whether the increased 11C-FMZ binding pattern observed results from an increase in receptor concentration, a deficit of the endogenous ligand competing for the same binding sites and/or to alterations in the affinity of the ligand/receptor complex. Moreover, some of these mechanisms can occur simultaneously and change their dynamics over disease progression.

The GABA<sub>A</sub> receptor is ligand-gated ion channel with five subunits out of six types of  $\alpha$  subunits, three subunits of  $\beta$  and  $\gamma$  as well as a subunit of the types  $\delta$ ,  $\epsilon$ ,  $\pi$  and  $\theta$  (Jacob, Moss et al. 2008). (Figure 26). There are numerous subunit isoforms for the GABA<sub>A</sub> receptor, which determine the receptor's agonist affinity, chance of opening, conductance, and other properties. GABA<sub>A</sub> receptor protein complex is also a molecular target for benzodiazepines. Benzodiazepines do not bind to the same receptor site on the protein complex as the endogenous ligand GABA (whose binding site is located between  $\alpha$ - and  $\beta$ -subunits), but bind to distinct benzodiazepine binding sites situated at the interface between the  $\alpha$ - and  $\gamma$ -subunits of  $\alpha$ - and  $\gamma$ -subunit containing GABA<sub>A</sub> receptors. Different benzodiazepines have different affinities for GABA<sub>A</sub> receptors made up of different collection of subunits, and this means that their pharmacological profile varies with subtype selectivity.

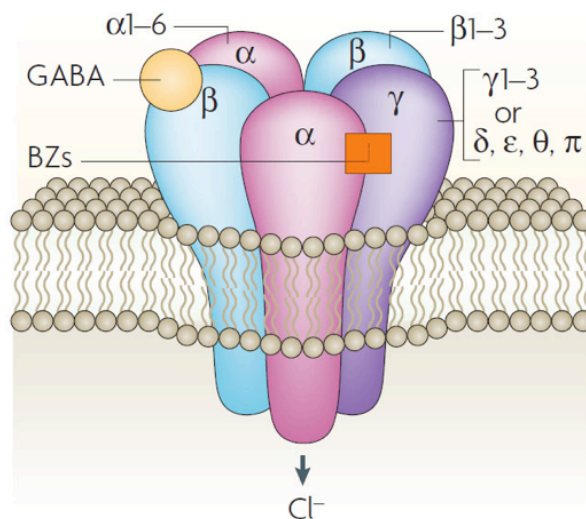


**Figure 26.** GABA<sub>A</sub> Receptor scheme (Jacob, Moss et al. 2008).

In particular, 11C-FMZ binds reversely with high affinity to the benzodiazepine site of GABA<sub>A</sub> receptors containing the  $\alpha_1$ -,  $\alpha_2$ -,  $\alpha_3$  or  $\alpha_5$ -subunits, and less so to those containing  $\alpha_4$ - or  $\alpha_6$ -subunits (Sieghart 1995).

Despite it is impossible to distinguish whether increased ligand binding results from decreased competition with endogenous benzodiazepines or an increased number or increased affinity of GABA<sub>A</sub> receptors, it is intriguing that  $\alpha_1^-/\alpha_1^-$  transgenic mice and patients with essential tremor respond to similar drugs (e.g., propranolol, primidone, and gabapentin), whereas the most significant tremorolytic effect in transgenic mice can be induced by low, non-sedating dosages of alcohol (Kralic, Criswell et al. 2005). This is an important analogy to the tremorolytic effect of alcohol in alcohol-responsive ET patients - an effect that is presumed to be mediated by GABAergic mechanisms as well. Ethanol reduces ET amplitude in up to 67% of patients, whereas the efficacy of diazepam is far lower (Zeuner, Molloy et al. 2003). This finding implies that alcohol is not acting solely via central benzodiazepine receptor agonistic action but may also have other effects - for example, suppressing sodium ion channel activity (Mullin and Hunt 1987) or transiently decreasing nerve membrane conductance (Reed and Chan 1980).

This study provides neuroimaging evidence of abnormally increased GABA<sub>A</sub> receptor binding in ET that is potentially linked to the rhythmic overactivity within the cerebellothalamic output pathways. Results support the GABA hypothesis of ET using in vivo 11C-FMZ PET in humans (Boecker, Weindl et al. 2010). The increased 11C-FMZ binding in cerebellothalamic pathways anatomically overlaps previous H<sub>2</sub><sup>15</sup>O PET regional cerebral blood flow increases (Colebatch, Findley et al. 1990; Wills, Jenkins et al. 1994; Boecker, Wills et al. 1996) and raised metabolism (Hallett and Dubinsky 1993; Louis, Shungu et al. 2002). This study demonstrates a GABAergic dysfunction in patients with ET, thus providing an independent measure of pathophysiologic and treatment-related interest in ET. Extending these studies to at-risk subjects for ET or using deep brain stimulation to test whether the changes in FMZ binding are normalized after this procedure would provide a means to understand whether the binding changes are primary or secondary phenomena.

PET imaging plays a critical role in both clinical and research applications with regard to neurological disorders. PET is useful in the initial diagnosis of patients presenting several neurological diseases and can help clinicians determine the best course of each therapy. PET studies can also be useful for studying the response to therapy. From the research perspective, the various neurotransmitter and other molecular tracers currently available or in development will provide substantial information about pathophysiologic process in the brain. As such applications become more widely tested, their introduction into the clinical arena will further advance the use of PET imaging in the evaluation and management of neurological disorders.

The widespread use of PET is at the moment limited by the high operational and maintenance costs of cyclotrons and radiochemistry equipment that are needed to produce the short-lived radioactive tracers for PET scanning and the need for specialized onsite chemical synthesis apparatus to produce radioactive tracers. In the future, the new microcyclotrons coupled with microchemistry labelling, already discussed in section 1.1.7, will likely overcome this limitation: the costs associated to the installation of cyclotrons in terms of space and shielding will certainly decrease (Nutt, Vento et al. 2007). The development of tracers with long half-life such as the ones labelled with  $^{18}\text{F}$  is highly desirable for use in a clinical setting and can overcome the financial and operational difficulties of running cyclotrons. Nevertheless,  $^{11}\text{C}$  tracers with the ability to enabling labelling of a number of molecules, remain essential for the development of new targets.

In addition, there are some regulatory limitations. One of the significant issues with biomarkers is that, from a process viewpoint, they are treated by the competent regulatory agencies in the same way as therapeutic drugs. This would not be significantly detrimental to the medical community except that financial justification cannot be made for the investment comparable to the investment the pharmaceutical industry makes to obtain EMEA or FDA approval for a single drug. Should the organizations create a specific and accurate protocol for PET radiotracers, this simplification could make important biomarkers available for clinical trials for therapeutic drugs and for use by physicians to diagnose, optimize, and personalize treatment of numerous diseases, resulting in reduced morbidity and mortality, as well as improve the cost effectiveness

of health care with a demonstrable return on investment. In vivo molecular imaging with PET biomarkers is therefore a significant public health issue that requires urgent dialogue and action (Nutt, Vento et al. 2007).

Regarding to PET image processing, improvements in the post-processing techniques continue apace, including partial volume effect correction, automated segmentation and co-registration. The major problem in the near future is the lack of expertise worldwide, both with respect to radiochemistry and data analysis (modelling). There clearly is an urgent need for more educational and training facilities. The lack of modelling expertise, in particular, has led to simplified (and sometimes inappropriate) scanning protocols, inaccurate image post-processing and quantification. These simplifications might be costly as they could lead to inaccurate results.



## 6. CONCLUSION

Several topics of dual-tracer molecular neuroimaging have been explored. The following contributions have been made in the course of the work presented in this dissertation:

\* It has been demonstrated, for the first time, that SDTT is practicable in vivo in rodent scanners. Besides, the impact of experimental settings on quantification accuracy has been studied. Using the SSRB with a span of 3 and a ring difference of 31, and acquiring for at least 20 min, independently of the frame duration, this technique does distinguish between the two-radiotracer images with similar SNR values to the initial dynamic image.

\* The SDTT procedure presented here does have its limitations; SDTT assumes that tracer concentrations do not change during the acquisition; therefore, SDTT is not applicable to kinetic studies. It can only be applied in static studies, when it can be ensured that both radiotracer concentrations do not vary. Nevertheless, these restrictions are similar to those usually found with diagnostic PET protocols using static imaging with  $^{18}\text{F}$ -FDG or  $^{13}\text{N}$ - $\text{NH}_4^+$ .

\* To apply SDTT using human scanners the number of coincidence events on human imaging voxel must be similar to that achieved on a typical rodent imaging 'voxel'. Apart from the difference between human and rodent scanners in terms of spatial resolution and sensitivity, there is another limitation in human studies; the injected radiotracer concentration. The per-voxel coincidence events achieved in this work were higher than those currently achievable in human studies. Reasonable per-voxel counting statistics on human scanners and, consequently, a reasonable SDTT performance, would require an increase in scanner sensitivity, an increase in voxel size or increase of total scanning time. However, this last option is limited to the kinetics of the employed radiotracers.

\* In the preclinical study, the SDTT have shown to be feasible in a rodent model of transient cerebral ischemia, obtaining results for both  $^{18}\text{F}$ -FDG and  $^{13}\text{N}$ - $\text{NH}_4^+$  very similar to those obtained in single tracer studies in

the same animal model (Martin, Rojas et al. 2009). Results from this study are encouraging and prove that this technique is practicable in rodent scanners.

\* In the clinical study, it has been demonstrated that ET symptomatology is associated with higher <sup>11</sup>C-FMZ binding in the cerebellum, suggesting a primary GABAergic deficiency or a functional abnormality at the level of GABA<sub>A</sub> receptor subtypes. The results reported are in agreement with the 'GABA hypothesis' in ET (Louis 1999) and with previous results with <sup>11</sup>C-FMZ PET in ET patients (Boecker, Weindl et al. 2010).

\* It has been also concluded that the serotonergic system probably is not involved in the pathophysiology of ET, since no serotonergic transporter dysfunction could be detected.

\* This preliminary study has several limitations. First, the relatively small number of patients included in the study might have impeded detecting subtler effects in either the GABAergic or serotonergic systems. Nevertheless, sample size is similar to those of previous PET studies. Second, PET does not allow discerning whether increased ligand binding results from decreased competition with endogenous neurotransmitter, increased concentration of the receptors, or altered receptor-ligand affinity. In addition, another limitation is that GABAergic effects may remain after the withdrawal of antitremoric drugs.

## REFERENCES

- Abe, O., S. Aoki, et al. (2002). "Normal aging in the central nervous system: quantitative MR diffusion-tensor analysis." *Neurobiology of aging* 23(3): 433-441.
- AIPES Conference. *Eur. J. Nucl. Med.*, MI 2007, 34, 806.
- Airey, D. C., F. Wu, et al. (2006). "Geometric morphometrics defines shape differences in the cortical area map of C57BL/6J and DBA/2J inbred mice." *BMC neuroscience* 7: 63.
- Archer, H. A., P. Edison, et al. (2006). "Amyloid load and cerebral atrophy in Alzheimer's disease: an 11C-PIB positron emission tomography study." *Annals of neurology* 60(1): 145-147.
- Arshaduddin, M., S. Al Kadasah, et al. (2004). "Citalopram, a selective serotonin reuptake inhibitor augments harmaline-induced tremor in rats." *Behavioural brain research* 153(1): 15-20.
- Ashburner, J. and K. J. Friston (2000). "Voxel-based morphometry--the methods." *NeuroImage* 11(6 Pt 1): 805-821.
- Backes, H., M. Walberer, et al. (2011). "Whiskers area as extracerebral reference tissue for quantification of rat brain metabolism using (18)F-FDG PET: application to focal cerebral ischemia." *Journal of nuclear medicine : official publication, Society of Nuclear Medicine* 52(8): 1252-1260.
- Badawi, R. D., P. K. Marsden, et al. (1996). "Optimization of noise-equivalent count rates in 3D PET." *Physics in medicine and biology* 41(9): 1755-1776.
- Badawi RD. *Aspects of Optimization and Quantification in Three-Dimensional Positron Emission Tomography* [PhD thesis]. London, U.K.: University of London; 1998:20–159. Bendriem B, Townsend DW. *The Theory and Practice of 3D PET*. Dordrecht, The Netherlands: Kluwer Academic; 1998.
- Badawi RD, Lodge MA, Marsden PK. Algorithms for calculating detector efficiency normalization coefficients for true coincidences in 3D PET, *Phys Med Biol* 1998;43:189–205.
- Badawi, R. D., M. P. Miller, et al. (1999). "Randoms variance reduction in 3D PET." *Physics in medicine and biology* 44(4): 941-954.
- Badawi RD, Marsden PK. Developments in component-based normalization for 3D PET. *Phys Med Biol* 1999;44:571–594.
- Badawi RD, Ferreira NC, Kohlmyer SG, Dahlbom M, Marsden PK,

- Lewellen TK. A comparison of normalization effects on three whole-body cylindrical 3D PET systems. *Phys Med Biol* 2000;45:3253–3266.
- Bailey, D. L. and S. R. Meikle (1994). "A convolution-subtraction scatter correction method for 3D PET." *Physics in medicine and biology* 39(3): 411-424.
- Bailey DL, Townsend DW, Kinahan PE, Grootenck S, Jones T. An investigation of factors affecting detector and geometric correction in normalization of 3-D PET data. *IEEE Trans Nucl Sci* 1996;43:3300–3307.
- Bailey, D. L., Karp, J. S., & S., S. Surti. *Positron emission tomography: Basic science and clinical practice*. Springer. 2003
- Bailey, D. L., Karp, J. S., & Surti, S. 2005. *Positron emission tomography: Basic sciences*. Springer. 2005
- Baron, J. C., M. G. Bousser, et al. (1981). "Reversal of focal "misery-perfusion syndrome" by extra-intracranial arterial bypass in hemodynamic cerebral ischemia. A case study with 15O positron emission tomography." *Stroke; a journal of cerebral circulation* 12(4): 454-459.
- Baron, J. C., D. Rougemont, et al. (1984). "Local interrelationships of cerebral oxygen consumption and glucose utilization in normal subjects and in ischemic stroke patients: a positron tomography study." *Journal of cerebral blood flow and metabolism : official journal of the International Society of Cerebral Blood Flow and Metabolism* 4(2): 140-149.
- Bartenstein, P., S. Asenbaum, et al. (2002). "European Association of Nuclear Medicine procedure guidelines for brain imaging using [(18)F]FDG." *European journal of nuclear medicine and molecular imaging* 29(10): BP43-48.
- Batini, C., C. Buisseret-Delmas, et al. (1981). "Harmaline-induced tremor. I. Regional metabolic activity as revealed by [14C]2-deoxyglucose in cat." *Experimental brain research. Experimentelle Hirnforschung. Experimentation cerebrale* 42(3-4): 371-382.
- Benamer, T. S., J. Patterson, et al. (2000). "Accurate differentiation of parkinsonism and essential tremor using visual assessment of [123I]-FP-CIT SPECT imaging: the [123I]-FP-CIT study group." *Movement disorders : official journal of the Movement Disorder Society* 15(3): 503-510.
- Bendriem B, Townsend DW. *The Theory and Practice of 3D PET*. Dordrecht, The Netherlands: Kluwer Academic; 1998.

- Bentourkia, M., P. Msaki, et al. (1995). "Assessment of scatter components in high-resolution PET: correction by nonstationary convolution subtraction." *Journal of nuclear medicine : official publication, Society of Nuclear Medicine* 36(1): 121-130.
- Bernard, J. F., C. Buisseret-Delmas, et al. (1984). "Harmaline induced tremor. III. A combined simple units, horseradish peroxidase, and 2-deoxyglucose study of the olivocerebellar system in the rat." *Experimental brain research. Experimentelle Hirnforschung. Experimentation cerebrale* 57(1): 128-137.
- Berti, V., A. Pupi, et al. (2011). "PET/CT in diagnosis of movement disorders." *Annals of the New York Academy of Sciences* 1228: 93-108.
- Bezard, E., A. R. Crossman, et al. (2001). "Structures outside the basal ganglia may compensate for dopamine loss in the presymptomatic stages of Parkinson's disease." *FASEB journal : official publication of the Federation of American Societies for Experimental Biology* 15(6): 1092-1094.
- Birattari, C., M. Bonardi, et al. (1987). "Biomedical applications of cyclotrons and review of commercially available models." *J Med Eng Technol* 11(4): 166-176.
- Bloomfield, P. M., S. Rajeswaran, et al. (1995). "The design and physical characteristics of a small animal positron emission tomograph." *Physics in medicine and biology* 40(6): 1105-1126.
- Boecker, H. and D. J. Brooks (1998). "Functional imaging of tremor." *Movement disorders : official journal of the Movement Disorder Society* 13 Suppl 3: 64-72.
- Boecker, H., A. Weindl, et al. (2010). "GABAergic dysfunction in essential tremor: an 11C-flumazenil PET study." *Journal of nuclear medicine : official publication, Society of Nuclear Medicine* 51(7): 1030-1035.
- Boecker, H., A. J. Wills, et al. (1996). "The effect of ethanol on alcohol-responsive essential tremor: a positron emission tomography study." *Annals of neurology* 39(5): 650-658.
- Boellaard, R., N. C. Krak, et al. (2004). "Effects of noise, image resolution, and ROI definition on the accuracy of standard uptake values: a simulation study." *Journal of nuclear medicine : official publication, Society of Nuclear Medicine* 45(9): 1519-1527.
- Boellaard, R., A. van Lingen, et al. (2001). "Experimental and clinical evaluation of iterative reconstruction (OSEM) in dynamic PET: quantitative characteristics and effects on kinetic modeling." *Journal of nuclear medicine : official publication, Society of Nuclear Medicine* 42(5): 808-817.

- Bohnen, N. I., D. S. Djang, et al. (2012). "Effectiveness and safety of 18F-FDG PET in the evaluation of dementia: a review of the recent literature." *Journal of nuclear medicine : official publication, Society of Nuclear Medicine* 53(1): 59-71.
- Bookstein, F. L. (2001). "'Voxel-based morphometry" should not be used with imperfectly registered images." *NeuroImage* 14(6): 1454-1462.
- Borghammer, P., M. Chakravarty, et al. (2010). "Cortical hypometabolism and hypoperfusion in Parkinson's disease is extensive: probably even at early disease stages." *Brain structure & function* 214(4): 303-317.
- Borghammer, P., P. Cumming, et al. (2009). "Subcortical elevation of metabolism in Parkinson's disease--a critical reappraisal in the context of global mean normalization." *NeuroImage* 47(4): 1514-1521.
- Brix, G., J. Zaers, et al. (1997). "Performance evaluation of a whole-body PET scanner using the NEMA protocol. National Electrical Manufacturers Association." *Journal of nuclear medicine : official publication, Society of Nuclear Medicine* 38(10): 1614-1623.
- Brooks, D. J. (1993). "PET studies on the early and differential diagnosis of Parkinson's disease." *Neurology* 43(12 Suppl 6): S6-16.
- Brooks, D. J., E. D. Playford, et al. (1992). "Isolated tremor and disruption of the nigrostriatal dopaminergic system: an 18F-dopa PET study." *Neurology* 42(8): 1554-1560.
- Broussolle, E., C. Dentesangle, et al. (1999). "The relation of putamen and caudate nucleus 18F-Dopa uptake to motor and cognitive performances in Parkinson's disease." *Journal of the neurological sciences* 166(2): 141-151.
- Browne, J. and A. B. de Pierro (1996). "A row-action alternative to the EM algorithm for maximizing likelihood in emission tomography." *IEEE transactions on medical imaging* 15(5): 687-699.
- Bruck, A., S. Aalto, et al. (2009). "A follow-up study on 6-[18F]fluoro-L-dopa uptake in early Parkinson's disease shows nonlinear progression in the putamen." *Movement disorders : official journal of the Movement Disorder Society* 24(7): 1009-1015.
- Bucher, S. F., K. C. Seelos, et al. (1997). "Activation mapping in essential tremor with functional magnetic resonance imaging." *Annals of neurology* 41(1): 32-40.
- Burn, D. J., G. V. Sawle, et al. (1994). "Differential diagnosis of Parkinson's disease, multiple system atrophy, and Steele-Richardson-Olszewski syndrome: discriminant analysis of striatal

- 18F-dopa PET data." *Journal of neurology, neurosurgery, and psychiatry* 57(3): 278-284.
- Cagnin, A., D. J. Brooks, et al. (2001). "In-vivo measurement of activated microglia in dementia." *Lancet* 358(9280): 461-467.
- Carmichael, S. T. (2005). "Rodent models of focal stroke: size, mechanism, and purpose." *NeuroRx : the journal of the American Society for Experimental NeuroTherapeutics* 2(3): 396-409.
- Carter, S. F., M. Scholl, et al. (2012). "Evidence for astrocytosis in prodromal Alzheimer disease provided by 11C-deuterium-L-deprenyl: a multitracer PET paradigm combining 11C-Pittsburgh compound B and 18F-FDG." *Journal of nuclear medicine : official publication, Society of Nuclear Medicine* 53(1): 37-46.
- Casey, M. E. and E. J. Hoffman (1986). "Quantitation in positron emission computed tomography: 7. A technique to reduce noise in accidental coincidence measurements and coincidence efficiency calibration." *Journal of computer assisted tomography* 10(5): 845-850.
- Casey ME, Gadagkar H and Newport D "A component based method for normalisation in volume PET" *Proceedings of the 3rd International Meeting on Fully Three-Dimensional Image Reconstruction in Radiology and Nuclear Medicine, Aix-les-Bains, France, 1995*
- Casteels, C., P. Vermaelen, et al. (2006). "Construction and evaluation of multitracer small-animal PET probabilistic atlases for voxel-based functional mapping of the rat brain." *Journal of nuclear medicine : official publication, Society of Nuclear Medicine* 47(11): 1858-1866.
- Cherry, S. R., M. Dahlbom, et al. (1991). "3D PET using a conventional multislice tomograph without septa." *Journal of computer assisted tomography* 15(4): 655-668.
- Cherry, S. R., S. R. Meikle, et al. (1993). "Correction and characterization of scattered events in three-dimensional PET using scanners with retractable septa." *Journal of nuclear medicine : official publication, Society of Nuclear Medicine* 34(4): 671-678.
- Cherry SR and Huang S-C (1995) "Effects of Scatter on Model Parameter Estimates in 3D PET Studies of the Human Brain" *IEEE Trans. Nucl. Sci.* 42(4), 1174-1179
- Cherry SR, Phelps ME. (1996) *Positron emission tomography: methods and instrumentation*. In: Sandler MP, Coleman RE, Wackers FJT, Patton JA, Gottschalk A, Hoffer PB, eds. *Diagnostic Nuclear Medicine*. 3rd ed. Baltimore, MD: Williams & Wilkins;139–159.

- Cherry, S. R., Sorenson, J. A., & Phelps, M. E. (2003) *Physics in nuclear medicine*. Saunders.
- Chesselet, M. F. (2005). "Animal models of neurological disorders." *NeuroRx : the journal of the American Society for Experimental NeuroTherapeutics* 2(3): 395.
- Choi, S. R., G. Golding, et al. (2009). "Preclinical properties of 18F-AV-45: a PET agent for Abeta plaques in the brain." *Journal of nuclear medicine : official publication, Society of Nuclear Medicine* 50(11): 1887-1894.
- Chow, P. L., F. R. Rannou, et al. (2005). "Attenuation correction for small animal PET tomographs." *Physics in medicine and biology* 50(8): 1837-1850.
- Colebatch, J. G., L. J. Findley, et al. (1990). "Preliminary report: activation of the cerebellum in essential tremor." *Lancet* 336(8722): 1028-1030.
- Daniels, C., M. Peller, et al. (2006). "Voxel-based morphometry shows no decreases in cerebellar gray matter volume in essential tremor." *Neurology* 67(8): 1452-1456.
- Davatzikos, C. (2004). "Why voxel-based morphometric analysis should be used with great caution when characterizing group differences." *NeuroImage* 23(1): 17-20.
- de la Fuente-Fernandez, R., V. Sossi, et al. (2004). "Levodopa-induced changes in synaptic dopamine levels increase with progression of Parkinson's disease: implications for dyskinesias." *Brain : a journal of neurology* 127(Pt 12): 2747-2754.
- de la Fuente-Fernandez, R., V. Sossi, et al. (2009). "Visualizing vesicular dopamine dynamics in Parkinson's disease." *Synapse* 63(8): 713-716.
- Defrise M, Townsend DW, Bailey D, Geissbuhler A, Michel C, Jones T. A normalization technique for 3D PET data. *Phys Med Biol* 1991;36:939-952. 18.
- Defrise, M., P. E. Kinahan, et al. (1997). "Exact and approximate rebinning algorithms for 3-D PET data." *IEEE transactions on medical imaging* 16(2): 145-158.
- Defrise, M. and G. T. Gullberg (2006). "Image reconstruction." *Physics in medicine and biology* 51(13): R139-154.
- Desco, M., Pascau, J., Reig, S., et al (2001) 'Multimodality image quantification using Talairach grid.' In *Proceedings of SPIE Medical Imaging*, vol. 4332, pp.1385-1392. San Diego, CA: IEEE.

- Devanand, D. P., A. Mikhno, et al. (2010). "Pittsburgh compound B (11C-PIB) and fluorodeoxyglucose (18 F-FDG) PET in patients with Alzheimer disease, mild cognitive impairment, and healthy controls." *Journal of geriatric psychiatry and neurology* 23(3): 185-198.
- Diehl-Schmid, J., T. Grimmer, et al. (2007). "Decline of cerebral glucose metabolism in frontotemporal dementia: a longitudinal 18F-FDG-PET-study." *Neurobiology of aging* 28(1): 42-50.
- Doder, M., E. A. Rabiner, et al. (2003). "Tremor in Parkinson's disease and serotonergic dysfunction: an 11C-WAY 100635 PET study." *Neurology* 60(4): 601-605.
- Drzezga, A., T. Grimmer, et al. (2008). "Imaging of amyloid plaques and cerebral glucose metabolism in semantic dementia and Alzheimer's disease." *NeuroImage* 39(2): 619-633.
- Drzezga, A., T. Grimmer, et al. (2005). "Prediction of individual clinical outcome in MCI by means of genetic assessment and (18)F-FDG PET." *Journal of nuclear medicine : official publication, Society of Nuclear Medicine* 46(10): 1625-1632.
- Drzezga, A., N. Lautenschlager, et al. (2003). "Cerebral metabolic changes accompanying conversion of mild cognitive impairment into Alzheimer's disease: a PET follow-up study." *European journal of nuclear medicine and molecular imaging* 30(8): 1104-1113.
- Dunphy, M. P. and J. S. Lewis (2009). "Radiopharmaceuticals in preclinical and clinical development for monitoring of therapy with PET." *Journal of nuclear medicine : official publication, Society of Nuclear Medicine* 50 Suppl 1: 106S-121S.
- Eckert, T., A. Barnes, et al. (2005). "FDG PET in the differential diagnosis of parkinsonian disorders." *NeuroImage* 26(3): 912-921.
- Edison, P., C. C. Rowe, et al. (2008). "Amyloid load in Parkinson's disease dementia and Lewy body dementia measured with [11C]PIB positron emission tomography." *Journal of neurology, neurosurgery, and psychiatry* 79(12): 1331-1338.
- Eidelberg, D., J. R. Moeller, et al. (1994). "The metabolic topography of parkinsonism." *Journal of cerebral blood flow and metabolism : official journal of the International Society of Cerebral Blood Flow and Metabolism* 14(5): 783-801.
- Engler, H., A. F. Santillo, et al. (2008). "In vivo amyloid imaging with PET in frontotemporal dementia." *European journal of nuclear medicine and molecular imaging* 35(1): 100-106.

- Fahey, F. H. (2002). "Data acquisition in PET imaging." *Journal of nuclear medicine technology* 30(2): 39-49.
- Fang, Y. H. and R. F. Muzic, Jr. (2008). "Spillover and partial-volume correction for image-derived input functions for small-animal 18F-FDG PET studies." *Journal of nuclear medicine : official publication, Society of Nuclear Medicine* 49(4): 606-614.
- Fearnley, J. M. and A. J. Lees (1991). "Ageing and Parkinson's disease: substantia nigra regional selectivity." *Brain : a journal of neurology* 114 ( Pt 5): 2283-2301.
- Fleming, S. M., P. O. Fernagut, et al. (2005). "Genetic mouse models of parkinsonism: strengths and limitations." *NeuroRx : the journal of the American Society for Experimental NeuroTherapeutics* 2(3): 495-503.
- Forsberg, A., H. Engler, et al. (2008). "PET imaging of amyloid deposition in patients with mild cognitive impairment." *Neurobiology of aging* 29(10): 1456-1465.
- Fox, S. H., R. Chuang, et al. (2009). "Serotonin and Parkinson's disease: On movement, mood, and madness." *Movement disorders : official journal of the Movement Disorder Society* 24(9): 1255-1266.
- Friedland, R. P., E. Koss, et al. (1993). "Functional imaging, the frontal lobes, and dementia." *Dementia* 4(3-4): 192-203.
- Frost, J. J., A. J. Rosier, et al. (1993). "Positron emission tomographic imaging of the dopamine transporter with 11C-WIN 35,428 reveals marked declines in mild Parkinson's disease." *Annals of neurology* 34(3): 423-431.
- Fu, Y. K., C. J. Chang, et al. (2009). "Imaging of regional metabolic activity by (18)F-FDG/PET in rats with transient cerebral ischemia." *Applied radiation and isotopes : including data, instrumentation and methods for use in agriculture, industry and medicine* 67(10): 1743-1747.
- Fukumoto, D., T. Hosoya, et al. (2011). "Multiparametric assessment of acute and subacute ischemic neuronal damage: a small animal positron emission tomography study with rat photochemically induced thrombosis model." *Synapse* 65(3): 207-214.
- Garnett, E. S., G. Firnau, et al. (1983). "Dopamine visualized in the basal ganglia of living man." *Nature* 305(5930): 137-138.
- Ghaemi, M., R. Hilker, et al. (2002). "Differentiating multiple system atrophy from Parkinson's disease: contribution of striatal and midbrain MRI volumetry and multi-tracer PET imaging." *Journal of neurology, neurosurgery, and psychiatry* 73(5): 517-523.

- Gholipour, A., N. Kehtarnavaz, et al. (2007). "Brain functional localization: a survey of image registration techniques." *IEEE transactions on medical imaging* 26(4): 427-451.
- Gjedde, A. and M. Rasmussen (1980). "Pentobarbital anesthesia reduces blood-brain glucose transfer in the rat." *Journal of neurochemistry* 35(6): 1382-1387.
- Goerendt, I. K., C. Messa, et al. (2003). "Dopamine release during sequential finger movements in health and Parkinson's disease: a PET study." *Brain : a journal of neurology* 126(Pt 2): 312-325.
- Grootenck, S., T. J. Spinks, et al. (1996). "Correction for scatter in 3D brain PET using a dual energy window method." *Physics in medicine and biology* 41(12): 2757-2774.
- Guttman, M., J. Burkholder, et al. (1997). "[<sup>11</sup>C]RTI-32 PET studies of the dopamine transporter in early dopa-naïve Parkinson's disease: implications for the symptomatic threshold." *Neurology* 48(6): 1578-1583.
- Hakim, A. M., A. C. Evans, et al. (1989). "The effect of nimodipine on the evolution of human cerebral infarction studied by PET." *Journal of cerebral blood flow and metabolism : official journal of the International Society of Cerebral Blood Flow and Metabolism* 9(4): 523-534.
- Hallett, M. and R. M. Dubinsky (1993). "Glucose metabolism in the brain of patients with essential tremor." *Journal of the neurological sciences* 114(1): 45-48.
- Hamacher, K., H. H. Coenen, et al. (1986). "Efficient stereospecific synthesis of no-carrier-added 2-[<sup>18</sup>F]-fluoro-2-deoxy-D-glucose using aminopolyether supported nucleophilic substitution." *Journal of nuclear medicine : official publication, Society of Nuclear Medicine* 27(2): 235-238.
- Harri, M., T. Mika, et al. (2007). "Evaluation of partial volume effect correction methods for brain positron emission tomography: Quantification and reproducibility." *Journal of medical physics / Association of Medical Physicists of India* 32(3): 108-117.
- Hartmann, M. and F. Hartmann-Vareilles (2006). "The clinical trials directive: how is it affecting Europe's noncommercial research?" *PLoS clinical trials* 1(2): e13.
- Heiss, W. D. (2000). "Ischemic penumbra: evidence from functional imaging in man." *Journal of cerebral blood flow and metabolism : official journal of the International Society of Cerebral Blood Flow and Metabolism* 20(9): 1276-1293.

- Heiss, W. D., M. Grond, et al. (1998). "Permanent cortical damage detected by flumazenil positron emission tomography in acute stroke." *Stroke; a journal of cerebral circulation* 29(2): 454-461.
- Heiss, W. D., M. Grond, et al. (1998). "Tissue at risk of infarction rescued by early reperfusion: a positron emission tomography study in systemic recombinant tissue plasminogen activator thrombolysis of acute stroke." *Journal of cerebral blood flow and metabolism : official journal of the International Society of Cerebral Blood Flow and Metabolism* 18(12): 1298-1307.
- Heiss, W. D., V. Holthoff, et al. (1990). "Effect of nimodipine on regional cerebral glucose metabolism in patients with acute ischemic stroke as measured by positron emission tomography." *Journal of cerebral blood flow and metabolism : official journal of the International Society of Cerebral Blood Flow and Metabolism* 10(1): 127-132.
- Heiss, W. D., J. Kessler, et al. (1993). "Cerebral glucose metabolism as a predictor of recovery from aphasia in ischemic stroke." *Archives of neurology* 50(9): 958-964.
- Heiss, W. D., J. Kessler, et al. (1999). "Differential capacity of left and right hemispheric areas for compensation of poststroke aphasia." *Annals of neurology* 45(4): 430-438.
- Hilker, R., K. Schweitzer, et al. (2005). "Nonlinear progression of Parkinson disease as determined by serial positron emission tomographic imaging of striatal fluorodopa F 18 activity." *Archives of neurology* 62(3): 378-382.
- Hjornevik, T., T. B. Leergaard, et al. (2007). "Three-dimensional atlas system for mouse and rat brain imaging data." *Frontiers in neuroinformatics* 1: 4.
- Hoekzema, E., S. Rojas, et al. (2011). "In vivo molecular imaging of the GABA/benzodiazepine receptor complex in the aged rat brain." *Neurobiology of aging*.
- Howells, D. W., M. J. Porritt, et al. (2010). "Different strokes for different folks: the rich diversity of animal models of focal cerebral ischemia." *Journal of cerebral blood flow and metabolism : official journal of the International Society of Cerebral Blood Flow and Metabolism* 30(8): 1412-1431.
- Huang, S. C., R. E. Carson, et al. (1982). "An investigation of a double-tracer technique for positron computerized tomography." *Journal of nuclear medicine : official publication, Society of Nuclear Medicine* 23(9): 816-822.

- Hudson, H. M. and R. S. Larkin (1994). "Accelerated image reconstruction using ordered subsets of projection data." *IEEE transactions on medical imaging* 13(4): 601-609.
- Hughes, J. L., P. S. Jones, et al. (2012). "A microPET study of the regional distribution of [11C]-PK11195 binding following temporary focal cerebral ischemia in the rat. Correlation with post mortem mapping of microglia activation." *NeuroImage* 59(3): 2007-2016.
- Hume, S. P., A. A. Lammertsma, et al. (1992). "Quantification of in vivo binding of [3H]RX 821002 in rat brain: evaluation as a radioligand for central alpha 2-adrenoceptors." *International journal of radiation applications and instrumentation. Part B, Nuclear medicine and biology* 19(8): 841-849.
- IAEA, 2006. *Directory of Cyclotron used for Radionuclide Production Members States 2006 Update*. IAEA-DCRP/2006.
- IAEA, 2009. *Cyclotron Produced Radionuclides: Physical characteristics and Production Methods*. Technical Reports series No. 468
- Ichise, M., J. S. Liow, et al. (2003). "Linearized reference tissue parametric imaging methods: application to [11C]DASB positron emission tomography studies of the serotonin transporter in human brain." *Journal of cerebral blood flow and metabolism : official journal of the International Society of Cerebral Blood Flow and Metabolism* 23(9): 1096-1112.
- Ido T, Wan CN, Fowler JS: Fluorination with F2: convenient synthesis of 2-deoxy-2-fluoro-d-glucose. *J Org Chem* 42:2341-2342, 1977
- Imaizumi, M., H. J. Kim, et al. (2007). "PET imaging with [11C]PBR28 can localize and quantify upregulated peripheral benzodiazepine receptors associated with cerebral ischemia in rat." *Neuroscience letters* 411(3): 200-205.
- Ingvar, M., L. Eriksson, et al. (1991). "Rapid feasibility studies of tracers for positron emission tomography: high-resolution PET in small animals with kinetic analysis." *Journal of cerebral blood flow and metabolism : official journal of the International Society of Cerebral Blood Flow and Metabolism* 11(6): 926-931.
- Innis, R. B., V. J. Cunningham, et al. (2007). "Consensus nomenclature for in vivo imaging of reversibly binding radioligands." *Journal of cerebral blood flow and metabolism : official journal of the International Society of Cerebral Blood Flow and Metabolism* 27(9): 1533-1539.
- Jack, C. R., Jr., H. J. Wiste, et al. (2010). "Brain beta-amyloid measures and magnetic resonance imaging atrophy both predict time-to-

- progression from mild cognitive impairment to Alzheimer's disease." *Brain : a journal of neurology* 133(11): 3336-3348.
- Jacob, T. C., S. J. Moss, et al. (2008). "GABA(A) receptor trafficking and its role in the dynamic modulation of neuronal inhibition." *Nature reviews. Neuroscience* 9(5): 331-343.
- Jagoda, E. M., J. J. Vaquero, et al. (2004). "Experiment assessment of mass effects in the rat: implications for small animal PET imaging." *Nuclear medicine and biology* 31(6): 771-779.
- Jankovic, J. (2002). "Essential tremor: a heterogenous disorder." *Movement disorders : official journal of the Movement Disorder Society* 17(4): 638-644.
- Karbe, H., J. Kessler, et al. (1995). "Long-term prognosis of poststroke aphasia studied with positron emission tomography." *Archives of neurology* 52(2): 186-190.
- Karbe, H., A. Thiel, et al. (1998). "Brain plasticity in poststroke aphasia: what is the contribution of the right hemisphere?" *Brain and language* 64(2): 215-230.
- Kemp, B. J., C. Kim, et al. (2006). "NEMA NU 2-2001 performance measurements of an LYSO-based PET/CT system in 2D and 3D acquisition modes." *Journal of nuclear medicine : official publication, Society of Nuclear Medicine* 47(12): 1960-1967.
- Kemppainen, N. M., S. Aalto, et al. (2006). "Voxel-based analysis of PET amyloid ligand [<sup>11</sup>C]PIB uptake in Alzheimer disease." *Neurology* 67(9): 1575-1580.
- Kim, C. K., N. C. Gupta, et al. (1994). "Standardized uptake values of FDG: body surface area correction is preferable to body weight correction." *Journal of nuclear medicine : official publication, Society of Nuclear Medicine* 35(1): 164-167.
- Koeppel, R. A., S. Gilman, et al. (2005). "<sup>11</sup>C-DTBZ and <sup>18</sup>F-FDG PET measures in differentiating dementias." *Journal of nuclear medicine : official publication, Society of Nuclear Medicine* 46(6): 936-944.
- Koller, W. C. (1989). "Tradozone in essential tremor. Probe of serotonergic mechanisms." *Clinical neuropharmacology* 12(2): 134-137.
- Koole, M., D. M. Lewis, et al. (2009). "Whole-body biodistribution and radiation dosimetry of <sup>18</sup>F-GE067: a radioligand for in vivo brain amyloid imaging." *Journal of nuclear medicine : official publication, Society of Nuclear Medicine* 50(5): 818-822.

- Kralic, J. E., H. E. Criswell, et al. (2005). "Genetic essential tremor in gamma-aminobutyric acidA receptor alpha1 subunit knockout mice." *The Journal of clinical investigation* 115(3): 774-779.
- Kralic, J. E., E. R. Korpi, et al. (2002). "Molecular and pharmacological characterization of GABA(A) receptor alpha1 subunit knockout mice." *The Journal of pharmacology and experimental therapeutics* 302(3): 1037-1045.
- Kuhl, D. E., M. E. Phelps, et al. (1980). "Effects of stroke on local cerebral metabolism and perfusion: mapping by emission computed tomography of 18FDG and 13NH3." *Annals of neurology* 8(1): 47-60.
- Lammertsma, A. A. and S. P. Hume (1996). "Simplified reference tissue model for PET receptor studies." *NeuroImage* 4(3 Pt 1): 153-158.
- Lassen, N. A. (1966). "The luxury-perfusion syndrome and its possible relation to acute metabolic acidosis localised within the brain." *Lancet* 2(7473): 1113-1115.
- Lee, C. C., G. Sui, et al. (2005). "Multistep synthesis of a radiolabeled imaging probe using integrated microfluidics." *Science* 310(5755): 1793-1796.
- Lee, C. S., A. Samii, et al. (2000). "In vivo positron emission tomographic evidence for compensatory changes in presynaptic dopaminergic nerve terminals in Parkinson's disease." *Annals of neurology* 47(4): 493-503.
- Leenders, K. L., E. P. Salmon, et al. (1990). "The nigrostriatal dopaminergic system assessed in vivo by positron emission tomography in healthy volunteer subjects and patients with Parkinson's disease." *Archives of neurology* 47(12): 1290-1298.
- Lenzi, G. L., R. S. Frackowiak, et al. (1982). "Cerebral oxygen metabolism and blood flow in human cerebral ischemic infarction." *Journal of cerebral blood flow and metabolism : official journal of the International Society of Cerebral Blood Flow and Metabolism* 2(3): 321-335.
- Levin CS, Dahlbom M and Hoffman EJ "A Monte-Carlo Correction for the Effect of Compton Scattering in 3-D PET Brain Imaging" *IEEE Trans. Nucl. Sci.* 42(4) 1181-1185, 1995
- Lin, K. J., Y. H. Weng, et al. (2010). "Whole-body biodistribution and radiation dosimetry of 18F-FP-(+)-DTBZ (18F-AV-133): a novel vesicular monoamine transporter 2 imaging agent." *Journal of nuclear medicine : official publication, Society of Nuclear Medicine* 51(9): 1480-1485.
- Llinas, R. and R. A. Volkind (1973). "The olivo-cerebellar system: functional properties as revealed by harmaline-induced tremor."

- Experimental brain research. Experimentelle Hirnforschung. Experimentation cerebrale 18(1): 69-87.
- Lonneux, M., I. Borbath, et al. (1999). "Attenuation correction in whole-body FDG oncological studies: the role of statistical reconstruction." *European journal of nuclear medicine* 26(6): 591-598.
- Loring, D. W., K. J. Meador, et al. (2002). "Now you see it, now you don't: statistical and methodological considerations in fMRI." *Epilepsy & behavior : E&B* 3(6): 539-547.
- Louis, E. D. (1999). "A new twist for stopping the shakes? Revisiting GABAergic therapy for essential tremor." *Archives of neurology* 56(7): 807-808.
- Louis, E. D. (2009). "Essential tremors: a family of neurodegenerative disorders?" *Archives of neurology* 66(10): 1202-1208.
- Louis, E. D., D. C. Shungu, et al. (2002). "Metabolic abnormality in the cerebellum in patients with essential tremor: a proton magnetic resonance spectroscopic imaging study." *Neuroscience letters* 333(1): 17-20.
- Louis, E. D., D. C. Shungu, et al. (2004). "Cerebellar metabolic symmetry in essential tremor studied with 1H magnetic resonance spectroscopic imaging: implications for disease pathology." *Movement disorders : official journal of the Movement Disorder Society* 19(6): 672-677.
- Lucignani, G., G. Paganelli, et al. (2004). "The use of standardized uptake values for assessing FDG uptake with PET in oncology: a clinical perspective." *Nuclear medicine communications* 25(7): 651-656.
- Luis, C. A., W. W. Barker, et al. (1999). "Sensitivity and specificity of three clinical criteria for dementia with Lewy bodies in an autopsy-verified sample." *International journal of geriatric psychiatry* 14(7): 526-533.
- Maetzler, W., M. Reimold, et al. (2008). "[11C]PIB binding in Parkinson's disease dementia." *NeuroImage* 39(3): 1027-1033.
- Marie, R. M., L. Barre, et al. (1995). "PET imaging of neocortical monoaminergic terminals in Parkinson's disease." *Journal of neural transmission. Parkinson's disease and dementia section* 9(1): 55-71.
- Martin, A., S. Rojas, et al. (2009). "Depressed glucose consumption at reperfusion following brain ischemia does not correlate with mitochondrial dysfunction and development of infarction: an in vivo positron emission tomography study." *Current neurovascular research* 6(2): 82-88.

- Matsumura, A., S. Mizokawa, et al. (2003). "Assessment of microPET performance in analyzing the rat brain under different types of anesthesia: comparison between quantitative data obtained with microPET and ex vivo autoradiography." *NeuroImage* 20(4): 2040-2050.
- Mazin, S. R. and N. J. Pele (2008). "Fourier rebinning algorithm for inverse geometry CT." *Medical physics* 35(11): 4857-4862.
- Miller, T. R. and J. W. Wallis (1992). "Clinically important characteristics of maximum-likelihood reconstruction." *Journal of nuclear medicine : official publication, Society of Nuclear Medicine* 33(9): 1678-1684.
- Miller, T. R. and J. W. Wallis (1992). "Fast maximum-likelihood reconstruction." *Journal of nuclear medicine : official publication, Society of Nuclear Medicine* 33(9): 1710-1711.
- Minoshima, S., N. L. Foster, et al. (2001). "Alzheimer's disease versus dementia with Lewy bodies: cerebral metabolic distinction with autopsy confirmation." *Annals of neurology* 50(3): 358-365.
- Mintun, M. A., G. N. Larossa, et al. (2006). "[11C]PIB in a nondemented population: potential antecedent marker of Alzheimer disease." *Neurology* 67(3): 446-452.
- Mirrone, M. M., W. K. Schiffer, et al. (2007). "A novel approach for imaging brain-behavior relationships in mice reveals unexpected metabolic patterns during seizures in the absence of tissue plasminogen activator." *NeuroImage* 38(1): 34-42.
- Montgomery, A. J., K. Thielemans, et al. (2006). "Correction of head movement on PET studies: comparison of methods." *Journal of nuclear medicine : official publication, Society of Nuclear Medicine* 47(12): 1936-1944.
- Mosconi, L. (2005). "Brain glucose metabolism in the early and specific diagnosis of Alzheimer's disease. FDG-PET studies in MCI and AD." *European journal of nuclear medicine and molecular imaging* 32(4): 486-510.
- Mosconi, L., M. Brys, et al. (2007). "Early detection of Alzheimer's disease using neuroimaging." *Experimental gerontology* 42(1-2): 129-138.
- Mosconi, L., R. Mistur, et al. (2009). "FDG-PET changes in brain glucose metabolism from normal cognition to pathologically verified Alzheimer's disease." *European journal of nuclear medicine and molecular imaging* 36(5): 811-822.
- Mullin, M. J. and W. A. Hunt (1987). "Effects of ethanol on the functional properties of sodium channels in brain synaptosomes." *Recent developments in alcoholism : an official publication of the*

- American Medical Society on Alcoholism, the Research Society on Alcoholism, and the National Council on Alcoholism 5: 303-311.
- Nagren, K., C. Halldin, et al. (2010). "Radiopharmaceuticals for positron emission tomography investigations of Alzheimer's disease." *European journal of nuclear medicine and molecular imaging* 37(8): 1575-1593.
- Nandhagopal, R., L. Kuramoto, et al. (2009). "Longitudinal progression of sporadic Parkinson's disease: a multi-tracer positron emission tomography study." *Brain : a journal of neurology* 132(Pt 11): 2970-2979.
- Neary, D., J. S. Snowden, et al. (1998). "Frontotemporal lobar degeneration: a consensus on clinical diagnostic criteria." *Neurology* 51(6): 1546-1554.
- Nelles, G., G. Spiekramann, et al. (1999). "Evolution of functional reorganization in hemiplegic stroke: a serial positron emission tomographic activation study." *Annals of neurology* 46(6): 901-909.
- Newberg, A. B. and A. Alavi (2005). "The role of PET imaging in the management of patients with central nervous system disorders." *Radiologic clinics of North America* 43(1): 49-65.
- Nutt, R., L. J. Vento, et al. (2007). "In vivo molecular imaging biomarkers: clinical pharmacology's new "PET"?" *Clinical pharmacology and therapeutics* 81(6): 792-795.
- O'Sullivan, S. S., K. Wu, et al. (2011). "Cue-induced striatal dopamine release in Parkinson's disease-associated impulsive-compulsive behaviours." *Brain : a journal of neurology* 134(Pt 4): 969-978.
- Ohyama, M., M. Senda, et al. (1996). "Role of the nondominant hemisphere and undamaged area during word repetition in poststroke aphasics. A PET activation study." *Stroke; a journal of cerebral circulation* 27(5): 897-903.
- Okello, A., P. Edison, et al. (2009). "Microglial activation and amyloid deposition in mild cognitive impairment: a PET study." *Neurology* 72(1): 56-62.
- Okello, A., J. Koivunen, et al. (2009). "Conversion of amyloid positive and negative MCI to AD over 3 years: an 11C-PIB PET study." *Neurology* 73(10): 754-760.
- Ollinger, J. M. (1996). "Model-based scatter correction for fully 3D PET." *Physics in medicine and biology* 41(1): 153-176.
- Panegyres, P. K., J. M. Rogers, et al. (2009). "Fluorodeoxyglucose-positron emission tomography in the differential diagnosis of

- early-onset dementia: a prospective, community-based study." *BMC neurology* 9: 41.
- Pascali, G., G. Nannavecchia, et al. (2011). "Dose-on-demand of diverse 18F-fluorocholine derivatives through a two-step microfluidic approach." *Nuclear medicine and biology* 38(5): 637-644.
- Phelps, M. E. (1977). "Emission computed tomography." *Seminars in nuclear medicine* 7(4): 337-365.
- Phelps, M. E. (2000). "Positron emission tomography provides molecular imaging of biological processes." *Proceedings of the National Academy of Sciences of the United States of America* 97(16): 9226-9233.
- Piccini, P., O. Lindvall, et al. (2000). "Delayed recovery of movement-related cortical function in Parkinson's disease after striatal dopaminergic grafts." *Annals of neurology* 48(5): 689-695.
- Piccini, P., N. Pavese, et al. (2003). "Endogenous dopamine release after pharmacological challenges in Parkinson's disease." *Annals of neurology* 53(5): 647-653.
- Poirier, L. J., T. L. Sourkes, et al. (1966). "Striatal amines, experimental tremor and the effect of harmaline in the monkey." *Brain : a journal of neurology* 89(1): 37-52.
- Politis, M., C. Loane, et al. (2011). "Serotonergic mediated body mass index changes in Parkinson's disease." *Neurobiology of disease* 43(3): 609-615.
- Politis, M. and P. Piccini (2012). "Positron emission tomography imaging in neurological disorders." *Journal of neurology*.
- Politis, M., P. Piccini, et al. (2008). "Evidence of dopamine dysfunction in the hypothalamus of patients with Parkinson's disease: an in vivo 11C-raclopride PET study." *Experimental neurology* 214(1): 112-116.
- Politis, M., K. Wu, et al. (2010). "Staging of serotonergic dysfunction in Parkinson's disease: an in vivo 11C-DASB PET study." *Neurobiology of disease* 40(1): 216-221.
- Politis, M., K. Wu, et al. (2010). "Depressive symptoms in PD correlate with higher 5-HTT binding in raphe and limbic structures." *Neurology* 75(21): 1920-1927.
- Politis, M., K. Wu, et al. (2010). "Parkinson's disease symptoms: the patient's perspective." *Movement disorders : official journal of the Movement Disorder Society* 25(11): 1646-1651.
- Price, J. C., W. E. Klunk, et al. (2005). "Kinetic modeling of amyloid binding in humans using PET imaging and Pittsburgh Compound-B." *Journal of cerebral blood flow and metabolism : official*

- journal of the International Society of Cerebral Blood Flow and Metabolism 25(11): 1528-1547.
- Rabinovici, G. D. and W. J. Jagust (2009). "Amyloid imaging in aging and dementia: testing the amyloid hypothesis in vivo." *Behavioural neurology* 21(1): 117-128.
- Rappaport, M. S., R. T. Gentry, et al. (1984). "Ethanol effects on harmaline-induced tremor and increase of cerebellar cyclic GMP." *Life sciences* 34(1): 49-56.
- Read, S. J., T. Hirano, et al. (2000). "The fate of hypoxic tissue on 18F-fluoromisonidazole positron emission tomography after ischemic stroke." *Annals of neurology* 48(2): 228-235.
- Reed, T. E. and J. Chan (1980). "Apparent rapid tolerance to ethanol for nerve conduction velocity." *Life sciences* 26(20): 1713-1720.
- Riddell, C., R. E. Carson, et al. (2001). "Noise reduction in oncology FDG PET images by iterative reconstruction: a quantitative assessment." *Journal of nuclear medicine : official publication, Society of Nuclear Medicine* 42(9): 1316-1323.
- Rinne, J. O., A. Laihininen, et al. (1995). "Increased density of dopamine D2 receptors in the putamen, but not in the caudate nucleus in early Parkinson's disease: a PET study with [11C]raclopride." *Journal of the neurological sciences* 132(2): 156-161.
- Rojas, S., J. R. Herance, et al. (2011). "Evaluation of hypoxic tissue dynamics with 18F-FMISO PET in a rat model of permanent cerebral ischemia." *Molecular imaging and biology : MIB : the official publication of the Academy of Molecular Imaging* 13(3): 558-564.
- Rojas, S., A. Martin, et al. (2007). "Imaging brain inflammation with [(11)C]PK11195 by PET and induction of the peripheral-type benzodiazepine receptor after transient focal ischemia in rats." *Journal of cerebral blood flow and metabolism : official journal of the International Society of Cerebral Blood Flow and Metabolism* 27(12): 1975-1986.
- Rojas, S., A. Martin, et al. (2011). "Positron emission tomography with 11C-flumazenil in the rat shows preservation of binding sites during the acute phase after 2h-transient focal ischemia." *Neuroscience* 182: 208-216.
- Rosen, H. J., S. E. Petersen, et al. (2000). "Neural correlates of recovery from aphasia after damage to left inferior frontal cortex." *Neurology* 55(12): 1883-1894.
- Rousset, O. G., Y. Ma, et al. (1998). "Correction for partial volume effects in PET: principle and validation." *Journal of nuclear medicine : official publication, Society of Nuclear Medicine* 39(5): 904-911.

- Rowe, C. C., U. Ackerman, et al. (2008). "Imaging of amyloid beta in Alzheimer's disease with 18F-BAY94-9172, a novel PET tracer: proof of mechanism." *Lancet neurology* 7(2): 129-135.
- Rowe, C. C., K. A. Ellis, et al. (2010). "Amyloid imaging results from the Australian Imaging, Biomarkers and Lifestyle (AIBL) study of aging." *Neurobiology of aging* 31(8): 1275-1283.
- Saita, K., M. Chen, et al. (2004). "Imaging the ischemic penumbra with 18F-fluoromisonidazole in a rat model of ischemic stroke." *Stroke; a journal of cerebral circulation* 35(4): 975-980.
- Salmon, E., D. J. Brooks, et al. (1990). "A two-compartment description and kinetic procedure for measuring regional cerebral [11C]nomifensine uptake using positron emission tomography." *Journal of cerebral blood flow and metabolism : official journal of the International Society of Cerebral Blood Flow and Metabolism* 10(3): 307-316.
- Sawamoto, N., P. Piccini, et al. (2008). "Cognitive deficits and striato-frontal dopamine release in Parkinson's disease." *Brain : a journal of neurology* 131(Pt 5): 1294-1302.
- Schneider, J. F., K. A. Il'yasov, et al. (2004). "Fast quantitative diffusion-tensor imaging of cerebral white matter from the neonatal period to adolescence." *Neuroradiology* 46(4): 258-266.
- Schulz, D. and P. Vaska (2011). "Integrating PET with behavioral neuroscience using RatCAP tomography." *Reviews in the neurosciences* 22(6): 647-655.
- Shao, L., R. Freifelder, et al. (1994). "Triple energy window scatter correction technique in PET." *IEEE transactions on medical imaging* 13(4): 641-648.
- Shimony, J. S., R. C. McKinstry, et al. (1999). "Quantitative diffusion-tensor anisotropy brain MR imaging: normative human data and anatomic analysis." *Radiology* 212(3): 770-784.
- Sieghart, W. (1995). "Structure and pharmacology of gamma-aminobutyric acidA receptor subtypes." *Pharmacological reviews* 47(2): 181-234.
- Sioka, C., A. Fotopoulos, et al. (2010). "Recent advances in PET imaging for evaluation of Parkinson's disease." *European journal of nuclear medicine and molecular imaging* 37(8): 1594-1603.
- Slifstein, M., R. V. Parsey, et al. (2000). "Derivation of [(11)C]WAY-100635 binding parameters with reference tissue models: effect of violations of model assumptions." *Nuclear medicine and biology* 27(5): 487-492.

- Snook, L., L. A. Paulson, et al. (2005). "Diffusion tensor imaging of neurodevelopment in children and young adults." *NeuroImage* 26(4): 1164-1173.
- Soto-Montenegro, M. L., J. J. Vaquero, et al. (2009). "Detection of visual activation in the rat brain using 2-deoxy-2-[(18F)]fluoro-D: -glucose and statistical parametric mapping (SPM)." *Molecular imaging and biology : MIB : the official publication of the Academy of Molecular Imaging* 11(2): 94-99.
- Spinks, T. J., T. Jones, et al. (2000). "Physical characteristics of the ECAT EXACT3D positron tomograph." *Physics in medicine and biology* 45(9): 2601-2618.
- Spires, T. L. and B. T. Hyman (2005). "Transgenic models of Alzheimer's disease: learning from animals." *NeuroRx : the journal of the American Society for Experimental NeuroTherapeutics* 2(3): 423-437.
- Stearns CW "Scatter correction method for 3D PET using 2D fitted Gaussian functions" *J. Nucl. Med.* 36 105P, 1995
- Su, K. H., J. S. Lee, et al. (2009). "Partial volume correction of the microPET blood input function using ensemble learning independent component analysis." *Physics in medicine and biology* 54(6): 1823-1846.
- Suzuki, Y., H. Matsuzawa, et al. (2003). "Absolute eigenvalue diffusion tensor analysis for human brain maturation." *NMR in biomedicine* 16(5): 257-260.
- Takasawa, M., J. S. Beech, et al. (2011). "Single-subject statistical mapping of acute brain hypoxia in the rat following middle cerebral artery occlusion: a microPET study." *Experimental neurology* 229(2): 251-258.
- Tantawy, M. N. and T. E. Peterson (2010). "Simplified [18F]FDG image-derived input function using the left ventricle, liver, and one venous blood sample." *Molecular imaging* 9(2): 76-86.
- Tartaglia, M. C., H. J. Rosen, et al. (2011). "Neuroimaging in dementia." *Neurotherapeutics : the journal of the American Society for Experimental NeuroTherapeutics* 8(1): 82-92.
- Tedroff, J., S. M. Aquilonius, et al. (1990). "Striatal kinetics of [11C]-(+)-nomifensine and 6-[18F]fluoro-L-dopa in Parkinson's disease measured with positron emission tomography." *Acta neurologica Scandinavica* 81(1): 24-30.
- Townsend DW, Defrise M. Image reconstruction methods in positron tomography. *CERN (European Organization for Nuclear Research) Report 93-0.2*. Ge-neva, Switzerland; 1993.

- Toyama, H., M. Ichise, et al. (2004). "Evaluation of anesthesia effects on [18F]FDG uptake in mouse brain and heart using small animal PET." *Nuclear medicine and biology* 31(2): 251-256.
- Vallabhajosula, S., L. Solnes, et al. (2011). "A broad overview of positron emission tomography radiopharmaceuticals and clinical applications: what is new?" *Seminars in nuclear medicine* 41(4): 246-264.
- Villemagne, V. L., K. Ong, et al. (2011). "Amyloid imaging with (18)F-florbetaben in Alzheimer disease and other dementias." *Journal of nuclear medicine : official publication, Society of Nuclear Medicine* 52(8): 1210-1217.
- Villemagne, V. L., K. E. Pike, et al. (2008). "Abeta deposits in older non-demented individuals with cognitive decline are indicative of preclinical Alzheimer's disease." *Neuropsychologia* 46(6): 1688-1697.
- Vingerhoets, F. J., M. Schulzer, et al. (1997). "Which clinical sign of Parkinson's disease best reflects the nigrostriatal lesion?" *Annals of neurology* 41(1): 58-64.
- Virdee, K., P. Cumming, et al. (2012). "Applications of positron emission tomography in animal models of neurological and neuropsychiatric disorders." *Neuroscience and biobehavioral reviews* 36(4): 1188-1216.
- Warburton, E., C. J. Price, et al. (1999). "Mechanisms of recovery from aphasia: evidence from positron emission tomography studies." *Journal of neurology, neurosurgery, and psychiatry* 66(2): 155-161.
- Wiley, C. A., B. J. Lopresti, et al. (2009). "Carbon 11-labeled Pittsburgh Compound B and carbon 11-labeled (R)-PK11195 positron emission tomographic imaging in Alzheimer disease." *Archives of neurology* 66(1): 60-67.
- Wills, A. J., I. H. Jenkins, et al. (1994). "Red nuclear and cerebellar but no olivary activation associated with essential tremor: a positron emission tomographic study." *Annals of neurology* 36(4): 636-642.
- Wimo, A., B. Winblad, et al. (2003). "The magnitude of dementia occurrence in the world." *Alzheimer disease and associated disorders* 17(2): 63-67.
- Wise, R. J., S. Bernardi, et al. (1983). "Serial observations on the pathophysiology of acute stroke. The transition from ischaemia to infarction as reflected in regional oxygen extraction." *Brain : a journal of neurology* 106 (Pt 1): 197-222.

- Woods, R. P., S. R. Cherry, et al. (1992). "Rapid automated algorithm for aligning and reslicing PET images." *Journal of computer assisted tomography* 16(4): 620-633.
- Yamamoto, S., M. Imaizumi, et al. (2010). "A compact and high sensitivity positron detector using dual-layer thin GSO scintillators for a small animal PET blood sampling system." *Physics in medicine and biology* 55(13): 3813-3826.
- Yoshiura, T., F. Mihara, et al. (2005). "Age-related structural changes in the young adult brain shown by magnetic resonance diffusion tensor imaging." *Academic radiology* 12(3): 268-275.
- Yui, J., A. Hatori, et al. (2011). "Visualization of early infarction in rat brain after ischemia using a translocator protein (18 kDa) PET ligand [<sup>11</sup>C]DAC with ultra-high specific activity." *NeuroImage* 54(1): 123-130.
- Yui, J., J. Maeda, et al. (2010). "<sup>18</sup>F-FEAC and <sup>18</sup>F-FEDAC: PET of the monkey brain and imaging of translocator protein (18 kDa) in the infarcted rat brain." *Journal of nuclear medicine : official publication, Society of Nuclear Medicine* 51(8): 1301-1309.
- Zasadny, K. R. and R. L. Wahl (1993). "Standardized uptake values of normal tissues at PET with 2-[fluorine-18]-fluoro-2-deoxy-D-glucose: variations with body weight and a method for correction." *Radiology* 189(3): 847-850.
- Zeng, G. L. (2001). "Image reconstruction--a tutorial." *Computerized medical imaging and graphics : the official journal of the Computerized Medical Imaging Society* 25(2): 97-103.
- Zeuner, K. E., F. M. Molloy, et al. (2003). "Effect of ethanol on the central oscillator in essential tremor." *Movement disorders : official journal of the Movement Disorder Society* 18(11): 1280-1285.